Vincenzo Afferrante, MSc

Gauge invariant spectra of theories with BEH effect

PhD Thesis
to achieve the university degree of
Doctor of Physical Sciences
Doctoral degree program: Physics

submitted to

University of Graz

Supervisor
Univ.-Prof. Dipl.-Phys. Dr.rer.nat. Axel Maas

Institute for Physics
Head: Univ.-Prof. Dipl.-Phys. Dr.rer.nat. Axel Maas

Graz, February 2021

Vincenzo Afferrante, MSc

Eichinvariante Spektren von Theorien mit BEH Effekt

Dissertation
zur Erlangung des akademischen Grades
Doctor of Physical Sciences
Doktoratsprogramm Physik

eingereicht an der

University of Graz

Betreuer
Univ.-Prof. Dipl.-Phys. Dr.rer.nat. Axel Maas

Institute for Physics
Leitung: Univ.-Prof. Dipl.-Phys. Dr.rer.nat. Axel Maas

Graz, February 2021

Affidavit

I declare that I have authored this thesis independently, that I have not used other than the declared sources/resources, and that I have explicitly indicated all material which has been quoted either literally or by content from the sources used. The text document uploaded to UNIGRAZonline is identical to the present doctoral thesis.

Date

Signature

Eidesstattliche Erklärung

Ich erkläre an Eides statt, dass ich die vorliegende Arbeit selbstständig verfasst, andere als die angegebenen Quellen/Hilfsmittel nicht benutzt, und die den benutzten Quellen wörtlich und inhaltlich entnommenen Stellen als solche kenntlich gemacht habe. Das in UNIGRAZonline hochgeladene Textdokument ist mit der vorliegenden Dissertation identisch.

Datum

Unterschrift

Abstract

Gauge invariance is a guiding principle for theoretical particle physics. We want to analyze the consequences of this principle for gauge theories with a Brout-Englert-Higgs effect. Requiring that the physics is not dependent on the redundant degrees of freedom can be achieved with a manifestly gauge invariant formulation. A proper description of physical states can be obtained with composite operators with a Higgs field insertion. The first goal of this work is to analyze the spectroscopical properties of these gauge-invariant operators with lattice methods since these objects are nonperturbative. The second is to obtain a prediction on these objects with the FMS mechanism and confront them with the lattice results. This procedure has been realized for the bosonic sector of the standard model, leading to results that resemble the phenomenology with great accuracy.

In this work, two novel cases are analyzed. The first is a SU(2) Georgi-Glashow model, which should allow for a massless composite vector state according to the FMS prediction. The lattice simulations support the FMS result. In the second case, the spectrum of a SU(2) Higgs theory coupled with vectorial fermions has been also analyzed on the lattice. The lattice implementation resembles the standard model setup with the addition of a Wilson mass term. The results support the FMS prediction also in this case, allowing the hypothesis of a Higgs valence contribution in leptons.

Kurzzusammenfassung

Die Eichinvarianz ist ein Leitprinzip für die theoretische Teilchenphysik. Die Konsequenzen dieses Prinzips sollen für Eichtheorien mit Brout-Englert-Higgs Mechanismus untersucht werden. Die Forderung, dass die Physik nicht von redundanten Freiheitsgraden abhängt, kann durch eine manifest eichinvariante Formulierung erreicht werden. Eine solche Beschreibung von physikalischen Zuständen kann durch zusammengesetzte Operatoren mit Higgs-Feld Einsetzungen erreicht werden. Das erste Ziel dieser Arbeit ist es, die spektroskopischen Eigenschaften solcher eichinvarianten Operatoren mit Gittermethoden zu analysieren, da diese Objekte von nichtstörungstheoretischer Natur sind. Das zweite Ziel besteht darin, eine Vorhersage für diese Objekte mit dem FMS-Mechanismus zu erhalten und diese mit den Gitterergebnissen zu vergleichen. Dieses Prozedere wurde bereits im bosonischen Sektor des Standardmodells durchgeführt, was zu einer detaillierten Übereinstimmung in der Phänomenologie führt.

In dieser Arbeit werden nun zwei Fälle analysiert. Der erste ist das SU(2) Georgi-Glashow Modell. Dieses besitzt ein masseloses zusammengesetztes Vektorteilchen gemäß der FMS Vorhersage. Die durchgeführten Gitteruntersuchungen unterstützen die FMS Resultate. Im zweiten Fall wird das Spektrum einer SU(2)-Higgs-Theorie mit vektoriellen Fermionen mit Hilfe von Gittersimulationen untersucht. Die Gitterimplementierung ähnelt der Struktur des Standardmodells wobei zusätzliche Wilson Massenterme mit berücksichtigt werden müssen. Die Ergebnisse stützen die FMS-Vorhersagen auch in diesem Fall und erlauben die Hypothese eines Higgs-Valenzbeitrages in Leptonen.

Contents

1. Introduction

Gauge theories are the cornerstone principle of the modern theoretical foundation of particle physics[1–3].

The first example of a quantum field theory with a gauge symmetry is *quantum electrodynamics* (QED) [4, 5]. The gauge group that characterizes the theory is $U(1)_{em}$, which is an abelian group. Its striking predictive properties led to many spectacular confirmations, starting from the calculation of the Lamb shift [6, 7].

A systematic set of rules for computing observables in QED via perturbation theory was found by Feynman, Schwinger, and Tomonaga [4, 5], which paved the road for all modern calculations, and many other predictions. All these results set local symmetries as the founding principle for a fundamental theory. In 1954 non abelian gauge theories were proposed by Yang and Mills [8]. A generalization of quantized gauge theories to non abelian groups has been achieved owing to the work of Feynman, Fadeev, Popov and deWitt. At first instance it was an exercise for the quantization of gravity, but later it was revealed to be the mathematical description of all elementary particles.

The *weak interactions* have been studied extensively in many experiments. A first theoretical approach has been realized with the non-renormalizable four-fermion Fermi interaction. The renormalizable model that fully describes these interactions is the Weinberg-Glashow-Salam (WGS) model [9]. Results obtained at the SppS and LEP colliders led to the discovery of the masses of the vector gauge weak mediators, and to many experimental precision tests of the theory. The WGS model has a $SU(2)_L \times U(1)_Y$ symmetry. In principle, a mass for the mediators of the gauge symmetry seems impossible, since it would violate the symmetry, but the WGS model is also equipped with a scalar doublet, giving rise to a Brout Englert Higgs (BEH) mechanism [10–12].

The BEH effect consists in the addition of a scalar field that is coupled to the weak mediators, and that in a precise phase lends some of its degrees of freedom to allow for longitudinal polarizations of the vector bosons. The discovery at LHC of a scalar particle in the mass range predicted by the theory in 2012 [13, 14], is the coronation of the theory, making theoretical understanding of the Higgs mechanism more important than ever.

Owing to the theoretical developments found for the weak interactions, a description for strong nuclear forces was made possible with the development of *quantum chromodynamics* (QCD) [15]. It was found that the partons, the components of the proton discovered in deep inelastic scattering experiments, are the quarks, the fundamental constituents of the QCD theory. These transform under the fundamental representation of $SU(3)_C$. The index C refers to the property that is represented by the additional quantum number that quarks and gluons possess, called the color. The observable particles that are obtained through their combination are singlets under the color symmetry, and are called hadrons. QCD has two really important properties. The first is asymptotic freedom [16, 17], which results in the property of the fundamental constituents of the theory to be essentially free at high energies. The other is called confinement, and refers to the property of the quarks to never be observable as physical particles, but only as components of physical bound states.

The resulting theory, which combines the electroweak theory of Weinberg-Glashow-Salam and the quantum chromodynamics is called the *Standard Model* (SM). It is the theory which is capable of describing all physical phenomena observed in modern colliders, except for gravity. At the current state, only some anomalous decays of the B and K meson seem to point at possible direct indications of the shortcomings of the theory at the colliders energy [18]. Also, the description of dark energy and dark matter is not included in the theory. Nonetheless, the phenomenological success of the Standard Model is an indication that, up to very high energy scales, the principles of relativity combined with the mathematical formalism of quantum mechanics can describe reality efficiently. But there are many indications that point to the fact that the Standard Model is not the definitive answer concerning high energy particles theory.

A problem of the Standard Model is called triviality, which is related to the renormalization group flow of theories with a scalar particle. The electroweak sector without a scalar field would be an asymptotically free theory, similarly to the QCD case. But scalar field theories perturbatively have a Landau pole in the ultraviolet, so they can only be without interactions, or trivial. This result also seems to be supported by non perturbative methods. In recent works, new renormalization group trajectories which circumvent the triviality problem, and that are not accessible with perturbation theory, have been found [19–21].

Another problem of the Standard Model is the seemingly arbitrary separation of scales that arise in the different parameters that describe nature. In particular, the difference between the scale of electroweak interactions, and the natural cutoff for the theory, which is usually considered to be the Planck scale. This is called the hierarchy problem. From a perturbative point of view, the scalar mass renormalization term is sensible to the cutoff of the theory, which is then represented by the gravitational force. This results in the bare mass parameter having corrections of the order of the ratio of the intensities of the weak and gravitational forces. The need for such small and precise determination of the bare parameter of the model is also known as fine tuning. Actually, more recent results on the physical Higgs propagator seem to suggest a lot less severe dependence on the couplings [22].

There have been many attempts of extending the Standard Model, in order to include gravity interactions, or to solve other conceptual problems just mentioned. One of these beyond the Standard Model (BSM) theories, are the *grand unified theories* (GUT) [23]. The main idea is that, since both quarks and leptons have fractions of the same electrical charge, there must be a bigger gauge group that transforms both under the same representation in a multiplet. In this way, the issue regarding the different scales of the Standard Model, is solved, since there is a common unification scale. The first proposed GUT group was $SU(5)$, which could break spontaneously to the group of the Standard Model $SU(3)_C \times SU(2)_L \times U(1)_Y$. There are many reasons why the theory has been abandoned, one of them is that it gave a decay rate for the proton which is very different from the experimental observations.

Various modifications of the Higgs sector of the SM have been proposed to address the issue of triviality. It can be circumvented, if the Higgs is a composite particle made of fermions states, since these do not suffer from the triviality problem. One of these is called technicolor [24]. In the technicolor framework there is an additional gauge group. The main idea is that the mass for the vector bosons is obtained by interactions with this bigger group. After the Higgs discovery, modifications of early technicolor theories have been proposed, that allow for a dynamical generation of a scalar as a condensate.

Also, many BSM theories propose new highly massive particles which have never been observed at colliders, since they couple very weakly at energies we can access with current apparatus, and thus are potential candidates for dark matter.

The modern interpretation of the the Standard Model is the one that treats it as an effective theory of an ultraviolet completion capable of describing gravity at a quantum level. In this sense both the triviality and the hierarchy problem become less severe. In the first case the ultraviolet completion of the Standard Model is not needed to describe low energy physics, since the description of reality at higher energies will be very different from the one we observe at the currently accessible energy scales. The second remains then a mostly aesthetical question. We will then assume the Lorentz symmetry and the gauge groups as guiding principles in the following. Even though it can be argued that at higher energy scales these symmetries will not be realized, due to the different mechanisms that can be involved in the physics of the Planck scale, these principles will still remain in the effective field theory of the Standard Model.

In this work, we want to point out a potential shortcoming of the spontaneous symmetry breaking treatment of gauge theories with a Higgs. This issue is of major interest in the context of the electroweak sector of the Standard Model. The main problem comes from the fact that the gauge variant elementary fields in the Lagrangian are used, in perturbation theory, as asymptotic states to identify the physical Higgs and the gauge bosons. But in principle, this issue can also be applied to any beyond the Standard Model theory that comprises a Higgs sector. It must first be pointed out that, since the physical states in this framework are gauge variant, the entire symmetry breaking procedure is then computed in a suitable fixed gauge. But in principle physical results should be independent of the gauge in which they are calculated.

This can be formulated in a coherent way owing to the result of Elitzur, which proves the impossibility of realizing the spontaneous symmetry breaking procedure for a local symmetry [25]. Also, in the case of the Standard Model weak sector, it was shown by Osterwalder and Seiler, as well as Fradkin and Shenker that no gauge invariant order parameter for the BEH phase transition exists [26–28]. This result implies that the QCD-like and BEH phases are indistinguishable, and their occurrence in a fixed gauge is an artifact.

The perturbative treatment can then potentially lead to nonphysical results. The gauge invariance of the theory is taken into account in the usual formulation of QCD, with the mechanism of confinement. But in the usual electroweak sector perturbative treatment this does not happen. The BRST singlets are capable of describing phenomenology, but they are not singlets of the full gauge group. Nonetheless results obtained using this approach led to many spectacular discoveries. Even though this observation being remarkable, in this work we want to point out that there can be in principle other contributions to the usual amplitudes calculated in perturbation theory. These contributions are not accessible by the current available experimental setups, but can potentially matter for the future colliders. Not taking them into account can then fake new physics effects.

Then a question naturally arises:

Why is perturbation theory so successful for the electroweak sector of the Standard Model? And also, should we expect then that the spontaneous symmetry breaking treatment of the Higgs sector lead to correct results in perturbation theory for all theories beyond the Standard Model?

The solution can only be achieved with a reformulation of the Higgs sector in terms of gauge invariant operators. One of the realizations of this idea is also known as *Fröhlich-Morchio-Strocchi (FMS) mechanism* [29, 30]. Alternatively, for particular models, the equations of motion of the gauge invariant degrees of freedom have been investigated [31], leading to nonlocal descriptions. However, the FMS mechanism is the framework of choice that drives the investigations in this manuscript. It is possible, using it, to understand why the usual procedure for the electroweak sector is so successful. More importantly, it will provide general rules to obtain results in gauge theories with Higgs sectors.

The starting principle of the FMS description is the gauge invariance of the observable physical particle states. This is analogous to what happens in the treatment of other non abelian gauge theories with confinement. The observable states, the hadrons, are gauge invariant combinations of the elementary constituents of the theory. The proposal in the original FMS work, is to treat the physical states in the electroweak theory with gauge invariant composite states with the required quantum numbers to describe phenomenology. This results in the addition of a Higgs field component to the elementary operators of the Lagrangian. The composite operators obtained in such a way are essentially nonperturbative objects. In principle, one can use lattice, or other nonperturbative methods to analyze them.

The FMS mechanism also provides a method to obtain perturbative results on the composite operators, that exploits properties of the theories that have a BEH effect. The n-point functions of the physical composite states can still be evaluated in a fixed gauge, since they do not depend on the gauge choice. In suitable gauges, this leads to an expansion in powers of the Higgs vacuum expectation value, that multiply n-point functions of elementary fields. The latter can be evaluated with perturbative techniques, and the ones that are multiplied by the greatest power of the vacuum expectation value will provide a good first approximation of the composite physical n-point correlation functions.

It will be shown that the usual classification of the states according to the gauge multiplets of $SU(2)_L$, is preserved in the gauge invariant formulation we are going to detail. The case of the Standard Model is special, in that it is an exact mapping to the remaining custodial symmetry of the Higgs sector. The custodial symmetry is an additional global symmetry that acts in the scalar sector. In the FMS setting, the physical states which contain a scalar field valence component, can be described as multiplets with the quantum number associated with this symmetry. This can be seen as an explanation for the success of perturbation theory in the Standard Model. For other gauge theories and Higgs representations, the broken gauge group and the custodial group are not the same. This can potentially lead to an inconsistency of the usual standard perturbation theory, and would prove the results obtained with it potentially unphysical.

Nonperturbative techniques have been used for the bosonic sector of the Standard Model [32, 33], confirming the predicted results. Also, a toy model of a GUT with a SU(3) gauge group has been studied, to check whether the inconsistencies predicted by the FMS mechanism are present in the physical spectrum calculated nonperturbatively. The FMS resulted in being successful also in this case [34].

1.1. Motivation and Background

All the Higgs theories analyzed on the lattice prior to this work are both merely bosonic and with a mass gap. A complete realization of the Standard Model, and a complete validation of the gauge invariant procedure to describe a phenomenologically viable theory, would require at least one massless vector particle, and a full set of fermion states. The goal of the work described in this manuscript is to give a lattice realization of these two cases.

The cases that are being described in this manuscript are of vital importance to the investigation of gauge theories coupled with a Higgs particle. The FMS mechanism has been used to describe the electroweak sector of the SM with great success. Also the spectroscopy of a SU(3) theory coupled with a fundamental scalar worked, but in both cases there were no massless states in the spectrum. Then the question arises whether it is possible to obtain a composite vector bound state operator which is massless. This would provide a physical photon state in a GUT setup in an unprecedented way.

The second question is if the FMS construction can also be validated for fermion states. In principle, this would result in a rethinking of the fermion states as composite objects, with a valence Higgs component. The phenomenological implications of this model are numerous, and potentially viable for discoveries in the near future, thanks to the new lepton collider facilities that have been proposed.

The first case can be explored in the SU(2) gauge theory coupled with a single Higgs in the adjoint representation. Analytical calculations with the FMS mechanism point to the existence of a composite vector operator with a vanishing mass [35]. A nonperturbative treatment is needed in order to prove this hypothesis, and lattice methods have been chosen for this goal. A positive result would result in a novel procedure to obtain a U(1) emergent symmetry at low energies for a beyond the Standard Model theory of a GUT type. But a realization of a theory with a massless state on the lattice is not trivial, since a truly massless state can only exist in an infinite volume. For scalar massless states we expect still then a nonzero mass in a finite volume. For vector states the behaviour is different, and will be explained thoroughly in this work.

The second question we answer in this work regards the fermion gauge invariant formulation. In principle, this is of enormous interest for phenomenology, since any left handed state in the Standard Model is not an $SU(2)_L$ singlet, and thus not an asymptotic observable state. A reformulation of the fermion observables has to be done, which will be associated with a composite bound state with fermionic quantum numbers. These new gauge invariant states cannot be analyzed straightforwardly on the lattice, as it has been done for the vector and scalar channel of gauge theories. The main obstacle is given by the fact that it is not possible to realize parity violation on the lattice [36]. In this work, we will depict a non chiral fermion lattice implementation, which is based on vectorial Wilson-Dirac fermions. A spectroscopic analysis for the bound states, in a quenched setting, has been done in order to analyze the spectrum. The FMS prediction gives a compatible mass between the bound state and the elementary mass in a suitable fixed gauge.

1.2. Outline

In chapter 2 we provide the details of the FMS framework for a gauge invariant formulation of theories with a BEH effect. In particular, we focus on the Standard Model case, both the bosonic and fermionic part, and the SU(2) gauge theory coupled with a Higgs in the adjoint representation. In this chapter we first illustrate the procedure with the elementary fields. Then the gauge invariant formulation is shown which is the main goal of this investigation. This formulation requires to treat physical observables as composite operators. The method chosen to analyze them is lattice field theory.

In chapter 3 we explain in detail all lattice techniques that are used in the following. It is first shown how to implement a scalar gauge theory on the lattice. Since one of the main goals of the investigation is to obtain masses of gauge invariant bound states, standard spectroscopical lattice methods are discussed. Fermions on the lattice require a special treatment. The method chosen to treat them in this work is the Wilson-Dirac approach. Further, the analysis is treated within the quenched approximation. Chapter 4 details a SU(2) gauge theory with an adjoint Higgs. The peculiarities of the lattice implementation are discussed, since the presence of a massless state requires a reinvention of the interpolators and the techniques with respect to the ones used in the case with a mass gap. The operator basis chosen and the obtained results are then presented in detail.

Chapter 5 describes the implementation of vectorial fermions on the lattice, due to the impossibility of the realization of a chiral implementation of fermion gauged theory with a Yukawa term on the lattice. Here the physical spectrum will be described as composite bound states with a Higgs valence contribution. Also a gauge fixed description of the gauge variant elementary propagator will be presented, and it will be fundamental to prove the FMS relations. The implementation of the extended Wilson-Yukawa operator is detailed. Spectroscopical results are then illustrated and discussed.

In chapter 6 the results are summarized, and put into perspective for future investigation about this topic.

2. Higgs theories and FMS mechanism

In this chapter we illustrate some notions about gauge theories in which the BEH effect is present. For our purposes, the focus will be on general unitary gauge theories.

This section serves as a basic introduction to the concepts needed for the spectrum formulation of SU(N) theories in the language of spontaneous symmetry breaking. The issue of the full gauge invariance of observables under the full gauge group is presented here as well. The reformulation of physical particles with gauge invariant operators is then used as a solution for the problem. For a review of the methods and the implications of this formulation see [37]. For the most recent analytical results on the scalar and vector channel in Higgs theories one can consult [38].

The chapter will first outline how the usual perturbative approach with the spontaneous symmetry breaking is realized. But the main focus of this section will then be a gauge invariant reformulation of the theory. This will result in the introduction of composite operators for the observable particles. Then we will also introduce a calculation tool for the composite operators when a BEH effect is present, the FMS mechanism. It will first be presented for general gauge theories, then we will give a description for the $SU(2)$ Higgs theory. A focus of the work is then thoroughly detailed, the fermions description as composite bound states with Higgs components. This will serve in order to analyze the electroweak sector in this new perspective, and then discuss the implications of the reformulation for the whole Standard Model. Then the second important case is explained, the Higgs in the adjoint representation. The section is concluded with an overview of the description of BSM theories in the FMS framework.

2.1. Perturbative treatment SU(N) Higgs theories

We first detail the case of a quantum field theory with a $SU(N)$ gauge group with a scalar particle in the fundamental representation. The general knowledge about these theories is that, based on the shape of the scalar potential, there are two possible realizations of the theory. The first is called the symmetric one, which has a behaviour which is similar to QCD, with $N^2 - 1$ massless gauge bosons. In this work we are interested in the other phase, which allows for the so called Brout-Englert-Higgs (BEH) effect. In this phase the scalar field can obtain a non zero vacuum expectation value (vev), in a suitable fixed gauge. Some of the degrees of freedom of the Higgs field are absorbed in the longitudinal polarization of the coupled gauge bosons, resulting then in the appearance of mass terms for these.

A prototype Langrangian for a $SU(N)$ gauge theory with a fundamental scalar and no fermions, which can allow the BEH effect, is written as

$$\mathcal{L} = -\frac{1}{4}W^a_{\mu\nu}W^{a\ \mu\nu} + \frac{1}{2}(D_\mu\phi)^\dagger(D^\mu\phi) - V(\phi^\dagger\phi)\,. \tag{2.1}$$

We use in this section the Minkowski spacetime. The gauge fields are indicated by W^a_μ, while the scalar is ϕ. The field strength tensor used in the Lagrangian reads

$$W^a_{\mu\nu} = \partial_\mu W^a_\nu - \partial_\nu W^a_\mu - gf^{abc}W^b_\mu W^c_\nu\,, \tag{2.2}$$

and the covariant derivative

$$D_\mu = \partial_\mu + igW^a_\mu T^a\,. \tag{2.3}$$

We can observe in the above equations the generators of the Lie algebra for SU(N) indicated by T_a, the relative structure constants f^{abc}, and the coupling constant g. The gauge transformations that leave the action invariant act as

$$\phi(x) \to U(x)\phi(x), \tag{2.4}$$

$$W_\mu \to U(x)W_\mu(x)U^\dagger(x) - \frac{i}{g}(\partial_\mu U(x)^\dagger)U(x)\,. \tag{2.5}$$

Here we wrote the transformation for the matrix valued gauge fields, defined by the expansion $W_\mu = W^a_\mu T^a$. The scalar field analyzed in this section is in the fundamental representation. We are interested in a potential which allows the BEH effect. We choose then a potential with the mexican hat shape, parametrized as

$$V(\phi^\dagger\phi) = \lambda\left(\phi^\dagger(x)\phi(x) - f^2\right)^2\,. \tag{2.6}$$

The parameters λ and f regulate the form of the potential. For a positive value of f^2 we have a classical minimum for $\phi^\dagger\phi = f^2$. At the quantum level the expectation value of the scalar field without gauge fixing vanishes. This is expected due to the Elitzur theorem [25], which states the impossibility of spontaneous breaking of local gauge symmetries. This theory can be analyzed in particular gauges which allow the split

$$\phi = \frac{fn}{\sqrt{2}} + \varphi\,. \tag{2.7}$$

Here n is a vector in $\mathbb{C}^N$ satisfying $n^\dagger n = 1$. The validity of this assumption, in particular regarding the choice of the direction is crucial in our discussion. If this is verified and well posed, we can then identify the Higgs expectation value modulo in a fixed gauge

$$\langle \phi \rangle = \frac{vn}{2} \tag{2.8}$$

with the parameter f of the Lagrangian, $v = f$. In this first analysis we do not include fermions, and the additional effects of a U(1) symmetry. The SU(2) case will be analyzed thoroughly afterwards. In order to solve the functional integral one must get rid of the gauge redundancy by fixing the gauge. In order to perform the split, we want to impose the Feynman-'t Hooft gauge condition, given by $\partial^\mu W^a_\mu + \frac{igv\zeta}{\sqrt{2}}\phi_i T^a_{il} n_l = 0$. It must be noted that, since the vector n is constant, this gauge fixes a direction for the vacuum expectation value. Using other gauges, like Landau gauge, would have provided a vanishing vev[1].

We choose to use the class of covariant R_ξ gauges, defined by adding the gauge fixing therm

$$\mathcal{L}_{gf} = -\frac{1}{2\xi}\left|\partial^\mu W^a_\mu + i\frac{gv\xi}{\sqrt{2}}(n^\dagger_i T^a_{ij}\phi_j - \phi^\dagger_i T^a_{ij} n_j)\right|^2 . \tag{2.9}$$

In this case, we imposed for simplicity that the parameter ζ of the 't Hooft gauge is the same as the ξ parameter for the R_ξ gauges, avoiding mixing of Goldstone bosons and gauge fields at tree level. This relation is not assured in higher loops calculations, but for the case we need to present it still works. By applying the Fadeev-Popov procedure one then obtain the ghost term in the Lagrangian

$$\mathcal{L}_{ghost} = -\bar{c}^a\left(\partial^\mu D^{ab}_\mu - \frac{\xi g^2 v}{\sqrt{2}} T^a_{ij} T^b_{jk}(\phi^\dagger_i n_k + n^\dagger_i \phi_k)\right) c^b . \tag{2.10}$$

We are interested in the elementary spectrum. It must be noted that in these gauges the Goldstone bosons obtain a mass term proportional to ξ. It can be shown, through the BRST procedure, that these additional unphysical degrees of freedom that depend on ξ, do not appear in the physical spectrum. We focus on the spectrum given by physical degrees of freedom. We can obtain it then by reinserting the scalar field after it has been split like in (2.7). The physical state masses are then obtained in the expansion of the kinetic term of the scalar field

$$(D_\mu\phi)^\dagger(D^\mu\phi) = \partial_\mu\phi^\dagger\partial^\mu\phi + \frac{g^2v^2}{2} n^\dagger_i T^a_{ij} T^b_{jk} n_k W^a_\mu W^{b,\mu} + \dots , \tag{2.11}$$

[1] On the other hand, the unitary gauge can be obtained by performing the limit $\xi \to \infty$ [3, 39]. By applying this limit, the masses of the unphysical degrees of freedom go to infinity, and then are decoupled from the dynamics of the theory. Its name derives then from the removal of the elements that violate the unitarity. But even if the decoupling appears evident at tree level, one must be careful in sending parameters to infinity at loop level. The renormalizability of the theory is not evident anymore. Since we want to focus on non-perturbative phenomena, and in general non tree level physics, we will not use it.

where the terms excluded here do not contribute to the masses of the physical states. A mass matrix appears for the gauge bosons

$$M^{ab} = \frac{g^2 v^2}{2} n_i^\dagger T^a_{ij} T^b_{jk} n_k \,. \tag{2.12}$$

With the convenient choice $n_i = \delta_{i,N}$ the mass matrix is

$$M = \frac{g^2 v^2}{4} \mathrm{diag}(0, \ldots, 0, 1, \ldots, 1, \frac{2}{N}(N-1)) \,. \tag{2.13}$$

The number of massless gauge bosons left is the same as the dimension of the group $SU(N-1)$, namely $N(N-2)$. There are then $2(N-1)$ massive bosons with mass $gv/2$, and one more with mass $gv\sqrt{(N-1)/2N}$. The breaking pattern that results from the coupling with a scalar in the fundamental representation is $SU(N) \to SU(N-1)$. The procedure we described is commonly regarded as spontaneous symmetry breaking of a gauge symmetry. The mass term for the scalar singlet is obtained by expanding the potential in equation (2.6).

Putting all the terms together we obtain

$$\begin{aligned}
\mathcal{L} \;=\; & -\frac{1}{4} W^a_{\mu\nu} W_a^{\mu\nu} + (\partial_\mu \varphi^\dagger)(\partial^\mu \varphi) \\
& + \frac{g^2 v^2}{2} n_i^\dagger T^a_{ij} T^b_{jk} n_k W^a_\mu W^{b\;\mu} - 2\lambda v^2 \,\mathrm{Re}[n^\dagger \varphi]^2 \\
& - \frac{g^2 \xi v^2}{2} \,\mathrm{Im}[\varphi T^a n]^2 + \xi g^2 v^2 n_i^\dagger T^a_{ij} T^b_{jk} n_k \bar{c}^a c^b \\
& - 2\sqrt{2}\lambda v \,\mathrm{Re}[n^\dagger \varphi](\varphi^\dagger \varphi) - \lambda(\varphi^\dagger \varphi)^2 + \xi g^2 v \bar{c}^a \,\mathrm{Re}[n_i^\dagger T^a_{ij} T^b_{jk} \varphi_k] c^b \\
& + \sqrt{2} g^2 v \,\mathrm{Im}[n_i^\dagger T^a_{ij} T^b_{jk} \varphi_k] W^a_\mu W^b_\mu + g^2 \varphi^\dagger W_\mu W^\mu \varphi + 2g \,\mathrm{Re}[(\partial_\mu \varphi^\dagger) W^\mu \phi] \\
& - \frac{1}{2\xi} (\partial^\mu W^a_\mu)^2 - \bar{c}^a \partial^\mu D^{ab}_\mu c^b \,.
\end{aligned} \tag{2.14}$$

In the first line we have the kinetic terms for the gauge bosons and the residual Higgs field. In the second there are the mass terms for the physical states. In particular, we can recognize the mass terms for the gauge bosons. In the third line there are the mass terms for the nonphysical additional states that appear in a fixed gague. We see then the mass terms for the Goldstone bosons, and the ghosts. We can observe how both terms depend on the gauge fixing parameter ξ. The fourth and fifth line contain interaction terms. The last line contains terms which are used for the gauge fixing.

2.2. Gauge invariant formulation and FMS mechanism

The scalar state and the gauge field are BRST singlets, and thus observable in perturbation theory. But it is evident that even these are not singlets under the full gauge group, but rather transform under a non-trivial representation of it. This problem was already known in the context of non-Abelian gauge theories. Another important result in this direction is given by Elitzur's theorem [25], which states that local gauge symmetries cannot be spontaneously broken. The symmetry breaking is actually obtained only by imposing gauge fixing. In this way gauge dependent correlation functions become nonvanishing. As a consequence, a correct treatment of these theories would require that the observable physical states must be singlets under the full gauge group. For non abelian gauge theories, these singlet states have to be composite operators. This is a procedure which is commonly accepted in the QCD case, where a nonperturbative treatment is essential, and the physical singlet states are called hadrons.

The idea to reformulate the spectrum of the theory in terms of gauge invariant composite operators comes from a seminal paper by Fröhlich, Morchio and Strocchi [29, 30, 40, 41]. The idea of readdressing the non abelian gauge theories with BEH effect in a similar fashion to theories with confinement, was also stated by G. 'T Hooft [42]. The main goals of the investigation described have a starting point and a foundation in these seminal ideas. In this part we now focus on readdressing the physics of these theories, by reformulating the observables in terms of gauge invariant operators.

In Landau gauge, or in any covariant R_ξ gauge, without fixing the global Higgs direction like in 't Hooft gauge, the expectation value of the Higgs vanishes

$$\langle \phi \rangle = 0\,. \tag{2.15}$$

In this gauge choice then no mass term for gauge bosons appears in the Lagrangian, which leaves the matter of the mass generations for the gauge bosons open. In principle it is evident that perturbation theory is not capable of describing the dynamics of the theory fully. It is not evident at all how the mechanism of generation of gauge boson masses works in such gauges. This becomes then a nonperturbative question.

But the Standard Model has been an extremely predictive theory using the paradigm of spontaneous symmetry breaking. This leads to the main questions. The first is why the Standard Model has such predictive power , even by using non physical operators [39, 43–45]. The second, is whether perturbation theory applied in the context of spontaneous symmetry breaking will be always equally predictive.

To address this questions, it is necessary to readdress the operators used to describe physical observables. In this section, we provide examples of operators with the same quantum numbers as the observable physical states. The theory can be reformulated with the physical observables described by gauge invariant operators. For the scalar channel we can construct one as

$$\mathcal{O}_{0^+}(x) = (\phi^\dagger \phi)(x)\,. \tag{2.16}$$

This operator is then the representation of the physical Higgs state. It is then possible to access its spectral properties from the connected 2 point function. But this would require a nonperturbative method to describe it, since it is a composite bound state. The FMS mechanism is the technique that allows to obtain analytical results about the composite object, relating it to perturbation theory techniques. To have a better understanding of the mechanism, we provide the FMS expansion of the two point function of the object just shown. It consists on expanding the Higgs field as in eq. (2.7), and then ordering the contributions by powers of the Higgs vev.

$$\begin{aligned} \langle \mathcal{O}_{0^+}(x)\mathcal{O}_{0^+}(y)\rangle &= cv^4 + 4v^2 \left\langle \mathrm{Re}\left[n_i^\dagger \varphi_i\right](x)\ \mathrm{Re}\left[n_j^\dagger \varphi_j\right](y)\right\rangle \\ &\quad +2v\left(\left\langle (\varphi_i^\dagger\varphi_i)(x)\ \mathrm{Re}\left[n_j^\dagger\varphi_j\right](y)\right\rangle + (x\leftrightarrow y)\right) \\ &\quad + \left\langle (\varphi_i^\dagger\varphi_i)(x)\ (\varphi_j^\dagger\varphi_j)(y)\right\rangle\ . \end{aligned} \tag{2.17}$$

This is basically a rewriting of the composite operator, thus the expression on the right hand side is gauge invariant. The individual terms are not. We can already get information about how the FMS mechanism works by analyzing the terms on the right hand side. The first one is a constant, which we indicated with c. The second one is more interesting from a dynamic point of view. It is formally the correlator of the Higgs field in the direction of the vev. It is also the dynamical component that is quantitatively more important, since it is the one which is multiplied by the biggest power of the Higgs vev. The other contributions are products of three and four fields, but they are quantitatively less relevant.

To estimate the contribution, it is possible to expand in the various couplings. If they are small enough it will be possible to use perturbation theory techniques. The expansion at the lowest order in the couplings reads as

$$\begin{aligned} \langle \mathcal{O}_{0^+}(x)\mathcal{O}_{0^+}(y)\rangle &= c'v^4 + 4v^2 \left\langle \mathrm{Re}\left[n_i^\dagger \varphi_i\left(x\right)\ \mathrm{Re}\left[n_j^\dagger \varphi_j\right](y)\right\rangle_{\mathrm{tl}} \\ &\quad + \left\langle \mathrm{Re}\left[n_i^\dagger\varphi_i\right](x)\ \mathrm{Re}\left[n_j^\dagger\varphi_j\right](y)\right\rangle_{\mathrm{tl}}^2 + \mathcal{O}(g^2,\lambda)\ . \end{aligned} \tag{2.18}$$

It is then instructive to analyze the spectral properties of the right hand side. There is a pole at the usual mass of the residual Higgs, due to the first dynamical term. Then a discontinuity from 2 times the Higgs mass is obtained. We are then capable of getting a first estimate about the properties of the bound state scalar operator, namely a tree level approximation of the position of its pole, and of its decay dynamics. Alternatively, one can keep all the terms in the coupling expansion, neglecting the terms multiplied by smaller powers of the vev

$$\langle \mathcal{O}_{0^+}(x)\mathcal{O}_{0^+}(y)\rangle_c = 4v^2 \left\langle \mathrm{Re}\left[n_i^\dagger\varphi_i\right](x)\ \mathrm{Re}\left[n_j^\dagger\varphi_j\right](y)\right\rangle_c + \mathcal{O}(v) = 4v^2 D_\varphi(x-y) + \mathcal{O}(v).$$

In this case, the full propagator of the elementary scalar is reproduced at the highest order in the vev. There are many remarks that can be made at this point. The first is that it must be noted how there is a strong dependence of the effectiveness of the FMS procedure, depending on the parameter of the theory. We are assuming in this expansion, that the fluctuating field φ is smaller than v. Lattice exploration of this hypothesis seems to support it [46]. The other regards the choice of the gauge. It appears that the method shown can only be applied with a gauge that allows the development of a vev, namely where $< \phi > \neq 0$. The expansion, with a vanishing vev, would become trivial and has only one term.

A gauge invariant vector state can be constructed similarly, with the insertion of a Higgs component in a composite operator. It must be taken into account, that there is a custodial $SU(2)$ left even in the broken phase for the SU(2) group, while for $SU(N)$ with $N > 2$ there is only a $U(1)$. The $SU(2)$ case will be analyzed in the next section.

We note now, concerning the treatment of Higgs theories, how the custodial symmetry can modify the values of the Higgs vev $\langle \phi \rangle$. The theory is thus invariant under a simultaneous custodial transformation and a global gauge transformation that leaves the vev unchanged. In this case, the theory is invariant under a diagonal subgroup, which contains partly the gauge symmetry. Hence the diagonal group is not observable, due to its gauge content.

With a U(1) custodial symmetry group, a single vector state can be written and expanded as

$$O_{1_0^-,\mu}(x) = \phi^\dagger(x) D_\mu \phi(x) = -\frac{v^2 g}{2}(n^\dagger W_\mu(x) n) + \mathcal{O}(\varphi)\,. \tag{2.19}$$

We can apply the expansion of the two point function

$$\left\langle O_{1_0^-,\mu}(x) O^\dagger_{1_0^-,\nu}(y) \right\rangle = \frac{v^4 g^2}{4} \left\langle n^\dagger W_\mu(x) n n^\dagger W_\nu(y) n \right\rangle + \mathcal{O}(\varphi)\,. \tag{2.20}$$

By setting the vev direction in the last component with $n_i = \delta_{i,N}$ we obtain then

$$\left\langle O_{1_0^-,\mu}(x) O^\dagger_{1_0^-,\nu}(y) \right\rangle = \frac{(N-1) v^4 g^2}{8N} \left\langle W_\mu^{N^2-1}(x) W_\nu^{n^2-1}(y) \right\rangle + \mathcal{O}(\varphi)\,. \tag{2.21}$$

There is a pole at the usual mass of the elementary gauge boson.

We can also construct non singlet U(1) vector states. An example for the group $SU(3)$ is given by the operator

$$\mathcal{O}^\mu_{1_1^-} = \epsilon^{abc} \phi^a (D^\nu \phi)^b (D_\nu D^\mu \phi)^c\,. \tag{2.22}$$

These ones have masses bigger than the singlet. These can be potential ground states of a different channel with different $U(1)$ quantum numbers. It can be obtained in an

FMS expansion as

$$\mathcal{O}^{\mu}_{1_1^-} = -g^2 v^3 \epsilon^{abc} n^a (W^\nu n)^b (D_\nu W^\mu n)^c + \mathcal{O}(\varphi) \tag{2.23}$$

We can observe a contradiction between the elementary description of the theory and the physical gauge invariant formulation. In order to prove these predictions, a $SU(3)$ theory has been simulated on the lattice. The results support the analytical relations we depicted in this section [34]. This still leaves open the question on the predictive power of the Standard Model in its spontaneous symmetry breaking interpretation.

2.3. SU(2) gauge theory coupled with a fundamental scalar

The $SU(2)$ gauge theory is special, and it is mostly due to the custodial group. As we have seen in the previous section, by using gauge invariant operators, it is not possible to classify states by the quantum numbers associated with the gauge group. It results then, that due to the Higgs insertion in those operators, the custodial symmetry of the Higgs group still allows for a classification of the states as representations of a symmetry group.

This will then result in a particular case of the general procedure presented in the previous section. The main point is that the custodial group is the same as the original gauge group. We now give more details about this interpretation, since it will be of much interest for the Standard Model, which we will discuss in greater detail in the next section.

We briefly detail the theory and how it is treated in usual perturbation theory. We describe the theory with the Lagrangian (2.1), but with the scalar fields in the fundamental representation of $SU(2)$, so complex vectors with two components. The generators of the group are then $T^a = \sigma^a/2$, where σ indicates the Pauli matrices, with structure constants given by the Levi-Civita symbol ϵ^{abc}. Also in this case in order to have results we need to do the split, but this can be done only in a gauge fixed setting, that assures $\langle\phi\rangle \neq 0$. An example of this is obtained with the 't Hooft gauge condition $\partial^\mu W^a_\mu + igv\zeta\phi_i T^a_{ij} n_j = 0$. After introducing the gauge fixing term (2.9) and ghost term (2.10), we can use the split (2.7) to analyze the mass spectrum.

It's important to discuss the custodial symmetry of the Higgs sector. We first have to analyze the Higgs doublet, by rewriting it as

$$\phi(x) = \begin{pmatrix} \varphi_1(x) + i\varphi_2(x) \\ \varphi_3(x) + i\varphi_4(x) \end{pmatrix} , \tag{2.24}$$

where the fields $\varphi_i(x)$ are all real. Analyzing the Higgs sector alone, consisting only of the kinetic term and the potential, in terms of the four real component of the complex doublet, a global $O(4)$ symmetry is manifest. The $O(4)$ symmetry can be decomposed into $SU(2) \times SU(2)$. When the Higgs field is gauged, then the decomposition can be written as $SU(2)_{gauge} \times SU(2)_{cust}$. After the spontaneous symmetry breaking procedure is applied, the $SU(2)_{cust}$ is still intact for the scalar field. This is due to the pseudoreality of the fundamental representation of the $SU(2)$ group. To make the invariance more explicit, we can write the Higgs field in a matrix form

$$X(x) = \begin{pmatrix} \tilde{\phi}(x) & \phi(x) \end{pmatrix} = \begin{pmatrix} -\phi_1^*(x) & \phi_0(x) \\ \phi_0^*(x) & \phi_1(x) \end{pmatrix} \tag{2.25}$$

The Higgs written in this way can be split as

$$X(x) = v\alpha + \chi(x) \tag{2.26}$$

where α is a $SU(2)$ matrix representing the direction of the vacuum, while χ is the remaining fluctuation field, with $\langle \chi \rangle = 0$. It can be observed how this object transforms under the gauge group on the left $X \to U(x)X$, while it transforms under the custodial group on the right $X \to Xc^\dagger$. It can then be used for constructing composite operators which are gauge invariant, but have an open custodial index.

The mass term for the scalar is obtained by examining the potential after the split, providing then the mass squared $m_h^2 = \lambda v^2$. The mass term of the gauge bosons is again obtained by the expansion of the kinetic term of the scalar field. A mass matrix is again obtained as

$$M^{ab} = \frac{g^2 v^2}{2} n^\dagger T^a T^b n \tag{2.27}$$

Given the properties of the $SU(2)$ group, the mass matrix is always diagonal. In this particular case $T^a T^b$ is proportional to δ^{ab} and $n^\dagger n = 1$. This gives a mass of $m_W = gv/2$ to all three gauge bosons W^a.

2.3.1. Gauge invariant spectrum

The physical spectrum is obtained by the two point functions of the physical (gauge invariant) operators. In this section we discuss the $J^P = 0^+, 1^-$ cases.

We can start by constructing a singlet scalar operator

$$O_{0^+}(x) = \phi^\dagger(x)\phi(x) \tag{2.28}$$

Its expansion works as described in section 2.2. By applying the FMS construction we obtain the same result. It is thus expected to have a single pole at $m_{0^+} = m_h = \sqrt{\lambda} v$. In the $SU(2) \to 1$ only one residual massive state is obtained, and this corresponds to the custodial scalar singlet in the FMS mapping. The results obtained in the $SU(N)$ case are still valid here then.

For the vector channel we construct a gauge invariant object in the following way

$$O^{\bar{a}}_{1^-\mu} = \mathrm{tr}\left(T^{\bar{a}}\frac{X^\dagger}{\sqrt{detX}}D_\mu\frac{X}{\sqrt{detX}}\right). \tag{2.29}$$

It is important to notice how the insertion of the generator and the trace operation is a projection over the direction of the $SU(2)_{cust}$ group. Barred indices denote indices of the global symmetry group. This operator is then called the custodial triplet. It can be mapped directly to the three vector gauge bosons obtained in perturbation theory. We can show this by its FMS expansion

$$O^{a}_{1^-\mu} = -i\frac{gv}{2}W^a_\mu\,\mathrm{tr}\left(T^{\bar{a}}\alpha^\dagger T^a\alpha\right) + \mathcal{O}(\varphi) \tag{2.30}$$

It can then be shown that the 2 point function is then

$$\left\langle O^{\bar{a}}_{1^-\mu}(x)O^{b\dagger}_{1^-\mu}(y)\right\rangle = \frac{g^2v^2}{4}c^{\bar{a}a}c^{\bar{b}b}\left\langle W^a_\mu(x)W^b_\nu(y)\right\rangle + \mathcal{O}(\varphi) \tag{2.31}$$

The constants we introduced are defined as $c^{\bar{a}b} = \mathrm{tr}\left(\alpha^\dagger T^b\alpha T^{\bar{a}}\right)$. So the pole masses are at the same position as the elementary ones, and also in the same multiplicity.

2.3.2. Fermion sector

The method outlined in this section is viable also for the fermion sector of a gauge theory. We will focus here on a case similar to the SU(2) case, without additional electromagnetic interaction, and with one lepton flavor. We will present then a single lepton generation case, described by the Lagrangian

$$\begin{aligned}\mathcal{L} = &-\frac{1}{4}W^a_{\mu\nu}W^{a\,\mu\nu} + \frac{1}{2}\mathrm{tr}\left[(D_\mu X)^\dagger(D^\mu X)\right] - \frac{\lambda}{4}\left(\mathrm{tr}\left(X^\dagger X\right) - v^2\right)^2 + \bar{\psi}^L\mathrm{i}\not{D}\psi^L + \bar{\chi}^R_f\mathrm{i}\not{\partial}\chi^R_f \\ &-\sum_f y_f\left(\bar{\chi}^R_f\left(X^\dagger\psi^L\right)_f + \left(\bar{\psi}^L X\right)_f\chi^R_f\right).\end{aligned} \tag{2.32}$$

This is an extension of the bosonic case, with the addition of two species of Weyl fermions. The first is ψ^L, which transforms under the fundamental representation of $SU(2)$, while χ^R_f consists of two singlets of $SU(2)$, which are Weyl ungauged fermions. A covariant derivative is used to ensure the gauge invariance of the Lagrangian for the ψ^L kinetic term. In the second line the Yukawa terms are present.

The two components of the ψ^L fermion cannot generate a flavor structure, since those are subject to the gauge group, like it happens for the quark, which are representations of the $SU(3)_c$ group, for every single flavor.

Name	Spin	$\mathrm{SU}(2)_{\mathrm{c}}$	$\mathrm{SU}(2)_{\mathrm{Rf}}$	Operator	LO FMS expansion
Higgs	0	0	0	$\mathrm{tr}\, X^\dagger X$	$\mathrm{Tr}(\eta)$
Gauge bosons	1	1	0	$\mathrm{tr}\, \tau^a X^\dagger D_\mu X$	W_μ^a
Left-handed fermions	$\frac{1}{2}$	$\frac{1}{2}$	0	$\Psi^L = X^\dagger \psi^{\mathrm{L}}$	$\psi^{\mathrm{L}} = \begin{pmatrix} \nu^{\mathrm{L}} \\ e^{\mathrm{L}} \end{pmatrix}$
Right-handed fermions	$\frac{1}{2}$	0	$\frac{1}{2}$	χ^R	$\chi^R = \begin{pmatrix} \nu^{\mathrm{R}} \\ e^{\mathrm{R}} \end{pmatrix}$

Table 2.1.: The physical states of a SU(2) Higgs theory with a fermion sector are summarized. The quantum numbers of the states are shown, along with their physical operators and their leading order FMS expansion.

If Yukawa interactions are switched off, three symmetries are present in the Lagrangian. The first is the local $SU(2)_W$. The second is a global symmetry that acts on the χ_f^R, that we call $SU(2)_{Rf}$. The third is the global custodial symmetry $SU(2)_c$. By switching on the Yukawa interactions with degenerate Yukawa couplings, the custodial and the right handed symmetry group get reduced to a single symmetry group that mix them, that we call $SU(2)_{df}$. It act as $\chi_f^R \to d^\dagger \chi_f^R$ on the fermion and as $X \to Xd$ for the Higgs in matrix form.

The masses for the fermion fields are obtained in a gauge with $\langle \phi \rangle \neq 0$, by performing the split (2.7) and substituting it in the Yukawa terms. This operation provides the masses

$$m_f = \frac{y_f v}{\sqrt{2}} . \tag{2.33}$$

But as discussed earlier, operators with open gauge indices cannot provide a reliable description of physical observable particles. We can introduce a gauge invariant operator that has the same quantum numbers as ψ^L, with $\Psi_L = X^\dagger \psi_L$. This one is a singlet under the gauge group, but it is in the fundamental representation of the custodial group.

Then one can perform the FMS expansion

$$\Psi^{\mathrm{L}} = X^\dagger \psi^{\mathrm{L}} = \left(\frac{v}{\sqrt{2}} \mathbb{1} + \eta \right) \psi^{\mathrm{L}} = \frac{v}{\sqrt{2}} \begin{pmatrix} \psi_1^{\mathrm{L}} \\ \psi_2^{\mathrm{L}} \end{pmatrix} + \mathcal{O}(\eta), \tag{2.34}$$

obtaining thus a mapping to the elementary components at the highest order in v.

We analyze then the two point function

$$\left\langle \Psi_{f_1}(x) \bar{\Psi}_{f_2}(y) \right\rangle = \frac{v^2}{2} \left\langle \psi_{f_1}^{\mathrm{L}}(x) \bar{\psi}_{f_2}^{\mathrm{L}}(y) \right\rangle + \mathcal{O}(\eta). \tag{2.35}$$

We obtain again that the structure of the propagator of the bound state operator expands at the highest order to the ordinary one. We thus can identify the physical doublet with the gauge invariant combination (Ψ^L, χ_f^R), with the mass m_f. One then obtains a complete description of a $SU(2)$ gauge theory coupled to the fermions. We summarize the states of the system in the table 2.1. The lattice implementation of this theory will be the focus of chapter 5.

2.4. Standard model interpretation with FMS

In this section we focus on applying the results obtained in the SU(2) Higgs theory to the whole Standard Model. It must first be noted how a rethinking of physical particles in the electroweak sector has to be done. Based on our results, the physical Higgs should be interpreted as composite Higgs-Higgs state, while the three weak gauge bosons are obtained from the custodial triplet object. We observed that there is a mapping of the gauge multiplets to custodial multiplets with the same quantum numbers, due to the special structure of the $SU(2)$ Higgs theory.

But in general, non-singlets of $SU(2)_L$ are used in all sections of the Standard Model, since the left handed fermions of the Standard Model are all gauged under $SU(2)_L$, and transform under the fundamental representation. One of the main points of this work, is that the same rethinking done for the bosonic part of the elecroweak sector is necessary also for all the left handed fermions. We then expect to use operators of the form of Ψ_L for indicating the new physical gauge invariant composite fermion operators, as described in subsection 2.3.2. This has to be done both for the leptons, and the quarks.

Once we acknowledged this, there is still the need of simulating the Higgs sector together with QED. The electromagnetic sector has an enormous relevance in modern physics. The physical states are defined by their electrical charge, since the group $U(1)_{em}$ is intact. But all charged states are not invariant under the gauge group. This is not an issue for an abelian gauge group. In fact gauge invariance in QED can always be obtained by using a photon dressing for the charged particles.

We should also mention the Gribov-Singer ambiguity of these models [47, 48]. We assume that it is going to be qualitatively irrelevant for our problems, even if some issues regarding the creation of a non Abelian local charge can be traced to it [49–51]. We will not discuss this here further. But it should be noted how the ambiguity distinguishes the non abelian case, and makes it necessary to apply the FMS construction, in contrast to the QED case.

Simulations of the SU(2) Higgs theory coupled to the $U(1)$ group have been already done [52–56], but never in the context of testing FMS. In principle, the same mixing between the third weak gauge boson and the hypercharge boson can be achieved in the FMS framework.

The inclusion of the full flavor structure causes no further problem in the FMS treatment. But the scale separations of the whole Standard Model make realistic lattice simulations impossible.

Quantum chromodynamics has an unbroken symmetry, which is $SU(3)_c$. The behaviour of this theory shows what happens in a non abelian gauge theory in the symmetric phase. Only gauge invariant states are present in the physical spectrum, the hadrons, while the elementary components only contribute in amplitudes, but are never asymptotic states. We will noto discuss the added complexities that arise in a gauge invariant formulation of QCD, given that with the interpretation of the left-handed quark as a composite operators, we still expect an expansion to the elementary quark state as the biggest contribution.

An analysis of the consequences of the FMS can also be done for dynamical observables, like decay rates and cross sections. But a systematic evaluation of the FMS effects on dynamic observables is hard to achieve, due to its mostly nonperturbative nature. For the evaluation of cross sections that involve bound states, like what happens in QCD with hadrons, a knowledge of the form factors and the pdfs is required, in order to get reliable Monte Carlo simulations. Nonetheless, a first effort in that direction has been done [57]. A preliminary study on the potential consequences of the substructure of the proton was conducted also with respect to actual datasets from CMS [58].

2.5. Higgs field in the adjoint representation

We illustrate a theory of major interest in this work. When formulating a gauge theory coupled to a scalar field, there has also been considered the possibility of a scalar that transforms in the adjoint representation. The theory can be described by the Lagrangian

$$\mathcal{L} = -\frac{1}{4} A^a_{\mu\nu} A^{a\mu\nu} + \text{tr}\left[(D_\mu \Phi)^\dagger (D^\mu \Phi)\right] - V(\Phi) \,.$$

Here we introduced the Higgs in the adjoint representation Φ. It transforms under a gauge transformation as $\Phi \to U(x)\Phi U^\dagger(x)$. It can be expanded in the generators of the algebra as $\Phi^a t^a$. The covariant derivative acts as $D^\mu \Phi = \partial^\mu \phi + ig[A^\mu, \Phi]$. The potential can then be written as

$$V(\Phi) = -\mu^2 \text{ tr}\left[\Phi\right]^2 + \gamma \,\text{tr}\Big[\Phi^3\Big] + \frac{\overline{\lambda}}{2} \text{ tr}\left[\Phi^2\right]^2 + \tilde{\lambda} \text{ tr}\left[\Phi^4\right] \,. \tag{2.36}$$

We will choose $\gamma = 0$. This will provide a Z_2 custodial symmetry.

The $SU(N)$ case with $N > 2$ leads to many difficulties. The most important one, is that there are multiple breaking patterns in these cases, due to the presence of more than one Cartan operator in the adjoint representation. This has potentially unknown consequences, especially in the gauge invariant formulation. A lattice exploration of a $SU(3)$ theory with an adjoint scalar is currently under investigation.

We focus on the $SU(2)$ case. We can then set $\bar{\lambda}$ to zero without loss of generality, since, the quantity $\mathrm{tr}\left[\Phi^2\right]^2$ is equivalent to $\mathrm{tr}\left[\Phi^4\right]$, since $\mathrm{tr}\left[\Phi^2\right]$ is the only non trivial Caisimir. Also, the Z_2 symmetry is not relevant in this case, due to the pseudo reality property.

We are interested in the realization of the BEH effect in this theory. We won't focus on the details of the gauge fixing, since they are analogous to the ones described in the fundamental case, but on the physical particles and their masses.

The only breaking pattern possible in the group is $SU(2) \to U(1)$. Given that we are in a fixed gauge with a non vanishing vacuum expectation value, we can then perform a split

$$\Phi(x) = \langle \Phi \rangle + \sigma(x) = w\Phi_0 + \sigma(x) \tag{2.37}$$

The field after the split can be reinserted into the Lagrangian. This leads to a mass matrix for the gauge bosons analogously to the fundamental case

$$(M_A^2)^{ab} = -2(gw)^2\, \mathrm{tr}\left([T^a, \Phi_0][T^b, \Phi_0] \right) \ . \tag{2.38}$$

We have then a massless gauge boson in the direction of the vacuum, and two massive gauge boson in the broken coset of $SU(2)$ with mass $M_W = gw$. For the scalar a mass term is obtained with mass $m_H = \sqrt{\lambda} w$.

2.5.1. Gauge invariant spectrum

The observations made for the fundamental case regarding the impossibility of spontaneous breaking of a local symmetry are valid also within other representations. Thus the necessity for a gauge invariant formulation of observables in the theory with an adjoint scalar.

We can construct a gauge invariant scalar operator as

$$O_{0^+}(x) = \mathrm{tr}\left[\Phi^2\right](x) \ . \tag{2.39}$$

We use the approach dictated by the FMS mechanism to obtain predictions for the spectrum. The expansion of the operator yields

$$O_{0^+}(x) = \frac{w^2}{2} + w\, H(x) + \mathcal{O}(w^0) \ , \tag{2.40}$$

where we obtained the Higgs field $H(x) = 2\,\mathrm{tr}(\Phi_0 \sigma(x))$. At highest order in the expansion of the correlator, the leading term with nontrivial dynamics is the elementary

Higgs field propagator. From this result we assess that the expected pole mass for the scalar operator is m_H.

The situation is less trivial in the vector channel. A gauge invariant operator can be written as

$$O^{\mu}_{1^-} = \frac{\partial_\nu}{\partial^2} \operatorname{tr}\left[\Phi F^{\mu\nu}\right] . \tag{2.41}$$

Its FMS expansion reads

$$O^{\mu}_{1^-} = -w \operatorname{tr}\left[\Phi_0 \overline{A}^{\mu}_{\perp}\right](x) + \mathcal{O}(w^0) , \tag{2.42}$$

where

$$\overline{A}^{\mu}_{\perp} = A^{\mu}_{\perp} + g\frac{\partial_\nu}{\partial^2}[A^\mu, A^\nu] , \tag{2.43}$$

the field-strength tensor with one index transversely contracted and

$$A^{\mu}_{\perp} = \left(\delta^{\mu}_{\nu} - \frac{\partial^\mu \partial_\nu}{\partial^2}\right) A^\nu ,$$

the transverse part of the gauge field. We can perform another expansion in the coupling constants, obtaining at tree level

$$O^{\mu}_{1^-} = -w \operatorname{tr}\left[\Phi_0 A^{\mu}_{\perp}\right](x) + \mathcal{O}(w^0, g^0, \lambda^0) . \tag{2.44}$$

It is evident how this expansion provides then, at leading order, a projection to the unbroken $U(1)$ group. The two point function would then provide a massless pole for this state. One can then expect a massless vector composite boson in the spectrum. This possibility can have important implications in GUT model building. The state constructed in this way can play the role of a photon in such scenarios. A non perturbative validation of this hypothesis is explored in chapter 4.

In an expansion of the two point function of (2.41), one can analyze the subleading term in the coupling constant, with the biggest power of the vev. One obtains then a non vanishing term multiplied by $g^2 w^2$, which has the form

$$C^{\mu\rho}(x,y) = \frac{1}{4}\frac{\partial_\nu}{\partial^2}\frac{\partial_\sigma}{\partial^2}\left[\left\langle A^{\mu}_{1}(x)A^{\rho}_{1}(y)\right\rangle \left\langle A^{\nu}_{2}(x)A^{\sigma}_{2}(y)\right\rangle - \left\langle A^{\mu}_{1}(x)A^{\sigma}_{1}(y)\right\rangle \left\langle A^{\nu}_{2}(x)A^{\rho}_{2}(y)\right\rangle + (1 \leftrightarrow 2)\right] . \tag{2.45}$$

We set $\Phi_0 = T_3$ for this calculation. We can interpret this term in a composite picture, with the gauge bosons as elementary constituents. A mass of twice the mass of the elementary gauge boson is then predicted in this channel, using a gauge invariant operator. It must be taken into account how the derivative can alter the shape of the propagator, and how the constituent picture is only an approximation of the full-fledged computation of the correlators. In any case, a non perturbative estimation, via lattice methods for instance, could help to validate this result.

2.6. BSM theories with a BEH effect

All the procedures we detailed in this chapter can be applied to various candidate BSM theories which have an extended Higgs sector. For those theories, spontaneous symmetry breaking is required to obtain the gauge groups of the Standard Model at low energies. But it should be kept in mind that the SSB procedure has many theoretical shortcomings, particularly in respect to the gauge variance of its fundamental constituents, as discussed in this chapter. We want to discuss potential implications of the FMS mechanism for some classes of BSM theories.

The adjoint Higgs case has particular relevance for its fundamental contribution in the Georgi-Glashow model of the SU(5) great unification theory [23]. Using this representation of the Higgs particle leads to the desired breaking pattern, which then results in principle in the Standard Model spectrum. For the $SU(5)$ case, coupled with two Higgs in the needed representations, it allow to obtain as little group the gauge group of the Standard Model $SU(3) \times SU(2) \times U(1)$.

The perturbative treatment of such a theory is obtained by realizing the spontaneous symmetry breaking with two scalar fields, one in the adjoint representation Σ, and the other in the fundamental representation ϕ. The custodial group is then $U(1)$, and if the potential is symmetric under $\Sigma \to -\Sigma$, then the custodial group is enhanced to $Z_2 \times U(1)$. The adjoint scalar allows the breaking to the Standard Model group, while the fundamental scalar breaks to $SU(3)_c \times U(1)_{ew}$.

In addition to the Standard Model particles, many other states are predicted, but at a mass scale of the order w, which is the vacuum expectation value of the adjoint scalar, and it is set to be far bigger than v, which is of the order of the electroweak scale. It needs a certain amount of fine tuning in order to set the masses of the unobserved additional states at the GUT scale.

In the FMS treatment, the spectrum is different from the elementary formulation. In the scalar channel, two fields with mass of order of the electroweak scale are expected, for instance, if a Z_2 symmetry of the adjoint Higgs is not enforced.

For the vector channel the situation is more involved. In the Cartan direction it is possible to obtain massless vectors. But the number of those it would be actually be different from the one required in the phenomenology. The main issue, is that when analyzing the FMS expansion in a fixed gauge, the correlators on the right hand side are invariant under the symmetry of the little group. If the little group comprises a $U(1)$ symmetry, then the state will not be charged under the symmetry. This construction would not allow the formation of charged massive vector bosons, like $W^{\pm}$. This prediction has still to be tested on the lattice fully, and the results from chapter 4 are not conclusive on the matter. Only a nonperturbative thorough investigation can give a strong hint concerning this matter.

It would be of outstanding importance to realize a nonperturbative description of a massless vector boson, obtained with the BEH effect on a larger symmetry group.

In this regard, the results of chapter 4 are fundamental for the exploration of BSM theories from a first principles realization.

Another possibility is the two Higgs doublet model ($2HDM$) [59]. This has been explored in the context of the FMS mechanism [60], resulting in a still viable solution, with no modification with respect to the spectrum of the elementary states.

For technicolor theories [61], in which the Higgs is replaced by a bound state of fermions which are representations of a technicolor group, the FMS interpretation is more subtle.

In the full technicolor theory, the electroweak sector is replaced by a set of fermions with two gauge interactions, and one is the usual weak one. In the analysis of the gauge invariant spectrum, one would have to obtain as the lightest state a vector triplet, and a then a slightly heavier scalar, to resemble the phenomenological situation. At the current moment, the usual spectrum of theories with only fermions and gauge interactions, have a pseudoscalar or a scalar as lightest state [61, 62]. As we discussed a physical triplet can only be obtained if there is a global symmetry that allows triplet representations.

For the minimal walking technicolor [61], where the technicolor sector consists of two colors of two flavors of adjoint quarks, one can build a vector operator as $\mathrm{tr}\left(t^a_{ij}\psi_i D_\mu \psi_j\right)$. We can insert one of the two gauge field in the covariant derivative, to construct the operator. Both gauge fields should exhibit a pole at the expected elementary gauge boson mass, with the further state being a scalar. In general it is expected that the two operators mix. The scalar state can either be a gauge-boson-ball, or a usual meson operator. The other states are expected at much higher energies. In any case, also here a nonperturbative exploration of the theory is needed.

There are other possibilities for beyond Standard Model theories that can be analyzed in the context of the FMS mechanism, but have never been analyzed in detail, like supersymmetry.

Lastly, the FMS should be intended as a general approach for theories with local symmetries, hence it has implications also for quantum theories of gravity. In this case, the local symmetry is the invariance under diffeomorphism. A preliminary effort in this direction has been done [63].

3. Lattice Field Theory

In this chapter we will detail the lattice techniques employed in the main part of the investigation. It should not be intended as an introduction to the topic, but more as a discussion over the topics which are relevant for our purposes.

Lattice field theory is a discretization of the usual quantum field theory, which can also be called continuum field theory in this context. The infinite degree of freedoms in the continuum spacetime are mapped to a finite number of degrees of freedoms on a lattice. The lattice introduces a regularization naturally through the lattice spacing. It is then our method of choice for solving the nonperturbative questions of chapters 4 and 5.

There are two main problems in our investigations that can not be straightforwardly solved when implemented on the lattice. The first is related to the introduction of a massless field. In principle, a massless state can be realized only in a infinite volume. The other problem is related to the lattice implementation of fermions. Parity violation cannot be implemented on the lattice, as stated in the Nielsen-Ninomiya theorem [64]. Hence, it is impossible to recreate the standard model fermionic setup with electroweak symmetry on the lattice.

In the following we detail the procedure to describe a bosonic gauge theory on the lattice, and how to extract masses of its constituent fields. Then the Wilson-Dirac formulation of fermionic gauge theories is discussed, followed by some details regarding the quenched approximation. This section will serve as a general background for the main investigations depicted later. The details on the setups and the techniques shown here follow closely [62, 65, 66].

3.1. Lattice scalar gauge theory

We want to discretize the Lagrangian for the $SU(N)$ gauge theory indicated in (2.1). We will focus on the $N = 2$ case. It will be the case of major interest, especially for chapter 5.

Scalar field theory is implemented almost straightforwardly on the lattice, even if the presence of gauge fields requires more attention. The main difference, is that it is necessary to change the degrees of freedom, using the links $U_\mu(x)$ to describe them. A discretized action for gauge theories coupled with a scalar in the fundamental representation is realized as

$$S = a^4 \sum_{x\in\Lambda} \left[-\frac{\beta}{2} \sum_{\mu<\nu} Re\,\mathrm{Tr}\big[U_{\mu\nu}(x)\big] + \phi^\dagger(x)\phi(x) \right. \tag{3.1}$$
$$\left. +\bar{\lambda}(\phi^\dagger(x)\phi(x) - 1)^2 - \kappa \sum_{\mu=\pm1}^{\pm4} \phi^\dagger(x) U_\mu(x)\phi(x+\hat{\mu}) \right] .$$

There are many elements that have been introduced in this formula which should be discussed. First, it must be noted how the action is realized as a finite sum of elements indicated by x, and comprised in the set $\Lambda = \{x_i = 0, 1, \ldots, L-1 | i = 1, 2, 3, 4\}$, where the integer L is the length of the lattice. The set Λ is then the set of all the points of a cubic lattice. In front of the sum with the dynamical fields there is the quantity a, which is the lattice spacing. In lattice field theory, the praxis is to make all dimensioned variables dimensionless, by extracting factors of the lattice spacing. For instance $\phi_{lat} = a\phi$, since the spacing has the dimension of the inverse of energy. In this chapter we will not use a subscript to indicate the lattice fields, but it should be accounted that the lattice fields are dimensionless.

Given these conventions, we describe the elements introduced in the Lagrangian. The first term is known as the Wilson action, which is constructed from the plaquette variable $U_{\mu\nu}(x)$. The plaquette is obtained from the link variables $U_\mu(x)$ as

$$U_{\mu\nu}(x) = U_\mu(x) U_\nu(x+\hat{\mu}) U_\mu(x+\hat{\nu})^\dagger U_\nu(x)^\dagger . \tag{3.2}$$

It can be shown that the plaquette is a discretization of the field strength tensor by taking the naive continuum limit $a \to 0$. The link variables are related to the continuum gauge field by $U_\mu(x) = \exp\big(iaA_\mu(x)^a T^a\big)$, where T^a are the generators of $SU(2)$. So, it can be observed that, while the continuum gauge fields are elements of the algebra $su(2)$, the links are elements of the gauge group $SU(2)$. The gauge transformations for the scalar field and the link are

$$\phi(x) \to g(x)\phi(x) \;\; ; \;\; U_\mu(x) \to g(x) U_\mu(x) g(x)^\dagger . \tag{3.3}$$

Given their construction, one can also verify the relation $U_{-\mu}(x) = U_\mu(x-\hat{\mu})^\dagger$. The scalar field and the gauge links obey periodic boundary conditions

$$\phi(x+\hat{\mu}L) = \phi(x) \;\; ; \;\; U_\nu(x+\hat{\mu}L) = U_\nu(x) \;\; , \;\; \forall x, \mu, \nu . \tag{3.4}$$

The three parameters in the action (3.1) are β, which is the inverse gauge coupling, $\bar{\lambda}$, which is the self interaction coupling parameter of the Higgs, and κ which is known as the hopping parameter, and it can be related to the inverse of the bare mass. We can write the relation to the continuum parameters as

$$\beta = \frac{4}{g^2} \;\; , \;\; a^2 m_0^2 = \frac{1-2\bar{\lambda}}{\kappa} - 8 \;\; , \;\; \lambda = \frac{\bar{\lambda}}{\kappa^2} . \tag{3.5}$$

These relations has been obtained by rescaling the scalar field with a factor $1/\sqrt{\kappa}$ and the gauge field by $1/\sqrt{\beta}$. This makes the the lattice action dimensionless.

We have then the following partition function

$$Z = \int \mathcal{D}[U,\phi] e^{-S[U,\phi]}, \tag{3.6}$$

where we introduced the following measure

$$\mathcal{D}[U,\phi] = \left(\prod_x \prod_{\mu=1}^{4} dU_\mu(x) \right) \left(\prod_x d\phi(x) \right) . \tag{3.7}$$

It is the product of a Haar measure, which is used for the integration over a compact continuous group [62, 65], and the measure over the scalar field, which is an integration over $\mathbb{C}^3$ at every point. These measures are both gauge invariant, thus the theory is fully gauge invariant.

The evaluation of this partition function is the main aim of a lattice investigation of quantum field theory. In order to perform this task, Monte Carlo techniques are used.

3.2. Generation of configurations

We can obtain information about the physics of a field theory by evaluating the vacuum expectation value of a gauge-invariant observable. This can be calculated with the formula

$$\langle O \rangle = \frac{1}{Z} \int \mathcal{D}[U,\phi] e^{-S[U,\phi]} O[U,\phi] \, . \tag{3.8}$$

This result can be achieved by Monte Carlo techniques, as anticipated. The idea is to approximate the integral over the whole space of configurations, to an average over a subset of N sample configurations $U_{(n)}, \phi_{(n)}$ of maximum probability, i.e., the configurations that minimize the action. When doing this, we note that the configurations in an Euclidean field theory are distributed according to the probability distribution density

$$dP(U,\phi) = \frac{1}{Z} e^{-S[U,\phi]} \mathcal{D}[U,\phi] \, , \tag{3.9}$$

which is also called Gibbs density.

In principle, the value of the observable is then obtained in the limit of the sample size going to infinity

$$\langle O \rangle = \lim_{N\to\infty} \sum_{n=1}^{N} O[U_{(n)}, \phi_{(n)}] \, . \tag{3.10}$$

But in actual computations it is desirable to have a finite sample that approximates the observable value. To have a reliable estimation, configurations with the highest probability are chosen.

A fundamental task in the simulations of lattice field theory is then to obtain a reliable algorithm that generates configurations in the maximum probability regions, so that the expected values of the observables can be calculated. Markov-chain Monte Carlo methods are used for this purpose. The idea of Markov-chain is to build a stochastic sequence that generates a new element with a probability distribution that depends only on the last element. This amounts to finding the transition probability $T(U', \phi' | U, \phi)$ which governs the generation of the new configurations U', ϕ' given the actual configuration U, ϕ. This transition probability has also to fulfill the detailed balance condition

$$T(U'|\phi'|U, \phi)P(U, \phi) = T(U, \phi|U'\phi')P(U', \phi') \,. \tag{3.11}$$

One of the most used algorithms that satisfy this condition is the metropolis one [67], which is characterized by the transition probability

$$T(U', \phi'|U, \phi) = \min[1, \exp(-\Delta S)] \,. \tag{3.12}$$

Here we used $\Delta S = S[U', \phi'] - S[U, \phi]$. This algorithm is assured to reach the equilibrium in the region of maximum probability, owing to the fixed point theorem [66].

For the action (3.1) the variation in the action for the proposed update to U' is

$$\begin{aligned} \Delta S_U = S[U', \phi] - S[U, \phi] = &- \frac{\beta}{2} \operatorname{Re}\operatorname{tr} \left[(U'_\mu(x) - U_\mu(x)) \sum_{\nu \neq \mu} C_{\mu\nu}(x) \right] \\ &- 2\kappa \operatorname{Re} \left[\phi^\dagger(x)(U'_\mu(x) - U_\mu(x))\phi(x+\hat{\mu}) \right] \,. \end{aligned} \tag{3.13}$$

Here we used the staple quantity, defined as

$$C_{\mu\nu}(x) = U_\nu(x+\hat{\mu})U_\mu(x+\hat{\nu})^\dagger U_\mu(x) + U_\nu(x+\hat{\mu}-\hat{\nu})^\dagger U_\mu(x-\hat{\nu})^\dagger U_\nu(x-\hat{\nu}) \tag{3.14}$$

For the update of the scalar field we have

$$\begin{aligned} \Delta S_\phi = &S[U, \phi'] - S[U, \phi] = \lambda \left[(\phi'(x)^\dagger \phi'(x) - 1)^2 - (\phi(x)^\dagger \phi(x) - 1)^2 \right] \\ &+ \phi'(x)^\dagger \phi'(x) - \phi(x)^\dagger \phi(x) - 2\kappa \sum_{\pm 1}^{\pm 4} \operatorname{Re} \left[(\phi'(x) - \phi(x))^\dagger U_\mu(x) \phi(x+\hat{\mu}) \right] \,. \end{aligned} \tag{3.15}$$

Multi-hit metropolis can then be used, to further update the link, with respect to the scalar field. This results in doing more update attempt on the links, and doing a single one for the scalar fields.

The proposed fields are obtained using random number generators. The widths of the proposals can be tuned by doing a systematic test of the acceptance rate, or by using an adaptive algorithm. Once it is possible to generate configurations that are in the maximum probability region, one says that the configurations are thermalized. For the actual evaluation of the observables, one also wants that the configurations are not correlated. To do so, some decorrelation steps are introduced in the generation of the configurations, to have statistically independent values of the observables.

3.2.1. Gauge fixing

One of the major goals of this work is to prove whether the FMS mechanism provides a correct mapping to the on-shell results on the gauge invariant operators, by using the gauge variant elementary correlators in a fixed gauge. It is then necessary to apply a gauge fixing procedure to the configurations generated with the methods described in the previous section. We discuss here the SU(2) theory with both the cases of the Higgs in the fundamental and in the adjoint representation.

We want to impose locally the Landau gauge condition $\partial_\mu A^\mu = 0$. On the lattice, this can be achieved by minimizing the functional

$$F_g[U] = -a^2 \sum_x \mathrm{Re}\,\mathrm{tr}\left[g(x)K_g[U](x)\right], \tag{3.16}$$

where we defined

$$K_g[U](x) = \sum_{\mu=1}^{4} \left(U_\mu(x) g(x+\hat{\mu})^\dagger + U(x-\hat{\mu})^\dagger g(x-\hat{\mu})^\dagger \right). \tag{3.17}$$

for every $U_\mu(x)$ using a gauge transformation $g(x)$. One has then to find the gauge transformation to be applied to the link in order to obtain the minimum of the functional. In principle, 1 it is possible to have more than one local minimum, due to the Gribov-Singer ambiguity. Hence, one tries to look for the global minimum. This procedure is also called *minimal Landau gauge* [68–70].

There are several algorhithms that allows obtaining the minimum of the functional [71]. In order to have an idea of how they work, we introduce, for the $SU(2)$ group, the quantity

$$w_g[K](x) = \frac{g(x)K_g[U]}{\sqrt{\det\left[g(x)K_g[U]\right]}}. \tag{3.18}$$

This one gives a local solution to the optimization problem. The Los Alamos algorithm consists in applying this quantity as a gauge transformation. It can also be shown that two consecutive applications of the quantity (3.18) give zero variation to the functional.

The method used for the configurations in this work is called stochastic overrelaxation. It works by doing the update

$$g(x) \to g^{(new)} = \begin{cases} [w_g[K](x)]^2 \quad g(x), & \text{with probability } p \\ w_g[K](x) \quad g(x), & \text{with probability } 1-p \end{cases} \tag{3.19}$$

where $p \in (0,1)$. This number has to be tuned in order to achieve the minimum in the smallest amount of iterations. This has been done with an adaptive algorithm.

In order to achieve a 't Hooft-Landau gauge condition, it is also necessary to fix the global direction of the scalar field. In the SU(2) case one can find a SU(2) transformation to apply to the vector in order to achieve this goal.

For the $SU(2)$ theory coupled to an adjoint scalar, one can use the $O(3)$ writing of the adjoint field. Then one has to apply two $O(3)$ rotations to the adjoint field, the first to put the first component to zero, and the last one points into the third direction as desired. In both cases one has to calculate the spatial average for every configuration

$$\bar{\phi} = \frac{1}{V} \sum_x \phi(x)\,, \tag{3.20}$$

then obtain the transformations needed, and apply them to the scalar and the gauge field. In this way we realize the so-called minimal 't Hooft Landau gauge.

3.3. Spectroscopy

The masses of the physical gauge invariant states can be extracted from two point functions. It is necessary to construct lattice quantities that reduce to the continuum operators, called *interpolators*. Those are the lattice realizations of the continuum operators that have an overlap with the physical states.

We can observe how the energy levels are obtained from the two point function of a generic interpolator $\mathcal{O}$ by expanding the correlator over a basis of energy eigenstates

$$< O(t)O^\dagger(t') >= \sum_n \langle 0|O|n\rangle \, \langle n|O^\dagger|0\rangle \, e^{-E_n(t-t')} = Ae^{-E_0(t-t')}(1+\mathcal{O}(e^{-\Delta E(t-t')}))\,. \tag{3.21}$$

Here E_0 indicates the energy of the ground state, and ΔE is the difference in energy between the ground state and the first excited state. We assumed here that there is a non zero overlap with the ground state for the operator, i. e. $\langle 0|O|n=0\rangle \neq 0$.

We are interested in the case where we can define a spatial momentum $\mathbf{p}$, so that we can Fourier transform the interpolator

$$\tilde{O}(\mathbf{p},t) = \frac{1}{\sqrt{L^3}} \sum_{\mathbf{x}} O(\mathbf{x},t) e^{-ia\mathbf{x}\cdot\mathbf{p}}, \tag{3.22}$$

where a sum over the spatial components $\mathbf{x} = (x_1, x_2, x_3)$ is done, while the spatial momenta $\mathbf{p}$ form a discrete set defined by the boundary condition $f(n + \hat{\mu}N) = f(n)$. The set can be written as

$$\tilde{\Lambda} = \left\{ p = (p_1, p_2, p_3, p_4) \mid p_\mu = \frac{2\pi}{aL} k_\mu \ , \ k_\mu = -\frac{L}{2} + 1, \ldots, \frac{L}{2} \right\} . \tag{3.23}$$

We then define at every time slice t a set of operators with definite spatial momentum $\mathbf{p}$ through the spatial Fourier transform. One can analyze the correlator of the operator in the momentum space using these operators

$$\begin{aligned} \left\langle \tilde{O}(\mathbf{p},t)\tilde{O}^\dagger(\mathbf{q},t') \right\rangle &= \frac{1}{L^3} \delta^{(3)}(\mathbf{p}-\mathbf{q}) \sum_{\mathbf{x},\mathbf{y}} e^{-ia(\mathbf{x}-\mathbf{y})\mathbf{p}} \left\langle O(\mathbf{x},t) O^\dagger(\mathbf{y},t') \right\rangle \\ &= A e^{-a(t-t')E(\mathbf{p})} \left(1 + \mathcal{O}(e^{-(t-t')a\Delta E}) \right) \delta^{(3)}(\mathbf{p}-\mathbf{q}) \, . \end{aligned} \tag{3.24}$$

The momentum-space delta is obtained due to the translational invariance. We have in the exponential the relativistic dispersion relation $E(\mathbf{p}) = \sqrt{m^2 + \mathbf{p}^2}$, with the physical mass m. It follows that $E(\mathbf{0}) = m$. Given this result, the ground state mass can be extracted via zero momentum projection by

$$\left\langle \tilde{O}(\mathbf{0},t)\tilde{O}^\dagger(\mathbf{0},t') \right\rangle = \frac{1}{L^3} \sum_{\mathbf{x},\mathbf{y}} \left\langle O(\mathbf{x},t) O^\dagger(\mathbf{y},t') \right\rangle = A' e^{-a(t-t')m} (1 + \mathcal{O}(e^{-(t-t')a\Delta E})) \, . \tag{3.25}$$

In doing this operation, we have assumed that the operator $\mathcal{O}$ has an overlap with the ground state, which has mass m. In general this can not be the case.

We define the zero momentum projected operator as

$$O(t) = \frac{1}{\sqrt{L^3}} \sum_{\mathbf{x}} O(\mathbf{x},t), \tag{3.26}$$

then, we define the time slice averaged correlation function as

$$C(t) = \frac{1}{L_t} \sum_{t'=0}^{L_t-1} \left\langle O(t') O^\dagger(t+t') \right\rangle_c \tag{3.27}$$

$$= \left\langle (O(t) - \langle O(t') \rangle)(O^\dagger(t+t') - O^\dagger(t+t')) \right\rangle , \tag{3.28}$$

where we used the connected correlation function, where the vacuum contributions $\langle O(t) \rangle$ are removed. This is usually done for operators with the quantum numbers of the vacuum, hence scalar operators. In this case, the vacuum contribution can be relevant and add statistical noise.

In order to obtain a better overlap with the ground state, but also to analyze the excited states of the system, it is preferable to use a set of interpolators that share the same quantum numbers, and consider their cross correlation matrix

$$C_{ij}(t) = \frac{1}{L_t} \sum_{t'=0}^{L_t - 1} \langle O_i(t) O_j(t + t') \rangle \ . \tag{3.29}$$

It is then possible to show that eigenvalues $\lambda_k(t)$ of the cross correlation matrix, which are also known as the principal correlators, have the biggest overlap with the physical states [72–74]

$$\lambda_k(t) \propto e^{-1tE_k} \left(1 + \mathcal{O}(e^{-at\Delta E_k})\right) \ , \tag{3.30}$$

where ΔE_k is the distance between the k-th energy level and the next energy level. This procedure is called *variational analysis*. It is now evident how this method can in principle disentangle the different energy levels, given that the interpolator basis chosen has enough overlap with them. It can also be used a generalized eigenvalue problem. In our case it is used the normalization given by the correlation matrix at the zero time slice

$$C(t)\mathbf{v} = \lambda(t) C(0) \mathbf{v} \, . \tag{3.31}$$

We expect that the eigenvalues (3.30) have the same exponential behavior, but with smaller amplitudes.

We can extract the energies from the principal correlators with the so called effective energies, defined as

$$aE_k(t + \frac{1}{2}) = \ln \frac{\lambda_k(t)}{\lambda_k(t+1)} \, . \tag{3.32}$$

Given the periodic boundary conditions of our lattice setting, the physical propagation in t starting from time 0, and the one in $L - t$ in the opposite direction, is the same. Thus, the exponential behavior is expected in the first half of the lattice $t = 0, \dots, L_t/2 - 1$. In the other half, we expect $\lambda_k \propto e^{-} E_k(L_t - t)$. The sum of the two contributions gives then a cosh ansatz for the correlators. One must also take into account the contribution from high energy states, which can then be parametrized as *cosh* addition. One of the fit functions that will be used the most in this work is the sum of two cosh functions as

$$\lambda_k(t) = A_k^{(1)} \cosh\left(aE_k^{(1)}(t - L/2)\right) + A_k^{(2)} \cosh\left(aE_k^{(2)}(t - L/2)\right) \ . \tag{3.33}$$

We have then the hypothesis of at least one excited states appreciable, for every principal correlator, which can also be only a lattice artifact. The masses will then be extracted from these fit assumptions, given that the operators have zero momentum.

3.4. Wilson-Dirac fermions

The implementation of fermions on the lattice is not straightforward due to the fermion doubling problem. The *Wilson-Dirac implementation* solves this problem by adding another operator which does not allow chiral symmetry.

The naive implementation of fermions on the lattice can be obtained by using the following Lagrangian

$$\mathcal{L}_F[\psi,\bar{\psi},U] = \bar{\psi}(x)\left(\sum_{\mu=1}^{4}\gamma_\mu \frac{U_\mu(x)\psi(x+\hat{\mu}) - U_{-\mu}\psi(n-\hat{\mu})}{2a} + m\psi(x)\right) . \tag{3.34}$$

This one is a straighforward discretization of the Dirac operator coupled to a gauge field. Since it is a bilinear in $\bar{\psi}$ and ψ, we can rewrite it in the form

$$S_F[\psi,\bar{\psi},U] = a^4 \sum_{x,y\in\Lambda}\sum_{a,b,\alpha,\beta} \bar{\psi}(x)_{\alpha,a} D(x|y)_{\alpha\beta,ab}\psi(y)_{\beta,b} \tag{3.35}$$

where we then introduced the naive discretized Dirac operator as

$$D(x|y)_{\alpha\beta,ab} = \sum_{\mu=1}^{4}(\gamma_\mu)_{\alpha\beta}\frac{U_\mu(x)_{ab}\delta_{x+\hat{\mu},y} - U_{-\mu}(x)_{ab}\delta_{x-\hat{\mu},y}}{2a} + m\delta_{\alpha\beta}\delta_{ab}\delta_{x,y} . \tag{3.36}$$

We can write its Fourier transform, with trival gauge fields $U_\mu(x) = \mathbb{1}$ as

$$\tilde{D}(p|q) = \delta(p-q)\tilde{D}(p) \tag{3.37}$$

$$\tilde{D}(p) = m\mathbb{1} + \frac{i}{a}\sum_{\mu=1}^{4}\gamma_\mu \sin(p_\mu a) . \tag{3.38}$$

Analyzing the inverted propagator, with zero mass, gives a set of unphysical poles, where $\sin(p_m ua) = 0$, at the positions

$$p = (\pi/a, 0, 0, 0) \ , \ (0, \pi/a, 0, 0) \ , \ \dots, (\pi/a, \pi/a, \pi/a, \pi/a) . \tag{3.39}$$

These unwanted poles are called doublers.

Wilson fermions get rid of them by the addition of an extra term. In momentum space the Wilson-Dirac free operator reads

$$\tilde{D}(p) = m\mathbb{1} + \frac{i}{a}\sum_{\mu=1}^{4}\gamma_\mu \sin(p_\mu a) + \mathbb{1}\frac{1}{a}\sum_{\mu=1}^{4}(1-\cos(p_\mu a)) . \tag{3.40}$$

The extra term, called also *Wilson term* vanishes for components with $p_\mu = 0$, while for every component with π/a it provides an extra contribution $2/a$. This results then in a mass term for the doublers, with mass $m + 2l/a$, where l is the number of components equal to π/a. It appears then that in the continuum limit $a \to 0$ the doublers become heavy and decouple. Thus only the physical pole in $\tilde{D}(p)^{-1}$ remains.

In position space, one obtains the Wilson term by inverse Fourier transform, so that we can write the full Wilson-Dirac operator

$$D(x|y)_{\alpha\beta,ab} = \left(m + \frac{4}{a}\right)\delta_{\alpha\beta}\delta_{ab}\delta_{x,y} - \frac{1}{2a}\sum_{\mu=\pm1}^{\pm4}(\mathbb{1} - \gamma_\mu)_{\alpha\beta}U_\mu(x)_{ab}\delta_{x+\hat{\mu},y}\,, \tag{3.41}$$

where we have defined $\gamma_{-\mu} = -\gamma_\mu$.

3.5. Quenched approximation

In general, given that we have an observable A which is a product of operators, we estimate it with

$$\langle A\rangle = \langle\langle A\rangle_F\rangle_G = \frac{1}{Z}\int \mathcal{D}[U]e^{-S_G[U]}\mathcal{D}[\psi,\bar{\psi}]e^{-S_F[\psi,\bar{\psi},U]}A[\psi,\bar{\psi},U]\,. \tag{3.42}$$

Given then an observable of the form

$$O_\Gamma = \bar{\psi}\Gamma\psi\,, \tag{3.43}$$

where Γ is a combination of gamma matrices, we can write its correlator as

$$\langle O_\Gamma(x)O_\Gamma(y)\rangle = -\frac{1}{Z}\int \mathcal{D}[U]e^{-S_G[U]}\det[D]\,\mathrm{tr}\Big[\Gamma D^{-1}(x|y)\Big]\,. \tag{3.44}$$

The Grassmann integration has been performed to obtain the determinant. In principle one can then do a Monte Carlo simulation with a probability density proportional to $\exp(-S_G[U])\det[D]$ to evaluate this quantity.

But the inclusion of the full fermion dynamics via the determinant is very computationally costly. In the QCD context, in the context of the first applications of lattice simulations with Monte Carlo methods, the *quenched approximation* was used to address the computational hardship.

The fermion determinant describes mainly the fermionic vacuum, hence processes where virtual pairs of quarks and antiquarks are involved. Then, putting the fermion determinant to unity is equivalent to neglecting the effects given by interactions with sea quarks. Also, one of the terms in the determinant expansion is a sum over plaquettes, hence its neglection would only result in a redefinition of the bare coupling.

The quenched approximation consists in the omission of the fermion determinant in the calculation of the observables. One can then write the correlator as

$$\langle O_\Gamma(x) O_\Gamma(y)\rangle_{\text{quenched}} = -\frac{1}{Z}\int \mathcal{D}[U] e^{-S_G[U]}\, \mathrm{tr}\Big[\Gamma D^{-1}(x|y)\Big]\,. \tag{3.45}$$

One can compute the configurations using Markov chain Monte Carlo, and evaluate then the quark propagator on those configurations, by inverting the Dirac operator. This procedure has been performed for spectroscopy of bound states, demonstrating a good predictive power.

3.6. Calculation of the propagator

The inversion of the Dirac operator can be done algorithmically. In this section we detail the idea behind a generic inversion algorithm, and then we provide a more detailed description of the one that has been employed for our purposes.

We start by detailing the fermion sources we used. Given the size of the Dirac operator, its calculation and storage would be wasteful. Instead we consider the propagator from a single site y_0, with fixed Dirac index α_0 and fixed gauge index a_0, to any other site of the lattice. This is only one column of the inverse Dirac operator

$$D^{-1}(x|y_0)_{\beta\alpha_0,ba_0} = \sum_{y,\alpha,a} D^{-1}(x|y)_{\beta\alpha,ba} S_0^{y_0,\alpha_0,a_0}(y)_{\alpha,a}\,. \tag{3.46}$$

Here we have the so called point sources

$$S_0^{y_0,\alpha_0,a_0}(y)_{\alpha,a} = \delta(y-y_0)\delta_{\alpha\alpha_0}\delta_{aa_0}\,. \tag{3.47}$$

The expression has still to be evaluated for the product of the Dirac indices and the dimension of the gauge group representation.

One has then to solve the equation $DG = S$, with G the unknown propagator vector. In order to invert the operators equation, given the source, one can rewrite D as a sum of a constant part and a nontrivial term $D = \mathbb{1} - Q$, then by expanding in series, one finds

$$G = (\mathbb{1} - Q)^{-1} S = (\mathbb{1} + Q + Q^2 + \dots) S\,. \tag{3.48}$$

Then the propagator is solved iteratively as

$$G^{(0)} = S\,,\ G^{i+1} = S + QG^{(i)}\,. \tag{3.49}$$

This method is called Jacobi iteration. It converges if the biggest eigenvalue of G is smaller than 1. The idea behind the inversion in the Jacobi iterations is the same for even more complicated methods. But reaching the convergence of the algorithm becomes a lot less trivial in these other cases.

In our calculations, we use a variant of the conjugate gradient (CG) method, called Bi-CGStab method. The conjugate gradient method consists in minimizing a quadratic functional

$$Q(x) = \frac{1}{2}\mathbf{x}^T A\mathbf{x} - \mathbf{x}^T\mathbf{b}\,. \tag{3.50}$$

The solution of the minimization problem solves $A\mathbf{x} - \mathbf{b} = 0$. The algorithm looks for search direction vector $\mathbf{p}^{(i)}$ such that iteratively $Q(\mathbf{x}^{(i)} + \alpha_i\mathbf{p}^{(i)})$ is minimized as a function of the parameter α_i. This is done then by applying the iteration $\mathbf{x}^{(i+1)} = \mathbf{x}^{(i)} + \alpha_i\mathbf{p}^{(i)}$. The vectors $\mathbf{p}^{(i+1)}$ is chosen such that it is A-orthogonal to all the other p vectors. Namely, it means that it is orthogonal to $A\mathbf{p}^{(i)}$. The space generated by the span of these vectors is called Krylov space.

But the CG method only works for positive definite symmetric matrices. Then for general matrices, like the case of our interest, the Dirac operator, the Bi-Conjugate Gradient (Bi-CGR) is needed. It is a generalization of the CG algorithm, that uses two sequences of search directions and residual vectors, by solving also the conjugate problem $A^T x^* = b^*$. The sequences obey a bi-orthogonality relation. The particular variant of the BiCG-Stab method we used is taken from [75]. It is shown in full detail in appendix A.

4. SU(2) lattice gauge theory coupled with an adjoint Higgs

The first lattice investigations of the gauge invariant spectrum of Higgs theories always displayed a mass gap. This can be observed in the analysis of the bosonic spectra of the SU(2) and SU(3) theories coupled with an Higgs in the fundamental representation [34, 35, 76]. This result seems to suggest that the composite bound states are massive. In this section we prove that this is not always the case.

The theory analyzed is a SU(2) one with an Higgs in the adjoint representation, as it has been presented in section 2.5. The expected breaking pattern in a fixed gauge leads to a $U(1)$ little group. Perturbation theory points then to the presence of a massless vector state. What is more interesting, is that also the FMS mechanism allows for a massless vector state, but composite and gauge invariant.

Here we will detail how this FMS result is obtained through nonperturbative means. We will focus on the lattice implementation of this model. After presenting the setup and the simulation points chosen, we will focus on the interpolators. Both gauge variant and gauge invariant vector degrees of freedom are explored, in order to prove the FMS predictions. Lastly, spectroscopical results are presented.

This chapter follows [77].

4.1. Setup

The lattice implementation of the SU(2) theory coupled with an adjoint Higgs can be obtained by simulating the following action [65]

$$\begin{aligned} S[\Phi, U] =& S_W[U] + \sum_x \Big(2 \text{ tr} \left[\Phi(x)\Phi(x)\right] + \lambda \big(2 \text{ tr} \left[\Phi(x)\Phi(x)\right] - 1\big)^2 \\ & - 2\kappa \sum_{\mu=1}^{4} \text{tr} \left[\Phi(x)\, U_\mu(x)\, \Phi(x+\hat{\mu})\, U_\mu(x)^\dagger\right] \Big) . \end{aligned} \tag{4.1}$$

Here we used the Wilson action, denoted by $S_W[U]$, and the links $U_\mu(x)$. In the case with the adjoint Higgs, one can make use of the expansion of the scalar over the generators of the algebra $\Phi = \sum \Phi^a T^a$, to rewrite the action as

$$\begin{aligned} S[\Phi, U] =& S_W[U] + \sum_x \left[\sum_{a=1}^{3} \left(\Phi^a(x)\Phi^a(x) + \lambda \left(\Phi^a(x)\Phi^a(x) - 1 \right)^2 \right) \right. \\ & \left. - 2\kappa \sum_{\mu=1}^{4} \sum_{a,b=1}^{3} \Phi^a(x)\, V_\mu^{ab}(x)\, \Phi^b(x+\hat{\mu}) \right] . \end{aligned} \tag{4.2}$$

We also introduced the links in the adjoint representation

$$V_\mu^{ab}(x) = \mathrm{tr}\left[T^a\, U_\mu(x)\, T^b\, U_\mu(x)^\dagger \right] , \tag{4.3}$$

that act on the Higgs in a similar way to the fundamental case.

In principle, the theory can be implemented quite straightforwardly on the lattice. For our purposes, a multi-hit Metropolis Monte-Carlo algorithm has proven successful for the configurations generation, like in [35, 78]. In an earlier stage of the work, an Hybrid Monte Carlo (HMC) algorithm, based on the Hirep code [79], which has been used for various lattice simulations also comprising a fundamental scalar, has been adapted for the simulation of this theory. The version of the code we augmented with an Higgs in the adjoint representation, had already implemented a scalar field in the fundamental representation [80]. The general performances of the algorithm were quite poor in comparison to the Metropolis algorithm. Thus, simulations were disbanded in favor of the Monte Carlo technique. As far as the author knows, there were no previous attempts of a HMC simulation with an adjoint Higgs. By our experience, the critical slowing down encountered can be the result of the particular dynamics of the theory in the broken phase, which was the interesting one for our investigation goals.

We analyzed lattices of sizes $L^4 = 8^4, 12^4, 16^4, 20^4, 24^4, 32^4$. In this case, the scalar fields were updated with a pseudo random flat distribution with support $[-\epsilon, \epsilon]$, while the gauge links used a $SU(2)$ transformation close to the identity, through the expansion $G(x) = x_0 \mathbb{1} + i x_i \sigma_i$. A multi hit Metropolis has been performed in our work, with five hits for the gauge fields.

The configurations are saved after a thermalization cycle of 1000 global updates. Then, a configuration is saved once every 50 update cycles, in order to have a decorrelated sample.

4.1.1. Phase diagram

Results on the phase diagram were already obtained in previous rougher simulations more then 30 years ago [81–85]. In our work, we want, in a first instance, to take advantage of the modern machine architectures and increased computational power to substantiate the results obtained in those early works. In particular we want to find a order parameter for the transition between the unbroken (QCD-like) phase and the broken phase with the BEH effect active.

When first exploring the phase diagram, similarly to what has been done in [34, 86], by simulating for various values of the lattice parameters (β, κ, λ), we still encountered slowing downs but not as severe as the one seen in the HMC algorithm. This is discussed more in detail in subsection 4.2.

Inspired by the previous results on the phase diagram in lattice Higgs theories, we decided to perform a scan over values of κ from $1/8$, which would provide a tree level massless scalar, to $\kappa = 2$, while keeping fixed values for $\beta = 4$ and $\lambda = 1$. It is expected that a QCD-like phase would apper for lower values of κ, and a BEH phase for higher values of it.

Our results validated this picture, with a phase transition around $\kappa \approx 0.5$. In the following sections, we will focus on values of $\kappa \in [0.5, 0.7]$, expecting to be closer to the continuum limit in this region. For the spectroscopy, in section 4.5, we focused on the two values $\kappa = 0.55, 0.65$.

The plaquette is used as a first approach to the phase diagram. As shown in figure 4.1, the high susceptibility around $\kappa = 0.5$ is a good sign a of a rapid transition between the two phases. But since there is no volume scaling for this phenomenon, we expect then a cross-over or a very small critical region.

While we cannot determine if it is an authentic second-order transition, even if it looks really close to one, we expect that this setup will serve our purposes. Nonetheless, it is important that the correlation lengths are sufficiently large. Moreover, even if there is no second-order phase transition, we expect that the low-energy observables to be still reliable [87]. We can then see the theory only as an effective theory, since we cannot push cutoff to zero, but this is also the case for the standard model Higgs sector [37].

Further, we will show that the setup we used for large statistics simulations in this investigation, with the parameter sets chosen with $\kappa = 0.55, 0.65$, is indeed suitable for out purposes. This is reported in section 4.5.

On the other hand, the behaviour of observables like the Polyakov loop norm didn't show a clear behaviour throughout a scan in the κ values while keeping β and λ fixed, as discussed in 4.2.

We want to summarize now the simulation setups chosen in detail. In total 12 setups have been used, all with $\beta = 4, \lambda = 1$. Two values of $\kappa = 0.55, 0.65$ have been simulated for 6 different lattice volumes $L^4 = 8^4, 12^4, 16^4, 20^4, 24^4, 32^4$.

For the calculation of gauge invariant observables we used: $(1-4) \times 10^5$ configurations for the smaller volumes 8^4 and 12^4, and $(1-3) \times 10^4$ for the remnant larger volumes. In the case of the gauge-fixed observables, discussed in 4.3, an order of magnitude of 10^3 has been used. The difference in the amount of configurations between gauge variant and gauge invariant degrees of freedom is due to two reasons. The

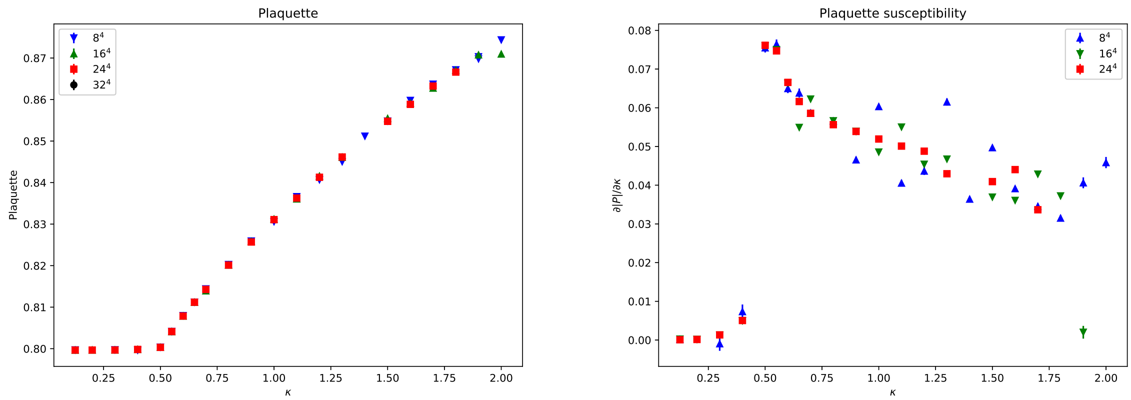

Figure 4.1.: The plaquette as a function of κ (left panel) for various volumes, as well as its derivative with respect to κ (right panel).

first reason is related to the high computational cost for the gauge fixing algorithm at higher volumes. With respect to the cost of the generations of non gauge fixed configurations, the increase with volume of the cost of the gauge fixing algorithm is one or two orders of magnitude larger. The second one is due to the lower amount of statistical noise for the gauge fixed observables. This is mostly due to the fact that the interpolators used contain less fields than the gauge invariant ones. Also, in general gauge invariant operators are calculated by averaging over a gauge orbit, thus resulting in added statistical noise for lattice estimation. This has been observed in many cases for lattice gauge fixed calculations [70, 88].

4.2. Thermalization properties

Before discussing the observables used for spectroscopy, we want to discuss the thermalization issues we encountered in more detail.

The ones we observed in the simulations with the HMC algorithm were far more severe. It was not possible to obtain thermalized observables of any kind for volumes of 24^4 and $\kappa > 0.2$. Different realizations of the Higgs field were implemented to solve the issue. In particular, a decoupling of the radial and angular modes of the Higgs has been simulated. Despite this attempt, performances did not change, every update required an extensive amount of time, and acceptance was drastically low for all values of κ bigger than 0.2. This resulted in the impossibility of computing, in the BEH phase which is the interestingone for our purposes, not only both the observables based on the scalar field, but also local observables like the plaquette. We don't know the exact causes of this behaviour of the algorithm. In principle, there can be a physical reason

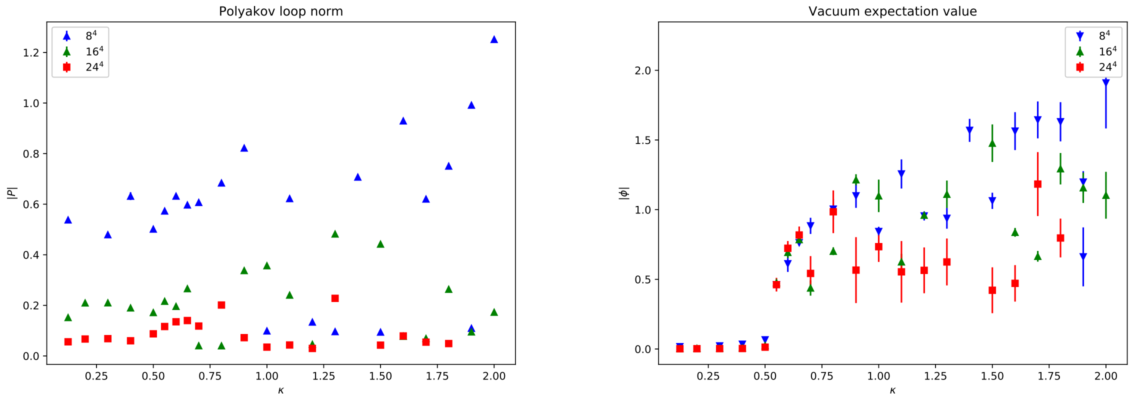

Figure 4.2.: The norm of the Polyakov loop (left panel) and the Higgs vacuum expectation value (right panel) for various volumes as a function of κ for $\beta = 4$ and $\lambda = 1$. For the Higgs vacuum expectation value the statistical error has been enlarged by a factor of ten to demonstrate that the observed effect is definitely not a statistical problem.

based on the shape of the potential, and then on the resulting change in the action for a global update, which we observed to be big in all the relevant cases we studied.

We then switched to a local multihit Metropolis algorithm, as it has already been applied successfully in other Higgs bosonic theories [34, 78]. By doing so, we managed to analyze successfully observables in the unbroken phase, which we found to be realized for $\kappa \gtrsim 0.5$. This region of parameters was inaccessible with the HMC algorithm.

But thermalization issues were also found in the local algorithm, in particular, for values of $\kappa \gtrsim 0.7$, as shown in figure 4.2. While the plaquette, as shown in figure 4.1, behaves in a regular way throughout all the values of κ analyzed, from 0.1 to 2.0, the Polyakov loop and the vev do not. We argue that a possible cause can be the locality of the plaquette variable.

It must be noted how the thermalization problems encountered in the two algorithms analyzed have quite different nature and severity. To summarize, we encountered many more difficulties when generating configurations with a global update, especially at increasing values of κ.

However, we analyzed the nature of the thermalization issues in the local algorhithm. These can be better recognized in the plots in figure 4.2. In particular, by observing the Monte-Carlo trajectories, we saw excursions to configurations which have vastly different values of the Polyakov loop and the Higgs vev. In other cases, we observe that the algorithm is stuck on certain values of these observables. Concerning the plaquette, we note that the change between the two phases is discontinuous. We thus hypothized that this can be a two-state system. In any case, the vacuum expectation value is nonzero in both phases, as it can be assessed in figure 4.2. In general, we can expect that the problem is more severe when the lattice is rougher, hence when it is farther from the phase transition. We interpret this behaviour as a sign of thermalization problems, since there is an excursion in the configurations generation. The resulting random values of the observables confirm this picture. We thus decided to not analyze extensively values of $\kappa \gtrsim 0.7$, redirecting our attention to lower values of κ for the spectroscopic analysis. For the parameters we choose, $\kappa = 0.55, 0.65$, we don't observe the problems described in this section, and the observables look thermalized.

4.3. Gauge fixed observables

For a global understanding of the system and its properties, we opted to check some gauge variant observables in a gauge fixed setting. This is of great importance especially given how the FMS mechanism works. It appears evident that the right hand side of an FMS expansion can be checked only if the gauge dependent observables are computed.

Gauge fixing has been performed as described in 3.2.1, by first obtaining a minimal Landau gauge fixing, then applying a global $SU(2)$ transformation to satisfy the 't Hooft condition, pointing the vev to a fixed Cartan direction. This is possible, because in minimal Landau gauge on a finite lattice, the expectation value of the Higgs is nonzero, while it would vanish in the infinite volume limit.

Given that the gauge is fixed, we focus now on the calculation of the gauge boson propagators. In particular, we calculate them separately in the Cartan direction and in the remainder direction, as done in [34]. Also, the ghost propagator is calculated, allowing us to determine the running gauge coupling in the minimal miniMOM scheme [89]. By doing so, we can verify whether we are in a weak coupling regime. Lastly, the scalar field propagator is investigated. In this way, it is possible to verify the existence of the Goldstone boson.

The results for the gauge boson propagator are shown in figure 4.3. For the fit shown in the figure, a fit function has been used of the form

$$D(p) = \frac{Z}{(ap)^2 + (am)^2}\,, \tag{4.4}$$

based on the three level propagator shape, where p is the standard lattice momentum $p_\mu = 2\sin\big(2\pi n_\mu/L\big)$. The fit describes the data points very well, except for the lowest two momenta. But observing the behaviour of these points, one can still notice strong finite-volume effects. Those can be safely dismissed from the fits.

The fit values are then listed in table 4.1. In principle, the masses of the elementary gauge boson in a fixed gauge are an important element in the analysis of the FMS mechanism. We will discuss in more detail about this in section 4.5. We can observe strong and qualitatively different volume dependencies of the masses for the two κ values. This behaviour can be explained in the context of the FMS mechanism. We

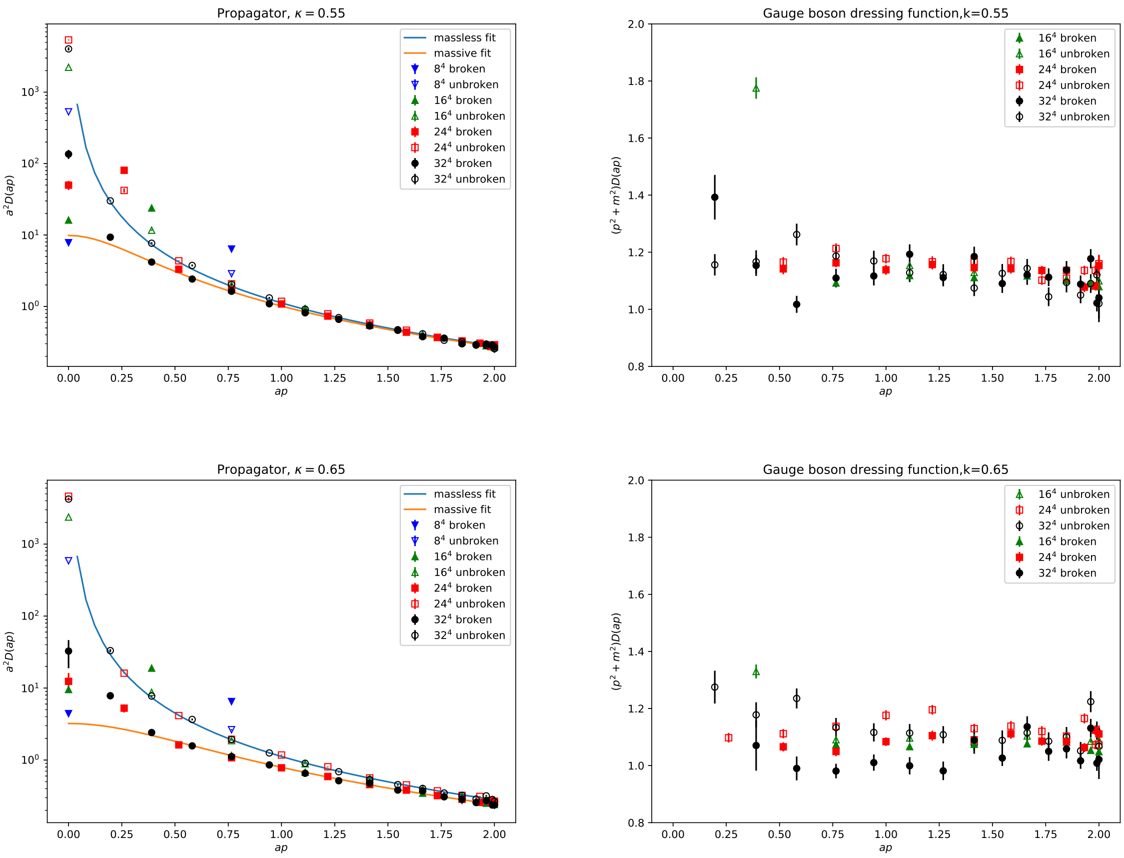

Figure 4.3.: The gauge boson propagator (left panels) and the dressing function (right panels) for $\kappa = 0.55$ (top panels) and $\kappa = 0.65$ (bottom panels) are shown, together with tree-level fits for the 16^4 case in lattice units. Momenta are along an edge of the lattice. The masses used to calculate the dressing functions are zero for the Cartan propagator. The fitted masses am_A are listed in Table 4.1 for the broken sector depicted in the right panels.

expect that this is due to the physical states possibility to cross decay thresholds as a function of the volume. This is discussed in detail in section 4.5, and it can be observed in figure 4.8.

We also perform a massless fit in the unbroken Cartan direction. It fits the data points well, validating the hypothesis of a massless state in the unbroken sector.

We can observe the running gauge coupling behaviour in the miniMOM scheme by using suitable combinations of the propagators. The values obtained are shown in figure 4.4. The results show a similar picture to what has been observed in [34]. For large momenta we see an unification of the broken and unbroken sector, going to a value for the gauge coupling $\alpha \approx 0.1$. We can focus on the value of the momenta where the split happens. It is generally larger than m_A, as could be expected. For the case

L/a	κ	am_A
32	0.55	0.338(1)
24	0.55	0.261(1)
16	0.55	0.207(2)
32	0.65	0.54(2)
24	0.65	0.623(3)
16	0.65	0.585(9)

Table 4.1.: The fit parameters for the fit form (4.4) of the gauge-fixed gauge boson propagator for different lattice sizes L/a. For the 8^4 lattice no stable fit was possible. In figure 4.3 the values for the 16^4 lattices have been used.

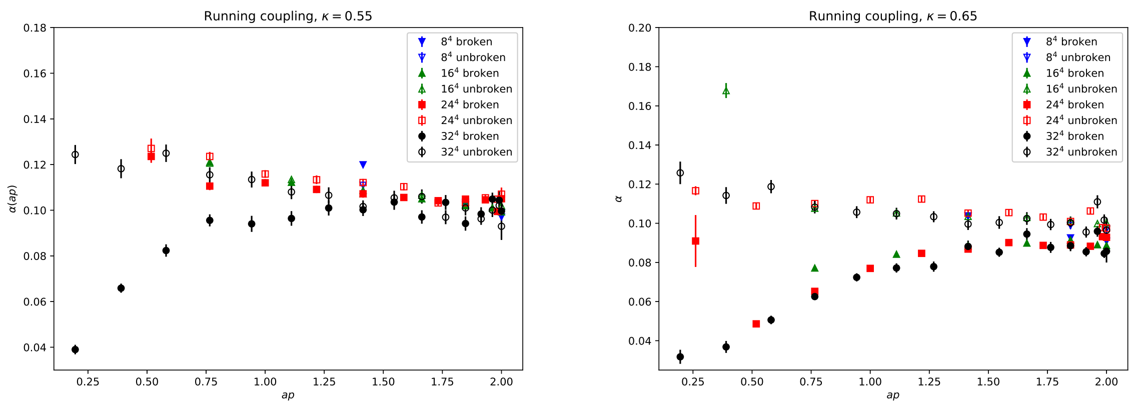

Figure 4.4.: The running gauge coupling in the miniMOM scheme. The left panel shows the result for $\kappa = 0.55$ and the right panel for $\kappa = 0.65$. Note that, the lowest momentum point is very strongly affected by finite volume effects, and thus often outside the plotting range. Momenta are along an edge of the lattice.

with $\kappa = 0.65$, where the lattice is rougher, the split is at $ap_{split} \approx 1.6$. For the finer setup with $\kappa = 0.55$ the split is at $ap_{split} \approx 1.1$. While the value at lowest momenta are indeed affected by heavy finite volume effects, the remaining values for the broken sector point to the typical situation for theories with the BEH effect [33]. The values of the coupling never exceed 0.1. The momentum dependence appears more prominent in the unbroken sector, but actually it never exceeds 0.12. We can then deduce that for both settings the gauge couplings are weak.

Lastly, the Higgs dressing function for both parameters is shown in figure 4.5. Analogously to the gauge boson propagator analysis we just detailed, also here it is necessary to choose a renormalization scheme. However, the scalar case is more involved, since there is an additional mass renormalization. The scheme choice has been done analogously to [90]. This choice appears to have almost no volume-dependence,

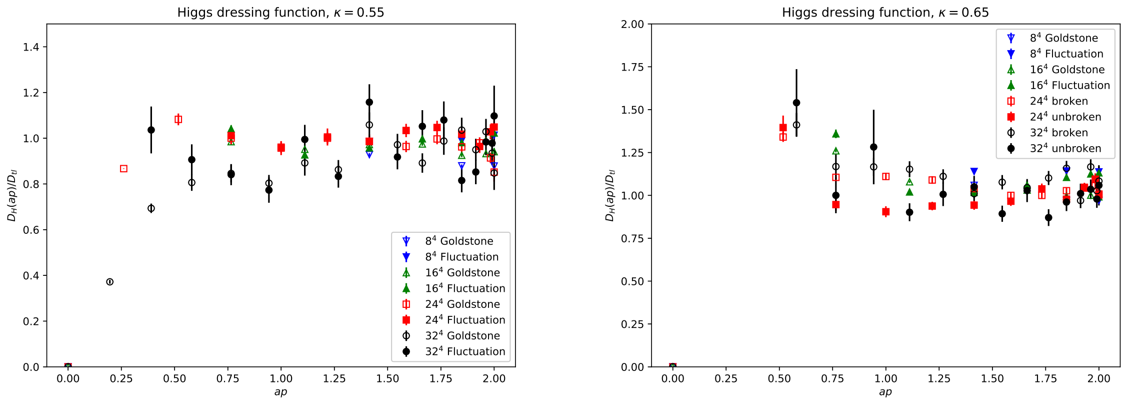

Figure 4.5.: The renormalized Higgs dressing function, normalized to the tree-level propagator, in the would-be pole scheme of [90]. The left panel shows the result for $\kappa = 0.55$ and the right panel for $\kappa = 0.65$. Note that the lowest momentum point is very strongly affected by finite volume effects, and thus often outside the plotting range. Momenta are along an edge of the lattice.

and also to be a good approximation for the pole scheme in the case of an Euclidean lattice.

The biggest problem is that the mass of the physical Higgs is currently not known. The amount of statistical fluctuations in the scalar channel madk it impossible to extract reliable values of the mass with our setup and amount of configurations. Thus we have no value for the scalar pole mass, which is required in our renormalization scheme. Nonetheless, for the Goldstone modes this is actually not an issue. In the 't Hooft-Landau gauge, those modes are massless.

For the fluctuation mode, the mass can then only be chosen arbitrarily. We set the normalized masses to 0.5 and 1.2 for the values $\kappa = 0.55$ and $\kappa = 0.65$, respectively. We observe that the results obtained are stable for all the volumes simulated, except for the fluctuation on the $\kappa = 0.65$, which is more unstable. It is visible that the dressing function for the fluctuation doesn't deviate much from 1, hence providing a tree-level shape for the propagator like $1/((ap)^2 + (am)^2)$. Even more interesting, this result for the Goldstone modes proves their compatibility with being actually massless. Also in this case a strong volume dependence is observed at small momenta.

4.4. Gauge invariant spectroscopic observables

As mentioned in the previous section, the scalar channel is affected by an high level of statistical noise. With the current amount of computational power available it was not possible to obtain spectroscopic results. Hence, in this work we focus on the vector channel.

The spectroscopical methods described in section 3.3 will then be used to analyze the observables we will describe in this section. Hence for the extrapolation of the effective values of the energies, a generalized eigenvalue problem, with a basis consisting of the operators we are going to describe, with different smearing levels, has been employed.

We now list the interpolators that have been used for the study of the $J^P = 1^-$ channel. The first interpolator we used, which is the ideal candidate to provide information about the spectrum, is the simplest discretization of the operator (2.41), namely

$$B^i_{1^-}(x) = \frac{\mathrm{Im}\,\mathrm{tr}\left[\Phi(x)U_{jk}(x)\right]}{\sqrt{2\,\mathrm{tr}[\Phi(x)^2]}}\,, \tag{4.5}$$

where $U_{jk}(x)$ is the plaquette in the spatial directions indicated by the indices jk. The index i of the interpolator (4.5), and the indices j, k of the relative plaquette are even permutations of the spatial indices $1, 2, 3$. We also consider other two interpolators with the same quantum numbers

$$\begin{aligned} B^{\Phi,i}_{1^-}(x) &= 2\,\mathrm{tr}\left[\Phi(x)^2\right] B^i_{1^-}(x)\,, \\ B^{2,i}_{1^-}(x) &= \left(\sum_{j=1}^{3} B^j_{1^-}(x) B^j_{1_-}(x)\right) B^i_{1_-}(x)\,. \end{aligned} \tag{4.6}$$

The first operator is constructed with the insertion of a scalar operator constructed from the elementary scalar field. The second also has a 0^+ operator inserted, but in this case it is constructed by taking the trace of the product of two vector operators. In both cases, the scalar insertion is multiplied with the simplest vector operator (4.5). From a more physical perspective, these two operators represent scattering states. The first is the scattering possibility with the Higgs, the second is the scattering with other gauge bosons.

In order to ameliorate the signal, by smoothing the contributions from higher excited energy states, a smearing procedure on the field is effectuated. In this way, the operators created with the smeared fields can contribute to enlarge the spectroscopical base.

The smearing procedure we decided to apply in this case is the APE smearing. We applied up to $n_{sm} = 5$ levels of smearing. The procedure is described by the replacement performed as

$$
\begin{aligned}
U_\mu^{(n)}(x) &= \frac{1}{\sqrt{\det R_\mu^{(n)}(x)}} R_\mu^{(n)}(x)\,, \\
R_\mu^{(n)}(x) &= \alpha\, U_\mu^{(n-1)}(x) + \frac{1-\alpha}{6} \sum_{\nu\neq\mu} \Big[U_\nu^{(n-1)}(x+\hat{\mu})\, U_\mu^{(n-1)}(x+\hat{\nu})^\dagger\, U_\nu^{(n-1)}(x)^\dagger \\
&\qquad + U_\nu^{(n-1)\dagger}(x+\hat{\mu}-\hat{\nu})\, U_\mu^{(n-1)}(x-\hat{\nu})^\dagger\, U_\nu^{(n-1)}(x-\hat{\nu}) \Big]\,, \\
\Phi^{a\,(n)}(x) &= \frac{1}{7} \Big[\Phi^{a\,(n-1)}(x) + \sum_\mu \Big(V_\mu^{ab}(x)\, \Phi^{b\,(n-1)}(x+\hat{\mu}) + V_\mu^{ba}(x-\hat{\mu})\, \Phi^{b\,(n-1)}(x-\hat{\mu}) \Big) \Big]\,,
\end{aligned}
\tag{4.7}
$$

when applied to the adjoint scalar field and the links. Here $U^{(0)} = R^{(0)}$ and $\Phi^{(0)}$ describe the unsmeared fields. We have selected the value $\alpha = 0.55$ for the tuning parameter. This procedure is performed analogously as in the fundamental case [76].

In a first exploration of the spectroscopical properties of the theory, done by analyzing the operator (4.5) in the zero momentum frame, we obtained no appreciable signal in that channel, with every time sliced point of the correlator compatible with zero. The main problem resides in the fact that, even in Euclidean space-time and on a finite lattice, massless vector particles cannot have a finite mass. Then we concluded that there is no signal if we analyze the correlator with zero momentum. In principle, it would be necessary to have a nonzero longitudinal degree of freedom of the operator to have a signal in this frame. Apparently then, even on a finite lattice, there is no appreciable contribution. Thus, in order to study a massless vector frame, one is required to work in a boosted frame[1].

The vector operators we illustrated in (4.5)-(4.6) are then boosted to a frame which is not at rest via

$$
O_j(\mathbf{p}, t) = \frac{1}{\sqrt{L^3}} \mathrm{Re} \sum_{\mathbf{x}} O_j(\mathbf{x}, t) e^{i\mathbf{p}\cdot\mathbf{x}}\,. \tag{4.8}
$$

Here O_j indicates any of the vector operator discussed. It has been checked numerically that the imaginary part of the Fourier transform is negligible. The momentum we chose has the only nonzero component in the z-direction

$$
\mathbf{p}_z(n_z) = \left(0, 0, p_z = \frac{2\pi}{L} n_z\right)\,. \tag{4.9}
$$

We then added in the new basis of boosted operators the three operators in (4.5)-(4.6) with $n_z = 1$, and also the operator (4.5) with $n_z = 2$, amounting then to a total of 4

[1] In principle, it is also possible to use twisted boundary conditions for this goal [91]. One can read in this context also [92, 93].

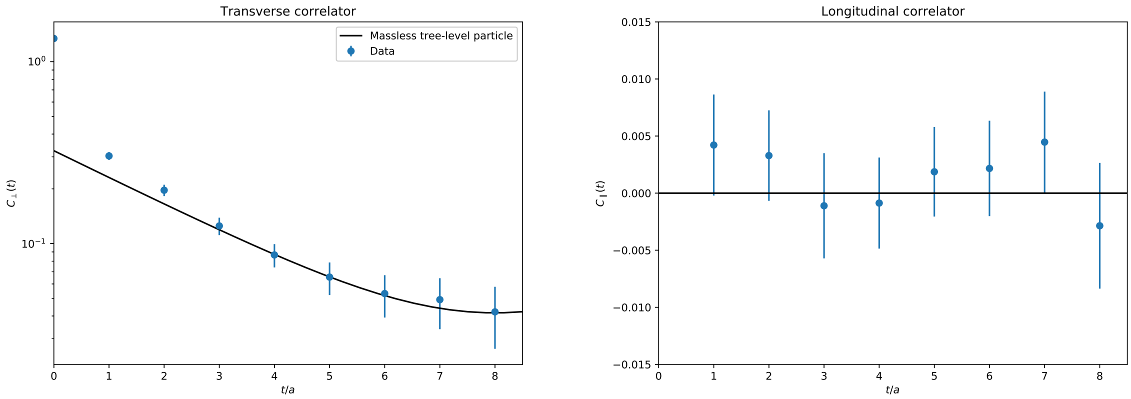

Figure 4.6.: Examples of the correlator decomposition (4.10). We show the transverse correlator (left panel) and longitudinal correlator (right panel) of the gauge-invariant vector state (4.5) in a boosted frame on a 16^4 lattice. The computation shown in this figure has been performed at $\kappa = 0.75$. In addition the expected behavior for a massless vector particle is plotted (solid lines).

operators in the basis. The last one has an evident overlap with the state with twice the energy of the ground state, and with this base we are also capable of capturing the physics of the scattering states, which is necessary for the analysis discussed in 4.5.

Once we have boosted the operators, we can then divide the correlators we construct from them in a transverse component $C_\perp$ and a longitudinal component $C_\parallel$ via the definitions

$$\begin{aligned} C_\perp(t) &= \frac{1}{L}\sum_{t'=0}^{L-1}\sum_{j=1}^{2}\langle O^j(\mathbf{p}_z(n_z),t')\,O^j(\mathbf{p}_z(n_z),t+t')^\dagger\rangle\,, \\ C_\parallel(t) &= \frac{1}{L}\sum_{t'=0}^{L-1}\langle O^3(\mathbf{p}_z(n_z),t')\,O^3(\mathbf{p}_z(n_z),t+t')^\dagger\rangle\quad, \end{aligned} \tag{4.10}$$

where a time slice averaging procedure is performed. The first analysis done for the longitudinal correlator shows that it is compatible with zero within statistical uncertainties, like it has been observed in the zero momentum projection case. See also [94]. We show an example of this observation in figure 4.6, together with the parallel correlator computed in the same setup. We already have a strong hint for the presence of a massless vector state. In the following, we will always then work with transverse correlators. Even for massive states, the longitudinal component will be at most constant.

We now discuss the energy predictions for boosted operators on an Euclidean lattice. This will be of fundamental importance in the following, since we will look mostly at

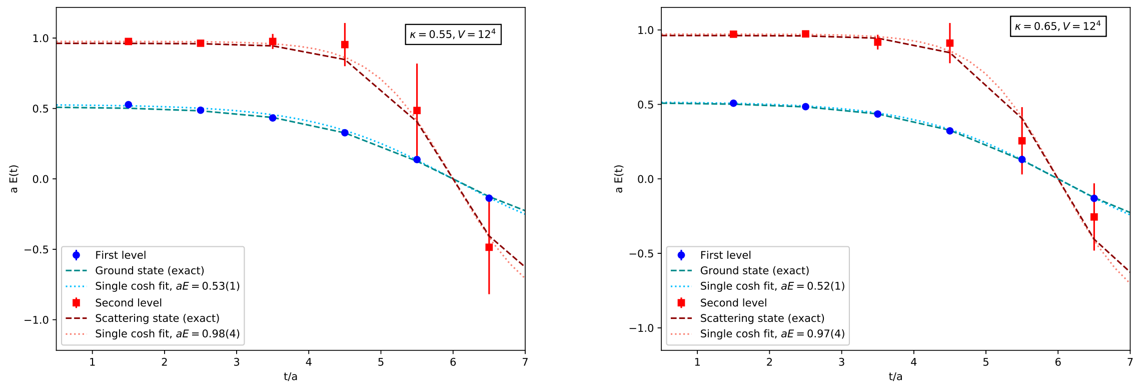

Figure 4.7.: The plots show the effective energies obtained at $\kappa = 0.55$ (left panel) and $\kappa = 0.65$ (right panel) at a volume of 12^4. These have been obtained in a basis with four operators smeared five times. Besides single-cosh fits to the data (dotted lines) also the expected behavior for a massless particle (4.12) with one unit of kinetic energy is shown (dashed lines).

the energy levels provided by the correlators. For this, we employ the lattice dispersion relation [62]

$$\cosh(aE) = \cosh(am) + \sum_{i=1}^{3}(1 - \cos(ap_i)) \, . \tag{4.11}$$

One can check immediately that this formula reduces to the usual dispersion relation $E^2 = m^2 + \mathbf{p}^2$ in the naive continuum limit. For the analysis of the massless state, we are interested in a particular case of (4.11). The dispersion relation for massless states on the lattice with only a non zero momentum component p_z in the third direction is

$$\cosh(aE) = 2 - \cos(ap_z). \tag{4.12}$$

We also can expect states with higher momenta. Due to the lattice formulation, these should be integer multiples of the momentum p_z.

Apart from the massless state, we also want to check whether there are massive states present in the channel. We could expect a state at the elementary boson mass, based on the usual perturbative treatment of Higgs theories, and one at twice the mass of the elementary state. This last one comes from the constituent picture of the FMS result discussed in 2.5.1. For these cases, we use equation (4.11) with the masses from the table 4.1 for the lattice predictions, setting then $m = m_A$ or $m = 2m_A$.

Before discussing the global results we obtained, we show an example of the effective energies we obtained together with the lattice predictions we just discussed. We can observe the two lowest effective energies one obtains from the principal correlators for a particular setup in figure 4.7. The predictions we show are taken from equation (4.12). We use the momentum values p_z and $2p_z$ for the functions, which are plotted along as dashed lines. Also single cosh fits are plotted as dotted lines. We can observe that the data points for the two eigenvalues are well described by the massless prediction. In this case only a single cosh is necessary for fitting the data. In other cases a double cosh fit is used due to the deviations caused by the higher energy levels at shorter times. Also in these cases, we can observe a good fit for the larger times, from which we can extract the energy levels. We have managed to obtain reliable predictions for the two lowest eigenvalues in all cases. We haven't managed to disentangle the higher energy levels. These resulted to be too noisy, except for the lower two volumes where it has been possible to get a rough estimate of the third energy level, which has been described with equation (4.12) with momentum $3p_z$ within the larger statistical errors.

4.5. Spectroscopic results

We now give some details about the predictions, before detailing the summary of our findings.

The first state we predict in the vector channel is the massless one. It is expected to provide energies which are integer multiples of the boosted momentum of the frame. This should provide values at the plateau like $aE(n_z) \approx 2\pi n_z/L$. The ground state is then given by $n_z = 1$, and the excited states by other integer multiples of this.

Then, there are two massive predictions. The first comes from the elementary perturbation theory computation, and it provides two degenerate massive states with mass m_A. The prediction obtained from the FMS mechanism is a state with mass $2m_A$. Given that we are in a boosted frame, the prediction for the effective energy is given by the dispersion relation (4.11), to take into account the nonzero momentum. Then a value of momentum $E(1)$ is a lower bound for the possible predicted energy of massive states.

One should also take into account the possibility for the massive states to decay into three massless states. This can happen provided that the kinematic condition

$$3 + \cosh(am) - \cos\frac{2\pi}{L} < 2 - \cos\frac{6\pi}{L} \tag{4.13}$$

is satisfied.

Concerning this relation, we will ignore the elementary mass dependence we encountered in the section 4.3, since the dependence of the kinetic term with respect to the volume is much stronger. In any case, for both the values of κ we considered, there is a crossing of the elastic region, which happens in two different volume values, since the predicted elementary masses are different.

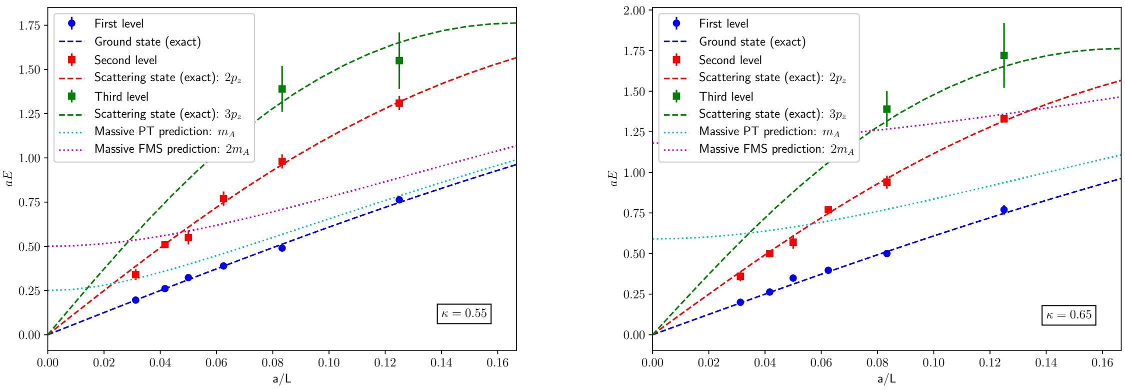

Figure 4.8.: The plots show the volume-dependent low-lying spectrum for $\kappa = 0.55$ (left) and $\kappa = 0.65$ (right). Besides the simulation results also shown are the predictions for the three lowest-lying massless states (dashed lines), the massive state from perturbation theory (cyan dotted lines) and the FMS prediction for an additional massive state (magenta dotted lines). In the latter cases masses $am_A = 0.25$ and $am_A = 0.6$, respectively, have been used, as reasonable proxies to the masses in Table 4.1. For the massive predictions effects from avoided level crossing have not been included in this plot.

Now we want to address the question of which states are actually observable, based on the symmetries of the theory. In principle, due to the impossibility of spontaneous breaking of a local symmetry [25], a state which transforms under a nontrivial representation of the gauge group cannot be observed, as discussed in chapter 2. Thus, we don't expect to observe the energy level associated with the elementary gauge boson. Also, in the FMS formalism, the states are described by gauge invariant operators, and their spectrum is obtained in a fixed gauge, where the global symmetry associated with the gauge symmetry is reduced to a residual one. In this case the residual gauge group is $U(1)$, hence the expected massless vector state associated with this symmetry. However, there is also the question of whether it is possible to have vector states which are charged under this residual $U(1)$ group, which would be an equivalent, in terms of their construction, of the charged $W^{\pm}$ bosons. Only a nonperturbative analysis can actually validate this hypothesis. The FMS expansion is still perturbation theory at its core, thus is not capable of capturing all the dynamical properties of the theory. Then the question of whether the state with twice the mass of the elementary boson, obtained in the constituent picture analysis of section 2.5, is present, is of vital importance, also from a purely field theoretical point of view.

We now show the final results in figure 4.8, together with the expectations we just discussed. The first two eigenvalues of the variational analysis have been determined for all the 12 lattice setups we simulated, consisting of two values of κ and 6 volumes.

Also, for the lowest two volumes, the third eigenvalue has been determined, but with a higher relative uncertainty. It is then evident that the ground state is well described by the dispersion relation (4.12) with $n_z = 1$. This gives a robust support for the hypothesis of a massless state in the vector channel. Thus, we confirm our prediction about the gauge invariant realization of the state. The second eigenvalue is also very well consistent with the dispersion relation (4.12) but with $n_z = 2$, supporting even more the massless state prediction, by showing the presence of a first excited state which is still massless, with twice the kinetic energy. Also, the 4 data points concerning the third eigenstates are compatible, though with a bigger uncertainty, with a massless state with three units of the basic momentum index n_z. This is another indication of the massless state in the channel.

On the other hand, we see no sign of massive states in our investigation results. The crossing point where the kinematic thresholds for the decay is reached can be observed in figure 4.8, by looking at the green scattering state line with $3p_z$, and by confronting it with the massive predictions. Even in the region where the decay is not allowed, there is no data point which is compatible with either the elementary or the composite massive state. Also, the energies can have a deformation effect which is due to avoided level crossing, or in general the presence of additional unpredicted states. Having made these observations, we conclude that no massive states are found in our investigation.

There can be multiple reasons for the lack of massive states in this investigation. The first and most prominent is the choice of the operator basis we made. In all our operators, the simplest operator (4.5) is present. Other operators [38], which do not contain the operator (4.5), will for sure be needed for a more thorough exploration of the energy levels. For instance, these other operators would be analogous to the ones used in [95]. We can also think about the presence of possible resonances which are not accessible with the techniques used. But unfortunately, there is no equivalent of the Lüscher analysis [96] for massless particles, as far as the author knows, which could have been used. The other reason is of a different nature, and it is only related to the presence of lattice artifacts. These can be due to the discretization process, but also finite volume effects, or simply lack of statistics. The latter would be true in the case that, for instance, two states are mixed in a subtle way, and one is predominating the other. In any case, ameliorating such lattice artifacts is a more straightforward operation than the rethinking of the operator base. But it would still require important computational resources to be achieved.

Even if the latter operations were to be performed, in order to find the massive states, without giving any further result, this would provide many implications. In principle, this would totally defy the standard perturbation theory prediction of two massive degenerate states. On the other hand, also the constituent prediction from the FMS would be invalidated. Then, model building done in the FMS picture would provide no way to construct charged vector bosons, if a $U(1)$ residual symmetry in the little group in a fixed gauge is present. Only a twisted GUT theory would be capable of allowing the charged gauge bosons. This discussion is outside the current state of the art of FMS nonperturbative findings. Further and more refined simulations will be able to resolve this important matter.

5. Lepton compositeness on lattice

One of the biggest challenges when realizing nonperturbative tests of the FMS, is the impossibility to reproduce the electroweak sector in its fermionic sector on the lattice. The main problem is the gauge anomaly introduced by the lattice regularization when simulating weak interactions with parity violation [36]. Despite numerous efforts, this problem is still unresolved [97–101]. Hence, all of the previous non perturbative tests of FMS mechanism that have been done in the past analyzed only bosonic Higgs theories.

In this section we show how to circumvent the hardships concerning chiral fermions, without losing the physical properties we are interested in. The biggest difference that characterizes our implementation is that the fermions are not chiral, but vectors of Dirac fermions. This setup will nonetheless emulate the weak sector of the Standard model with a single associated lepton flavor. But at the same time it can be simulated on the lattice with standard techniques, without the hardships we mentioned.

The continuum theory for vectorial leptons is introduced in section 5.1. The lattice setup associated with it, also known as Wilson-Yukawa model [102–105] is then explained in 5.2. For the simulation of this model the quenched approximation discussed in 3.5 is performed. We believe that, concerning our goals for the bound state fermion operator spectrum, doing this will not affect the FMS prediction. We discuss the lattice interpolators used for spectroscopy in section 5.3. The results obtained with such operators will be listed and discussed in section 5.4.

The techniques and the results shown in this chapter are found also in [106].

5.1. Vectorial leptons

In section 2.3.2 the chiral version of the theory is presented in the light of the FMS construction. Here we present a continuum theory that shares many properties with it, but also an important modification to the fermionic fields. The introduction of vectorial Dirac fermions, in contrast to Weyl fermions in the theory we are going to present, is the main difference with respect to the fermion description in the weak sector of the Standard Model. This modification is required to construct a lattice simulation that could circumvent the problems related to the chiral nature of the theory. We keep all the main features we are interested from the Standard Model setting, by imposing a similar symmetry structure. However, this is analogous to an approach that has been studied extensively in the past, namely the addition of a further generation of spinors with opposite helicities, called mirror fermions. One can consult [103, 104] for an earlier introduction to the topic.

The theory is a $SU(2)_w$ gauge theory coupled to a scalar field in the fundamental representation, like the one explained in 2.3, with the addition of another Dirac fermion ψ which is also gauge coupled. Two other flavors of Dirac fermions χ_f are present in the theory, which are $SU(2)_w$ singlets. These fields are coupled to the Higgs field and the fermion ψ via Yukawa interactions. Since all the fermion species are now of the Dirac type, the theory can be put straightforwardly into a lattice setup. On the other hand, we can see how the gauged fermion ψ can be seen as a non chiral equivalent of a $SU(2)_W$ Weyl lepton doublet, and the two flavors of χ_f can be compared to the right handed lepton and neutrino. Given this analogy, we will refer to the fields as vectorial leptons, or just leptons, when there is no need to specify if we are referring to the Standard Model leptons or the ones proposed here.

We can write the Lagrangian of this theory as

$$\begin{aligned}\mathcal{L} = &-\frac{1}{4}W^a_{\mu\nu}W^{a\,\mu\nu} + \frac{1}{2}\,\mathrm{tr}\left[(D_\mu X)^\dagger(D^\mu X)\right] - \frac{\lambda}{4}\left(\mathrm{tr}\left(X^\dagger X\right) - v^2\right)^2 \\ &+ \bar{\psi}\left(\mathrm{i}\not{D} - m_\psi\right)\psi + \sum_f \bar{\chi}_f\left(\mathrm{i}\not{\partial} - m_{\chi_f}\right)\chi_f - \sum_f y_f\left((\bar{\psi}X)_f\chi_f + \bar{\chi}_f(X^\dagger\psi)_f\right).\end{aligned} \tag{5.1}$$

The similarity to the Lagrangian in section 2.3.2 is evident. The main difference is the introduction of the tree-level Dirac masses m_ψ, m_{χ_f}. The discussion on the symmetries we made in 2.3.2 remains mostly valid, with the exception of another flavor symmetry breaking pattern, realized by setting $m_{\chi_1} \neq m_{\chi_2}$. To summarize the symmetries, there is a gauge symmetry $SU(2)_w$, a global $SU(2)_c$ symmetry, if the Yukawa couplings y_f vanishes, and also a $SU(2)_f$ flavor symmetry if $m_{\chi_1} = m_{\chi_2}$ and the coupling y_f vanish again. The other explicit breaking patterns are the same as in the Standard Model. One is obtained by having non vanishing Yukawa couplings, the other with a BEH effect in a fixed gauge.

It can be verified that in the limit $m_\psi = m_{\chi_f} = 0$ an additional discrete chiral symmetry

$$\psi \to \mathrm{e}^{\mathrm{i}\frac{\pi}{2}\gamma_5}\psi, \quad \chi_f = \mathrm{e}^{\mathrm{i}\frac{\pi}{2}\gamma_5}\chi_f, \quad X \to -X, \tag{5.2}$$

appears, with $\gamma_5 = i\gamma^0\gamma^1\gamma^2\gamma^3$. In the following, we will not take into account for this discrete symmetry, since we will set the the Dirac masses to a nonzero value. The discrete chiral symmetry is them explicitly broken in our implementation. This is because the additional masses do not interfere with the FMS predictions, and make the theory discretization feasible.

As in the Standard Model case, the physical spectrum in the fermion channel is again described by the gauge invariant bound state

$$\Psi = X^\dagger\psi\,, \tag{5.3}$$

since ψ is not a gauge singlet. We again constructed a $SU(2)_c$ doublet. Moreover, the two gauge singlets χ_f are also directly observable. What has been said about the diagonal flavor symmetry with $y_f \neq 0$ in 2.3.2 is once again valid here. We can then interpret the components Ψ_1 and χ_1 as two vectorial neutrino-like operators, in analogy to the Standard Model left handed and right handed neutrino. Then, Ψ_2 and χ_2 are a vectorial analogy of the left handed and right handed electron.

5.1.1. Elementary spectrum

We discuss the elementary spectrum, in the case that a BEH effect is present. We then assume that the split in equation 2.7 is justified by an appropriate gauge fixing.

We begin by analyzing the tree level physics of the problem. This is quite different from the Standard Model one in 2.3.2. Instead of obtaining Dirac mass terms from the product of Weyl fermions with the Higgs vev, here a non-diagonal mass matrix for the four Dirac fields arises. This is expected, since the number of degrees of freedom is effectively doubled.

By using the vector notation for the four fermion species $(\psi_1\ \psi_2\ \chi_1\ \chi_2)^{\mathrm{T}}$, we have the mass matrix

$$M = \begin{pmatrix} m_\psi & 0 & \frac{v}{\sqrt{2}}y_1 & 0 \\ 0 & m_\psi & 0 & \frac{v}{\sqrt{2}}y_2 \\ \frac{v}{\sqrt{2}}y_1 & 0 & m_{\chi_1} & 0 \\ 0 & \frac{v}{\sqrt{2}}y_2 & 0 & m_{\chi_2} \end{pmatrix} . \tag{5.4}$$

We can solve the associated eigenvalue problem, and obtain the four tree-level eigenmasses

$$M_f^\pm = \frac{m_{\chi_f} + m_\psi}{2} \pm \frac{1}{2}\sqrt{(m_{\chi_f} - m_\psi)^2 + 2v^2 y_f^2} . \tag{5.5}$$

Given the five parameters available, it is then possible to form values for the tree level masses which can have multiple different scales. The nontrivial mixing is due to the BEH effect and the Yukawa coupling for the Dirac fields. The mixing, with respect to the eigenvalues of the tree level mass matrix, can be parametrized by a rotation in the field ψ, χ space, where there are two different rotation angles θ_f for the two different flavors of ψ_f and χ_f

$$\begin{aligned} \begin{pmatrix} \zeta_f^+ \\ \zeta_f^- \end{pmatrix} &= \begin{pmatrix} \cos\theta_f & \sin\theta_f \\ -\sin\theta_f & \cos\theta_f \end{pmatrix} \begin{pmatrix} \psi_f \\ \chi_f \end{pmatrix} , \\ \frac{1}{\sin(2\theta_f)} &= \sqrt{1 + \frac{(m_\psi - m_{\chi_f})^2}{2y_f^2 v^2}} . \end{aligned} \tag{5.6}$$

Here we introduced the eigenvector fields $\zeta_f^\pm$, which have associated eigenmasses $M_f^\pm$.

Given the mainly computational purpose we have in mind, we will refer to a specific subset of the parameter space, in order to make the scan of the phase diagram easier. We then set $m_{\chi_f} = m_\psi = m$ and $y_f = y$. The parameter space dimensionality is then reduced from five to two. Then there is an effective flavor symmetry $SU(2)_{df}$, which is unbroken, with this choice of parameters at tree level. We can then describe the fermion fields as two degenerate doublets with masses

$$M^\pm = m \pm \frac{yv}{\sqrt{2}}. \tag{5.7}$$

In the case we just detailed, the mass eigenstates are obtained from the flavor eigenstates by

$$\zeta^\pm = \frac{1}{\sqrt{2}}(\chi \pm \psi)\,. \tag{5.8}$$

We can improve the predictions by going beyond the three level analysis. We must keep in mind that while the relations $m_{\chi_1} = m_{\chi_2} = m$ and $y_f = y$ are protected by the $SU(2)_{df}$ symmetry, the relation $m_\psi = m_\chi$ is not. This is due to the fact that the gauged and ungauged fermion species couple in different ways with the gauge bosons and the scalar. While the former have a direct gauge coupling, the latter couples directly only to the Higgs particle via Yukawa couplings. Hence one can expect a splitting of the mass terms when quantum corrections are taken into account.

The one loop correction of the mass parameters can be parametrized as

$$\begin{aligned} m_\psi^{(1)} &= m(1 + c_\mathrm{y} y^2 + c_\mathrm{W}\alpha_\mathrm{W}), \\ m_\chi^{(1)} &= m(1 + c_\mathrm{y} y^2), \end{aligned} \tag{5.9}$$

where we introduced the dimensionless constants c_y and c_W, which stem from the one loop integrals. The first refers to internal fermion lines, while c_W can have a scalar or gauge internal line. Also, we have used in the parametrization the fine structure constant for the weak coupling $\alpha_W = \frac{g^2}{4\pi}$.

Including the one loop correction for the mass terms, the eigenvalues of the fermion mass matrix become

$$\begin{aligned} M^\pm &= \frac{m_\psi^{(1)} + m_\chi^{(1)}}{2} \pm \frac{1}{2}\sqrt{\left(m_\psi^{(1)} - m_\chi^{(1)}\right)^2 + 2y^2v^2} \\ &= m\left(1 + c_\mathrm{y}y^2 + \frac{c_\mathrm{W}}{2}\alpha_\mathrm{W}\right) \pm \frac{1}{2}\sqrt{c_\mathrm{W}^2\alpha_\mathrm{W}^2 m^2 + 2v^2y^2}. \end{aligned} \tag{5.10}$$

In this calculation, the one loop corrections to the Yukawa coupling have been neglected. This is due to the fact that these are more strongly suppressed for small gauge couplings. We expect them to be of order $y\alpha_W$ and y^3. It is expected that also the tree level mixing (5.8) is modified by the quantum corrections. The mixing angle θ that characterizes the relation between the two mass eigenvalues $\zeta^{\pm}$ with respect to the flavour eigenstates ψ, χ by $\zeta^+ = \psi \cos\theta + \chi \sin\theta$ and $\zeta^- = \chi\cos\theta - \psi\sin\theta$ is obtained from the one loop parameters via

$$\frac{1}{\sin(2\theta)} = \sqrt{1 + \frac{c_W^2 \alpha_W^2 m^2}{2y^2 v^2}}\,. \tag{5.11}$$

The relation, which in the tree level case gives the maximal split for the degenerate case $m_\psi = m_\chi$, is altered. We expect θ to be close to zero in the case that y is small, at fixed α_W, causing no mixing between m_ψ and m_χ, since ψ and χ are close to be eigenstates in this case. As we will see, this will be the case in some of our simulations in section 5.4. For the case of large y we don't have a precise prediction, and a nonzero θ can be expected.

5.1.2. FMS prediction

The application of the FMS mechanism is qualitatively unaltered in respect to the Standard Model case discussed in 2.3.2. The bosonic sector provides essentially the same results. We will look in more detail the hybrid field Ψ. By applying the FMS mechanism we obtain the relation

$$\Psi = X^\dagger \psi = \frac{v}{\sqrt{2}} \begin{pmatrix} \psi_1 \\ \psi_2 \end{pmatrix} + \mathcal{O}(\eta).$$

We see that, again, we map the Ψ bound state to the gauge-dependent elementary fermion ψ. Thus, we expect that Ψ is not a mass eigenstate at leading order in the FMS expansion. This is because ψ is a linear superposition of the mass eigenstates $\zeta^{\pm}$. We then expect two poles at $M^{\pm}$ for the correlator of Ψ, analogously to what happens for ψ in a fixed gauge. Then a gauge invariant mass eigenstate is constructed from a linear combination of Ψ and the gauge singlet χ, by applying a suitable rotation of the fields, like in the elementary case. A FMS expansion for the full correlation matrix of the gauge invariant singlets, which include terms like $\langle \Psi\bar{\chi}\rangle$ and $\langle \chi\bar{\Psi}\rangle$, is required to study the rotation. If one treats the FMS expanded terms perurbatively, one obtain as a prediction that the mixing of Ψ and χ is the same as the one of ψ and χ in a fixed gauge, at the leading order in v.

One can obtain this result by applying on-shell renormalization conditions for both the correlators of elementary and composite operators, like it has been done in [22]. One can observe how the poles and their residue of the gauge-invariant correlators are the same as correlators of elementary operators, obtained as leading terms in the FMS expansion.

Anyway, it has to be kept in mind how this is a perturbative statement. A nonperturbative bound state can still have some dynamics that is not captured by this calculation. However, we expect that in a weak couplings regime, with a large enough value of v, the relations still hold.

5.2. Lattice Wilson-Yukawa setup

We want now to focus on the lattice implementation of the theory in 5.1. [1] The fermion sector of it can be rewritten as an operator which acts on the 4 component vector of the Dirac fields as [65]

$$(\bar{\psi} \quad \bar{\chi}) D \begin{pmatrix} \psi \\ \chi \end{pmatrix} = (\bar{\psi} \quad \bar{\chi}) \begin{pmatrix} D^{\bar{\psi}\psi} & D^{\bar{\psi}\chi} \\ D^{\bar{\chi}\psi} & D^{\bar{\chi}\chi} \end{pmatrix} \begin{pmatrix} \psi \\ \chi \end{pmatrix}, \tag{5.12}$$

with

$$\begin{aligned} D^{\bar{\psi}\psi}_{ij} &= \left(\mathrm{i}\partial\!\!\!/ - m_\psi\right)\delta_{ij} - g\,\gamma^\mu A^a_\mu T^a_{ij}, \\ D^{\bar{\chi}\chi}_{ff'} &= \mathrm{i}\partial\!\!\!/ \delta_{ff'} - m_{\chi 1}\delta_{f1}\delta_{1f'} - m_{\chi 2}\delta_{f2}\delta_{2f'}, \\ D^{\bar{\psi}\chi}_{if} &= -y_1 X_{i1}\delta_{1f} - y_2 (X^\dagger)_{2i}\delta_{2f}, \\ D^{\bar{\chi}\psi}_{fj} &= (D^{\bar{\psi}\chi})^\dagger_{jf}. \end{aligned}$$

This a block diagonal operator, where the interactions with the Higgs field in the Yukawa terms is explicitly encoded in the off-diagonal sections.

In order to obtain the lattice action, we opt for a discretization of the bosonic sector is done analogously to what we discussed in chapter 3, or in [65, 76]. Configurations for the bosonic sector are then generated accordingly to this action. The Lagrangian of the fermion model on the lattice can be described by the action of the Wilson-Yukawa operator [65, 102, 103, 105] on a vector made of the two fermions species ψ and χ, that we introduced in the continuum discussion. We now discuss a general case with non degenerate parameters, before specializing to the case we simulated, with only two parameters.

The first block diagonal term in the operator is a standard $SU(2)$ Wilson-Dirac operator

$$D^{\overline{\psi}\psi}(x|y)_{ij} = \mathbb{1}\delta_{ij}\delta_{xy} - \kappa_\psi \sum_{\mu=\pm 1}^{\pm 4} (\mathbb{1} - \gamma_\mu)\, U_\mu(x)_{ij}\, \delta_{x+\hat{\mu},y}\ , \tag{5.13}$$

[1] Other gauge-Higgs-fermions theories without Yukawa interactions have been investigated on the lattice [107, 108].

with the links $U_\mu(x)$, where $U_{-\mu}(x) = U_\mu(x-\hat{\mu})^\dagger$, and the definition $\gamma_{-\mu} = -\gamma_\mu$. It must be noted, that with this notation we have the following relation between the hopping and the mass parameter $\kappa_\psi = \frac{1}{2(m_\psi+4)}$. We use Euclidean γ-matrices in the chiral representation, as in [62], and as usual, $\gamma_5 = \gamma_1\gamma_2\gamma_3\gamma_4$.

The second diagonal block is the free Wilson-Dirac operator for the two ungauged fermions χ_1 and χ_2:

$$D^{\bar{\chi}\chi}(x|y)_{ff'} = \mathbb{1}\delta_{ff'}\delta_{xy} - \left(\kappa_{\chi_1}\delta_{f1}\delta_{1f'} + \kappa_{\chi_2}\delta_{f2}\delta_{2f'}\right)\sum_{\mu=\pm1}^{\pm4}\left(\mathbb{1}-\gamma_\mu\right)\delta_{x+\hat{\mu},y}\,, \tag{5.14}$$

where $\kappa_{\chi_f} = \frac{1}{2(m_{\chi_f}+4)}$, $f = 1,2$ are the hopping parameters for the two ungauged fermions.

The off diagonal blocks are Yukawa terms that couple the two different kinds of fermions. Due to the rotation to the Euclidean spacetime those get a minus sign factor. Aside from this change, they are close to their continuum equivalent.

$$\begin{aligned} D^{\bar{\psi}\chi}_{if}(x|y) &= \delta_{xy}\mathbb{1}\left(Y_1X_{i1}\delta_{1f} + Y_2X^\dagger_{i2}\delta_{2f}\right), \\ D^{\bar{\chi}\psi}_{fi}(x|y) &= D^{\bar{\psi}\chi\dagger}_{if}(x|y). \end{aligned} \tag{5.15}$$

In the rest of the chapter, we will set $\kappa_F = \kappa_\psi = \kappa_{\chi_1} = \kappa_{\chi_2}$ and $Y = Y_1 = Y_2$. It must be noted how, because of the rescaling of the Higgs field and the fermion fields, the lattice Yukawa coupling Y_f obeys $Y_f = y_f\sqrt{\kappa}\kappa_F$.

5.2.1. Inverter

The inversion of of the Wilson-Yukawa operator is needed for the calculation of the observables, like introduced in 3.6. In the software we developed, a biconjugate gradient method is employed, the BiCGStab-M, which is fully outlined in appendix A.

In our implementation, the full Wilson-Dirac operator is applied on a vector $v(x)_{\alpha,i}$, which is then the fermionic source discussed in 3.6. The index α is a Dirac index, while the index i refers to the fermionic species, by counting over the gauge components of ψ and the flavor components of χ. Thus, it is a four dimensional Dirac source vector.

The implementation has been cross checked by calculating the trace of the full operator on a smaller volume (hence using $16\times V$ point sources), in the free case $U_\mu(x) = \mathbb{1}$ and with a static Higgs, and then comparing the results for different values of m and Y with ones calculated in an algebraic computation software.

Also parallelization has been included in the inversion algorithm, by using the openMP API to speed up the applications of the Wilson-Yukawa operator, that are necessary for the inversion algorithm. The parallel implementation has been tested against the serial results.

For the following part of this chapter, which is mostly focused on the spectroscopy, we use a single point source located in the origin. With this choice, only 16 inversions are necessary, given the 4 Dirac components and 4 different fermionic species that make up the multifield. It will be shown that this strategy allowed us to reach a clear statistical estimation of the observables in 5.4.

5.2.2. Simulation points and phase diagram

We expect that the computational costs for the simulation of the full theory are very high. This is mostly due to the implementation of the dynamical fermions in the theory, as it has been assessed in previous simulations without additional ungauged fermions in a QCD-like setting [80].

Anyway, we don't expect that the effects of sea fermion quantum corrections will provide a substantial change to the FMS prediction for the spectrum of the theory. Thus, we decided to use a quenched approximation, like it has been described in 3.5, in order to have a first qualitative evaluation of the theory.

The spectrum is calculated by inverting the Wilson-Yukawa operator on configurations with dynamical gauge and scalar fields, generated using the methods of [33, 76]. Also, a subset of gauge fixed configurations in the minimal Landau-'t Hooft gauge, generated with the method detailed in 3.2.1, is included for our calculations. The latter are necessary to compute the propagator of the gauge variant field ψ.

Like mentioned before, the subset of gauge fixed configurations is sensibly smaller than the set of non gauge fixed configurations. While for the former $\mathcal{O}(50)$ configurations are needed, due to reduced statistical noise, for the latter $\mathcal{O}(1000)$ have been used. Given the additional complexity of the gauge fixing procedure, this leads to roughly the same amount of time for creation of the two sets. But, the most computationally costly procedure remains the one related to the fermion observables, due to the size of the Wilson-Yukawa operator and its inversion.

The parameters chosen in the bosonic sector, used for the spectroscopic calculation, are listed in table 5.1. These five sets of parameters have been selected due to their similarity with the Standard Model case. These have also a weak gauge coupling in the last three cases, and a stronger coupling in the first two. It will be shown in 5.4, that the behaviour for all five sets is essentially similar. We haven't done a systematic continuum limit by analyzing lines of constant physics in this work, but having the results reproduced in all of the parameters sets gives us a good hint of their soundness.

After the validity of the inversion procedure has been established, and the parameters for the bosonic section have been provided, a systematic scan of the fermionic sector parameters has been done. In the more general version of the theory we have five parameters, three hopping parameters $\kappa_\psi, \kappa_{\chi_f}$ and two Yukawa couplings Y_f. As already mentioned, we reduced the number of parameters to two by setting $\kappa_F = \kappa_\psi = \kappa_{\chi_f}$

#	β	κ	λ	a^{-1} [GeV]	$m_{0_0^+}$ [GeV]	α_W	$v = \frac{m_{1_3^-}}{\sqrt{\pi\alpha_W}}$ [GeV]
1	2.7984	0.2954	1.328	384	118(9)	0.544	39
2	2.7984	0.2978	1.317	326	129(12)	0.495	64
3	3.9	0.2679	1	509	116(19)	0.140	121
4	5.082	0.249	0.7	636	123(19)	0.170	110
5	5.082	0.2552	0.7	427	131(5)	0.0794	161

Table 5.1.: Parameters of the bosonic sector configurations and related physical observables are listed. Quantities without explicit uncertainties have a statistical error below 1%. The scale was set by fixing the mass of the physical W/Z bosons, hence the custodial vector triplet, to $m_{1_3^-} = 80.375$ GeV. $m_{0_0^+}$ is the mass of the scalar bound state $\mathrm{tr}\left(X^\dagger X\right)$, which is the Higgs boson in our model. The running coupling α_W, and thus the vacuum expectation value v, are in the miniMOM scheme [33, 89] evaluated at 200 GeV. The results are from the largest volumes employed here, 24^4.

and $Y = Y_1 = Y_2$. We only have to analyze a two dimensional phase diagram spanned by the parameters κ_F and Y. We want to obtain values of these two parameters that reproduce the expected physics for the vectorial leptons, but that can still be analyzed with a suitable computational effort, appropriate to the resources we have available.

Many different values of the fermion sector parameters have been investigated in order to attain this goal. As expected, combinations of parameters that resulted in a lower tree level mass required substantially more time for the inversion. This happens in the case with $\kappa \gtrsim 1/8$, which corresponds to three level negative masses. Then we proceeded to analyze smaller values of κ_F, given the much smaller inversion time. On the other hand, choosing a value κ_F sensibly smaller than $1/8$ results in heavier tree level fermion masses, way above one in lattice units. Higher tree level masses then provide easily higher effective masses, hence very small auto correlation lengths. The increased masses could potentially be of an order of magnitude bigger than the masses of the vector and scalar states, but this would result in physical scenario which is not interesting for our purposes. The suitable simulation points we have found are a compromise. These are close to the zero tree level mass point at $\kappa_f = 0.125$, namely at $\kappa_F = 0.11, 0.12$. For the Yukawa coupling we chose $Y = 0.01, Y = 0.05, Y = 0.1$. In an earlier stage of the work, we observed how higher values of the Yukawa coupling provided small effective masses, thus resulting again in long inversion times. This can be expected, through equations (5.7) and (5.10). In principle we can also approach the zero Dirac mass case, thus increase the inversion time of more than one order of magnitude. On the other hand, small values of Yukawa coupling can result in effects which are too weak in order to be detected within our precision, basically leaving the physics unchanged. We also observed that the results are symmetric under a change of the sign of the Yukawa coupling. We then will use only positive values of the couplings in the following.

In order to understand the volume dependence of the observables, we analyzed 5 different lattice volumes, $8^4, 12^4, 16^4, 20^4$ and 24^4. We found that the finite volume effects were negligible already at a volume of 20^4, even for the lattice parameter set with the finer lattice spacing. Thus, the lattice volumes we used are enough for our purposes. We discuss the finite volume behaviour in more detail in B. Then, in total 150 different sets of parameters and volumes have been investigated, which resulted in a little more than 50000 configurations. The biggest statistical noise appears when investigating the hybrid field Ψ, mostly due to its strongly fluctuating scalar insertion. This is expected, and observed in [33, 76].

5.3. Spectroscopic observables

Usual observables in the context of non abelian gauge theories with fermions are hadrons, in the QCD setting. Those are gauge invariant combinations of the fermions of the theory under the SU(3) group. In our case we want to discuss the possibility of gauge invariant combinations of the Higgs particle and the elementary gauged fermion, as a physical realization of the fermion particle. We are interested in a spectroscopic analysis, so the interesting observables for our goals will be given by time sliced two point functions of gauge invariant operators.

In particular, with our setup, we have two possible realization of the bound state operator

$$
\begin{aligned}
O_1(x) &= (\phi^\dagger \psi)(x) \\
O_2(x) &= (\tilde{\phi}^\dagger \psi)(x)\,,
\end{aligned}
\tag{5.16}
$$

which are the two components of the custodial doublet Ψ. Given the symmetry of our setup with only two fermionic parameters, we expect the same result for both. Other two interesting gauge invariant operators are given by the two singlet fermion fields χ_i. We also expect the same result for both the components. We also want to analyze the gauge variant fermion ψ.

On the surface, Ψ and χ have the same quantum numbers. By looking exclusively at them, we then expect to obtain the ground state and the first excited state. If we take into account the possibility of a decay of the first excited state, a Lüscher-type analysis would be required. But the results we obtained show an agreement with the predictions from section 5.1. This is a good indication that the states are stable. It is confirmed in a few cases that decays and scattering states are kinematically forbidden. In the fermion spectrum, only two stable states are observed. We deduce that the Lüscher analysis is not required. Therefore, the straightforward procedure we are going to describe for the discretization of the propagators of the fields is sufficient for our purposes.

In the gauge invariant sector we define a full cross-correlation matrix based on the gauge invariant fields Ψ and χ. We write it by combining the inverted Dirac operator

(5.12) sectors in an appropriate way with the Higgs in the matrix embedding. This result for the cross correlation matrix can be obtained by doing Wick contractions on the hybrid field Ψ and the singlet χ_i two point functions. The matrix is

$$M_{\mathrm{GI}}(x|y) = \begin{pmatrix} X^{\dagger}(x)(D^{-1})_{\bar{\psi}\psi}(x|y)X(y) & (D^{-1})_{\bar{\psi}\chi}(x|y)X(y) \\ X^{\dagger}(x)(D^{-1})_{\bar{\chi}\psi}(x|y) & (D^{-1})_{\bar{\chi}\chi}(x|y) \end{pmatrix}. \tag{5.17}$$

Here the fermionic species have been used to distinguish the sections of the inverted Wilson-Yukawa operator. Those should not be confused with the elements of the operator (5.12). It should be noted that all the elements of the matrix (5.17) have a full Dirac matrix structure. For spectroscopy we use only their trace. In the following we will omit the trace symbol, but we will refer to it when extracting masses.

The off-diagonal blocks of the matrix (5.17) give the possibility of mixing between the bound state Ψ and the elementary fermion χ. This is analogous to the mixing of left handed and right handed particles in the Standard Model [57]. We can get a good sense of the mixing by performing variational analysis with the matrix. Unfortunately, results on the principal correlators of (5.17), with our available statistics, are not sufficient for a quantitative statement, but we obtained sensible information about the system nonetheless. In the following, both the diagonal elements and the eigenvalues from (5.17) will de discussed.

It is possible to supplement the components of the ψ doublet as observables. In order to have non zero matrix elements for it, we must perform the inversion of the propagator on gauge fixed scalar and gauge configurations. We can include them in a matrix of cross correlations between the elementary fermions of the theory, resulting in

$$M_{\mathrm{GF}}(x|y) = \begin{pmatrix} (D^{-1})_{\bar{\psi}\psi}(x|y) & (D^{-1})_{\bar{\psi}\chi}(x|y) \\ (D^{-1})_{\bar{\chi}\psi}(x|y) & (D^{-1})_{\bar{\chi}\chi}(x|y) \end{pmatrix}, \tag{5.18}$$

in analogy to the matrix for the gauge invariant case. To test the FMS mechanism, it will be required to confront the results from the variational analysis of both the matrices (5.17) and (5.18). Naturally, the matrix (5.18) must be computed in a gauge fixed setting, otherwise all its elements will vanish, except for $(D^{-1}_{\bar{\chi}\chi})$. But this is exactly how the FMS mechanism works, and the matrix (5.18) is the first term in the expansion.

But, since the variational analysis proved to be too expensive for analyzing the excited states of (5.17), we will focus on the diagonal elements. They will prove to contain enough information for computing the spectrum. Concerning the propagator of the gauge invariant fields Ψ and χ, it is irrelevant whether it is calculated on a gauge fixed subset of configurations or if it is calculated in the full set of non gauge fixed configurations. We use the results from the set of unfixed configurations for those, and we will use the gauge fixed subset only for the propagator of the gauge variant field ψ.

Given the subset of gauge fixed configurations, where the gauge symmetry and the global custodial symmetry are broken to a common subgroup, like explained in section

5.1, we define a matrix of the extended propagators, which now connects ψ also to the gauge invariant bound state

$$M_{\mathrm{GF}}^{\mathrm{ext}}(x|y) = \begin{pmatrix} X^{\dagger}(x)D^{-1}_{\bar{\psi}\psi}(x|y)X(y) & D^{-1}_{\bar{\psi}\chi}(x|y)X(y) & D^{-1}_{\bar{\psi}\psi}(x|y)X(y) \\ X^{\dagger}(x)D^{-1}_{\bar{\chi}\psi}(x|y) & D^{-1}_{\bar{\chi}\chi}(x|y) & D^{-1}_{\bar{\psi}\chi}(x|y) \\ X^{\dagger}(x)D^{-1}_{\bar{\psi}\psi}(x|y) & D^{-1}_{\bar{\chi}\psi}(x|y) & D^{-1}_{\bar{\psi}\psi}(x|y) \end{pmatrix} . \tag{5.19}$$

We added new off-diagonal matrix elements which represent the gauge dependent overlap of the elementary field ψ and the gauge invariant hybrid field Ψ. A complete understanding of the system can be achieved by performing variational analysis on (5.19). This has not been achieved, given our computational possibilities. Hence, we are interested only in a qualitative understanding of the FMS mechanism for fermions. We thus decided to analyze separately (5.17) and $(D^{-1})_{\bar{\psi}\psi}$. This proved to be sufficient for our purposes.

For spectroscopy, we perform zero momentum projection, like explained in 3.3. In this case it is performed on the inverted matrix elements as

$$M(t) = \sum_{\mathbf{x}\in\Lambda_{\mathbf{x}}} M(0,\mathbf{0}|t,\mathbf{x}) \,. \tag{5.20}$$

This is obtained by performing the inversion with a single point source in the origin. We additionally define the effective masses with the quantity

$$m_{eff}(t) = \log\left(\frac{M(t)}{M(t+1)}\right) . \tag{5.21}$$

Using this notation, we indicate both the diagonal elements of the matrix which provide

$$m^{(i)}_{eff}(t) = \log\left(\frac{M_{ii}(t)}{M_{ii}(t+1)}\right) , \tag{5.22}$$

but also the eigenvalues of the matrix M, the principal correlators λ , with effective masses

$$m^{\lambda,i}_{eff}(t) = \log\left(\frac{\lambda_i(t)}{\lambda_i(t+1)}\right). \tag{5.23}$$

Both the diagonal correlators $M_{ii}(t)$ and the principal correlators $\lambda_i(t)$ show a sum of cosh behavior. A double cosh fit like in equation (3.33) proved to be a good description of many of the correlators analyzed.

5.4. Spectroscopic results

We detail now the results obtained in our investigation. Before discussing the lattice results, we discuss the effects of the quenching approximation on the predictions we detailed in sections 5.1.1 and 5.1.2. Then our spectroscopic findings are shown and discussed. Lastly the volume effects encountered in this work are also treated in appendix B.

5.4.1. Quenching effects on spectroscopic results

In principle, lattice investigations can give more detailed information on the system than the one loop approximation in section 5.1. But while such predictions are derived in the context of fully dynamical fermions, in our lattice setup a quenching of the dynamics of the fermions is performed. In order to compare these tqo, we can either do the FMS analysis in the quenched approximation, or do the lattice calculations in an unquenched setting. This latter option is beyond the scope of this work, and computationally substantially expensive. Another alternative in this context would be to perform partial quenching, by extrapolating the lighter degrees of freedom in an effective field theory setup, but his direction has not been explored in this work. We focus then on analyzing the effects of quenching on the analytical predictions listed in 5.1. A direct translation of the quenched approximation in the continuum formulation is however challenging.

We begin this task by redoing the analytical calculations assuming that the mass of the fermions is much larger than any momentum scale for the internal fermion lines. This works well for all the observables which have fermion loops in the calculation, since it suppresses the fermion fluctuations, thus reproducing the quenching effect. But the analysis for fermion observables is less straightforward. In particular, the mixing effect which we discussed for dynamical fermions in 5.1 is not reproduced in this analysis of the quenched approximation. We can observe this in the pole structure of the propagators $\langle\bar{\chi}\chi\rangle$ and $\langle\bar{\psi}\psi\rangle$. In the dynamical case, we can observe two distinct poles in both propagators, due to the mixing.

But in our modeling of the quenched approximation, we find that each propagator contains only one pole, given by the quenched quantum corrected versions of m_ψ and m_χ, for the propagators of ψ and χ, respectively. We will observe in the next subsection that similar results are obtained from the lattice investigations, giving consistency to this analysis. Then, in the following we will denote these mass terms as M_ψ and M_χ, not to confuse them with the bare parameters.

However, despite the reproduction of some lattice results, our modeling of the quenching effects has some ambiguities in the resumming of the propagators. This is due to the fact, that by treating internal and external fermion lines differently, not only simple poles $\sim 1/(p^2 - m^2)$ are obtained, but also terms like $\sim 1/(p^2 - m^2)^2$. This is mostly due to our somewhat naive modeling of the quenching. More sophisticated methods have been used for the modeling. One of them introduces additional ghosts that cancel the fermion determinant precisely. This one has been used in the context

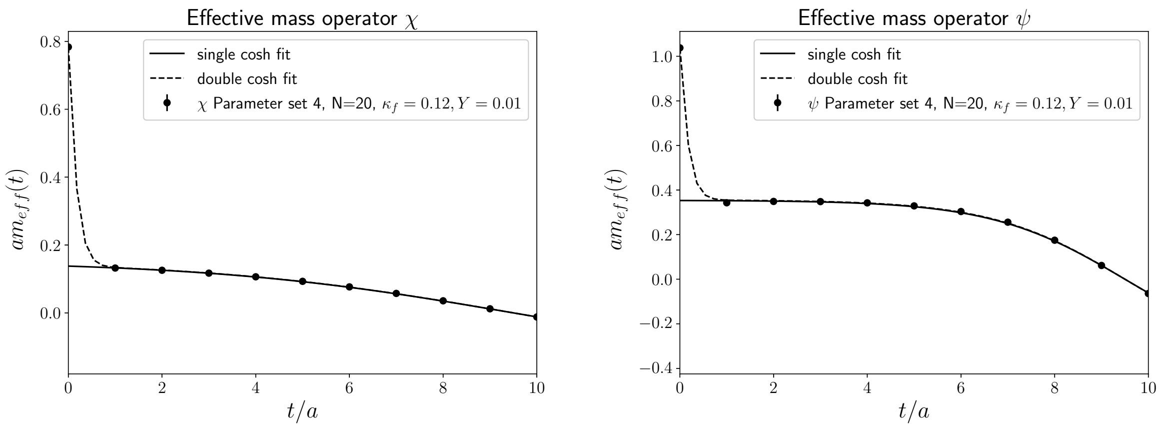

Figure 5.1.: On the left, an example of the effective mass from the gauge-invariant propagator of the χ fermion for system 4 on a 20^4 lattice at $\kappa_F = 0.12$ and $Y = 0.01$. The fit is performed with a two-cosh ansatz. A single cosh fit is also shown alone to emphasize its dominance at long times. Errors are smaller than the symbol size. On the right, an example of the effective mass from the gauge-fixed propagator (5.18) for system 4 on a 20^4 lattice at $\kappa_F = 0.12$ and $Y = 0.01$. The same fitting procedure performed for χ is applied here.

of quenched chiral perturbation theory [109–113]. Unfortunately, when applying this method to our case, the influence of the ghost fields appears only at higher loop terms. Also, unitarity issues have arised in the application of this procedure for our case.

5.4.2. Lattice spectroscopic results

In this section we present the results obtained from our investigations with the methods discussed in 3.3. The values we are interested into are the effective masses of the fermion states that can be extracted from the correlators. We will exclusively list the infinite volume extrapolated masses. Even though, this problem is of small concern, since the values at 20^4 are compatible within statistical uncertainties with the infinite volume result.

The first interesting physical question we analyze is obtaining the ground state with gauge invariant operators. We detail now the pattern we found. Performing the variational analysis on the matrix (5.17), we find that the lowest level is the same as it had been obtained by performing spectroscopy on the ungauged fermion χ alone. More precisely, by analyzing only the lower right part of the matrix. In particular, the correlator of the χ operator has very little statistical noise and it is well described by a double cosh fit of the form (3.33). An example of the effective mass with a fit is shown on the left panel of figure 5.1. We then deduce that the χ operator has an optimal overlap with the ground state. It is then the lightest particle in the fermion channel. Also, being a fermion, it cannot decay into bosons, and thus is stable. It can also be observed how, for this and other channels, the correlator at small times $t/a \lesssim 2$ is affected by a mode with associated mass bigger than 3 lattice units. We deduce that it is a lattice artifact, and we will not consider it in the spectrum.

The next object we discuss is the propagator of the gauge variant field ψ, which is analyzed on the subset of gauge fixed configurations. Due to the gauge dependence [33], we find a small non monotonous behavior of the correlator at short times. At larger times, the effective masses show a well behaved plateau. We then can use a single cosh fit to describe them. We show an example of a fit in figure 5.1. From the plateau we can then extract the mass of the gauge variant fermion ψ. From this result we deduce that there is only a single state in this channel.

Both of the elementary fields have an important overlap with the physical state in their channel, by showing only one mass level. This is in contradiction with the dynamical analysis in 5.1, but can be explained through the effects of the quenched approximation as discussed in 5.4.1. We find also other evidences for this hypothesis. We can analyze then the mixed correlators, which are present as off-diagonal terms in (5.18), which describe the overlap of the elementary fields ψ and χ. The results are computed on the subset of gauge fixed configurations. We then observe in figure 5.2 how the results are compatible with zero for all times bigger than zero. On the other hand, we can also expect that the lack of mixing is due to the particular symmetry structure of the quenched case. Mostly, the two global symmetries acting on the scalar and the χ field are independent at the path integral level. Then, since the interaction does not lock them, in opposition to the dynamical case, this can also explain the results obtained. Also, the spectrum is not affected in this interpretation of the quenching. Consequently, We do not expect deviations in the masses extracted.

We now observe that the mass M_ψ obtained from the correlator of the ψ operator is bigger than the mass M_χ obtained from the correlator of χ. This fits into our interpretation of the theory, since the gauged field receives additional corrections due to the gauge interactions, which are not present at the one loop level for the χ field. This can be observed in equations (5.9).

We list the results for the masses M_χ and M_ψ in table 5.2. We can observe how the values of M_χ do not depend on the gauge coupling. They vary only with the Yukawa parameter, and more indirectly with the parameters of the scalar sector. On the contrary, the mass M_ψ is dependent on the gauge coupling. In particular, the ratio M_ψ/M_χ decreases with smaller gauge couplings, as expected.

We can describe the dependence of mass on the Yukawa couplings by using the fit form

$$aM_\chi = am + r_\chi Y^2 \tag{5.24}$$

$$aM_\psi = am + r_W + r_\psi Y^2 \tag{5.25}$$

which is motivated by the small y expansion in equation (5.9). We provide for this

#	κ_F	Y	aM_χ	aM_ψ	r
1	0.11	0.01	$0.421^{+0.001}_{-0.008}$	0.817(3)	5.7
1	0.11	0.05	0.407(6)	0.77(3)	0.5
1	0.11	0.1	0.353(9)	0.54(1)	0.3
1	0.12	0.01	0.137(1)	0.58(1)	2.1
1	0.12	0.05	0.111(1)	0.45(1)	0.2
1	0.12	0.1	0.044(5)	0.21(1)	0.2
2	0.11	0.01	0.422(3)	0.810(4)	6.1
2	0.11	0.05	0.406(3)	0.75(2)	0.8
2	0.11	0.1	0.352(2)	0.62(3)	0.6
2	0.12	0.01	0.136(1)	0.583(4)	2.6
2	0.12	0.05	0.103(1)	0.49(2)	0.4
2	0.12	0.1	0.032(2)	0.17(1)	0.3
3	0.11	0.01	$0.422^{+0.001}_{-0.006}$	0.674(3)	9.2
3	0.11	0.05	0.407(5)	0.645(2)	0.7
3	0.11	0.1	0.357(3)	0.574(4)	0.2
3	0.12	0.01	0.136(1)	0.426(5)	20.0
3	0.12	0.05	$0.112^{+0.004}_{-0.002}$	0.385(2)	0.4
3	0.12	0.1	0.043(1)	0.24(1)	0.1
4	0.11	0.01	0.422(1)	0.604(2)	17.9
4	0.11	0.05	0.402(2)	0.54(1)	1.2
4	0.11	0.10	0.331(7)	0.43(1)	0.3
4	0.12	0.01	0.136(3)	0.346(2)	767.0
4	0.12	0.05	0.098(1)	0.27(2)	0.8
4	0.12	0.10	0.036(9)	0.09(1)	0.2
5	0.11	0.01	0.422(5)	0.599(2)	10.0
5	0.11	0.05	0.39(1)	0.51(1)	2.0
5	0.11	0.1	0.305(5)	0.35(1)	0.6
5	0.12	0.01	0.126(4)	0.347(6)	315.9
5	0.12	0.05	0.086(2)	0.22(1)	1.3
5	0.12	0.1	0.03(2)	$0.1^{+0.09}_{-0.05}$	0.1

Table 5.2.: The infinite-volume extrapolated results for the ground-state mass in the gauge-invariant and gauge-dependent channel, which are identified with the masses of the ψ and χ fermions, see text. The value of r from (5.26) is given for the 20^4 lattice, see also appendix B.

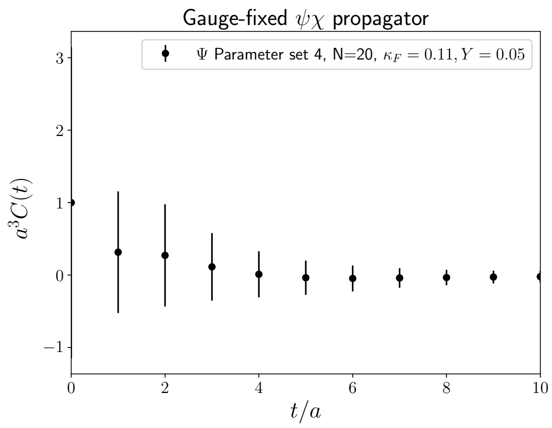

Figure 5.2.: Example of the two point function between ψ and χ for the parameter set 4 on a 20^4 lattice at $\kappa_{\mathrm{F}} = 0.11$ and $Y = 0.05$. By being compatible with zero, it clearly shows a nonoverlap phenomenon.

purpose the parameters obtained from the fits in table 5.3. In principle, we could use the results we obtained from the fits and translate them directly to the mass and r parameters in (5.9). But this is incorrect, since that calculation has been done in the full dynamical theory, while the masses have been obtained in the quenched approximation. Also, the fits have been done with respect to the lattice Yukawa couplings. The continuum Yukawa couplings y have a rescaling factor $\sqrt{\kappa\kappa_F}$. This value is on average ≈ 0.06. By doing the rescaling, one can nonetheless obtain reasonable results.

Lastly, we now analyze the bound state Ψ. This presents more complications with respect to the the states we previously discussed. Firstly, it is significantly noisier than the other two states. But we observed soon that, for the largest and smallest value of the Yukawa coupling, the bound state correlator provides a mass which is compatible with the χ field and the ψ field, respectively. This can be observed in figure 5.3. This result is also confirmed in the variational analysis performed on the matrix (5.17), by showing a second eigenvalue at the mass M_ψ. But the uncertainties found in the variational analysis are in some cases significantly large. Thus requiring more statistics than what we have available, in order to have a reliable results for all the cases we simulated.

Conversely, the picture is less clear when analyzing the intermediate Yukawa coupling case. If one employs spectroscopical methods naively, by performing a two cosh fit, an intermediate value of the mass is obtained, with slightly larger errors. However, one can find a systematic trend of the correlators upon a closer inspection. What is actually happening, is that the bound state correlator is a combination of the correlators of the two elementary states, due to the mixing. We will show that this assumption

#	κ	am	r_W	r_χ	r_ψ
1	0.11	0.423(8)	0.41(2)	-6.9(7)	-28.6(2)
1	0.12	0.1363(5)	0.43(2)	-9.3(5)	-36.1(1)
2	0.11	0.423(4)	0.38(1)	-7.1(2)	-19(3)
2	0.12	0.1334(9)	0.46(2)	-10.3(2)	-41.9(1)
3	0.11	0.423(6)	0.250(3)	-6.5(3)	-9.9(2)
3	0.12	0.136(2)	0.294(4)	-9.3(1)	-18.9(7)
4	0.11	0.424(1)	0.172(6)	-9.3(7)	-16.9(7)
4	0.12	0.131(2)	0.21(1)	-9.7(8)	-25.4(4)
5	0.11	0.421(8)	0.167(6)	-11.7(2)	-24.2(5)
5	0.12	0.119(2)	0.197(2)	-9(2)	-22(9)

Table 5.3.: Fit parameters for the masses $M_{\psi/\chi}$ according to the one-loop motivated fit form (5.24-5.25). Note that the fit is done in the lattice Yukawa coupling Y and not the continuum y.

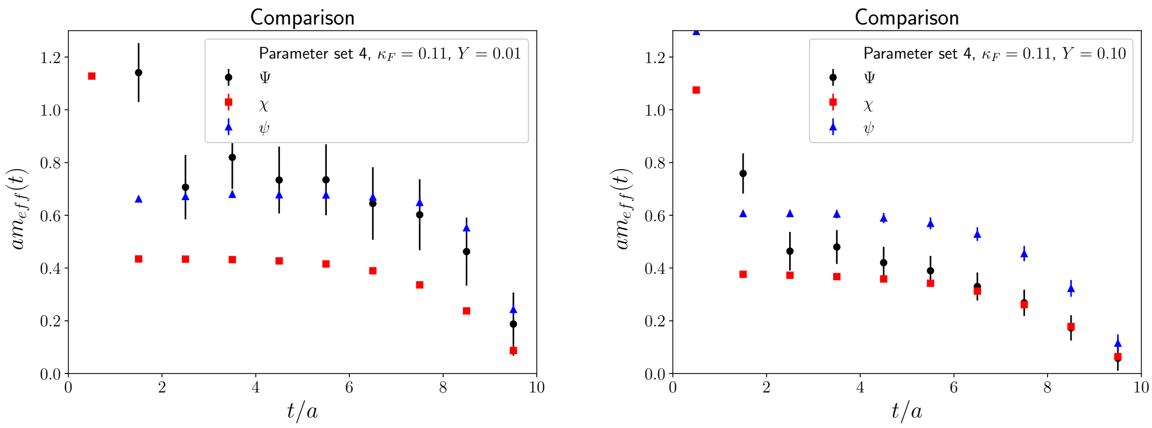

Figure 5.3.: The effective mass of the bound state operator Ψ compared to the effective masses of the elementary fermions ψ and χ at small Yukawa couplings (left panel) and large Yukawa couplings (right panel) for parameter set 4 at $\kappa_F = 0.11$ on 20^4.

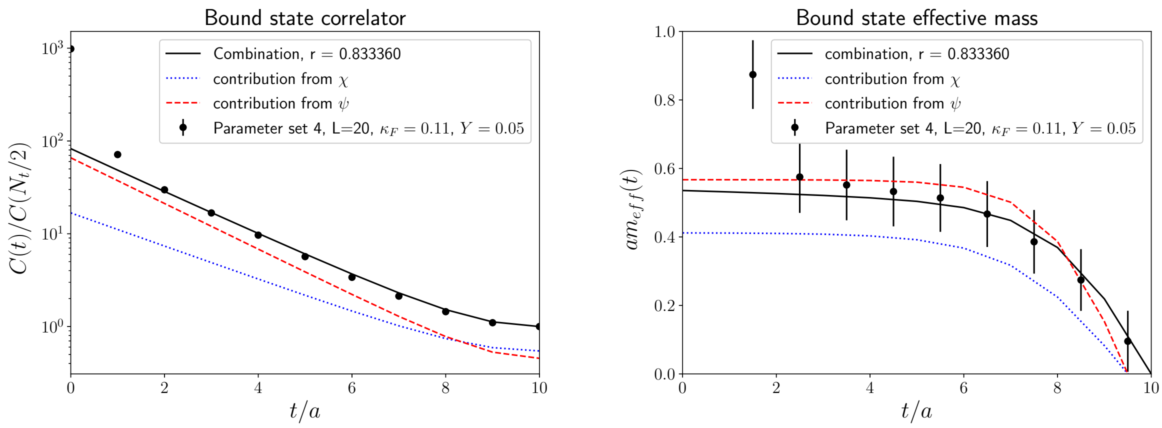

Figure 5.4.: Example of the mixing effect for the bound state correlator (left panel) and the effective mass (right panel) for parameter set 4 on 20^4 at $\kappa_{\mathrm{F}} = 0.11$ and $Y = 0.05$, using the infinite-volume extrapolated masses from table 5.2.

can actually solve the puzzle related to the mass spectrum of the bound state. We then performed single parameter fits based on

$$\frac{C(t)}{C(N_t/2)} = \frac{1}{1+r}\left[\cosh\left(M_\chi(t-N_t/2)\right) + r\cosh\left(M_\psi(t-N_t/2)\right)\right], \tag{5.26}$$

where the parameter r has to be fitted, while the value of the masses in the cosh functions are fixed. The fit is performed at later times, excluding the first two time slices, to avoid the contamination from lattice artifacts. This result is again supported by the variational analysis, which find the second eigenvalue systematically at the mass M_ψ, even if with significantly larger uncertainty. We can then perform the same fit on the data for the bound state Ψ with larger and smaller Yukawa values. We again find that the correlator is well described by 5.26, but the value of r obtained in those cases suggests that the correlator is dominated by either one of the two cosh functions, depending on the value of the Yukawa parameter. This is consistent with the picture we obtained for the bound state data, when comparing them with the elementary correlators, as in figure 5.3. Also, we can look at the matrix elements that couple different flavors of Ψ and χ. We observed a non negligible overlap, indicating a mixing effect, due to the Yukawa interactions.

We show an example of substantial mixing in figure 5.4, for a particular setup. The values of r we obtained from all the parameter sets are listed in table 4.1. We can also note how the mass difference of the the two states is less than the mass of the scalar singlet, or twice the mass of the vector triplet. Then, the heavier state cannot decay into the ground state, making it stable.

When analyzing the r parameter, we have to take into account some subtleties. Those stem from the fact that the bound state effective mass is significantly noisier than the elementary state ones. But, according to equation (5.26), the upper fluctuation of the effective mass is bounded by the error of the the larger mass M_ψ. Analogously, the lower fluctuation of the bound state effective mass, is limited by the error of the smaller mass M_χ. Then, when one tries to find the uncertainty related to the parameter r, one should take into account the relative errors for the input masses in (5.26) which are larger than the ones listed in 5.2. In principle, the error band should be of the same relative magnitude as the one of the bound state. It is evident that this procedure would be artificial. Furthermore, it would be even more complicated due to the closeness of the masses M_ψ, M_χ. This is reason for showing only an optimal result of r in table 5.2, obtained by varying the parameter while keeping the elementary masses fixed, and going through the error bands of the effective masses. A fit example with relative optimal value of r is shown in figure 5.4.

Our results show clearly that the bound state operator can be described as a mixture of the two mass states, which are obtained from the correlators of the elementary fields ψ and χ. Although this picture is compatible with the FMS description, the quenched analysis introduces some conceptual difficulties. In section 5.1 we showed that at leading order in the FMS expansion, we have a projection of the on shell properties of Ψ onto the gauge variant fermion ψ, when using dynamical fermions. This would then result in Ψ having an overlap with two mass eigenstates, and a mixing angle between Ψ and χ which is the same as the one between ψ and χ in a perturbative gauge fixed setup. From our current understanding concerning the effects of the quenched approximation on the system, we know that it does not allow the mixing between the elementary states. Then, one would expect that the bound state is only described by a mass level with mass M_ψ, as it would stem from a naive expansion of the Ψ operator.

But actually, only a quenched full analysis of the FMS mechanism would resolve this matter. We already performed a first quenched continuum analysis for the elementary fields, but we decided that a detailed analysis for the bound state would be beyond the scope of this work. We then conjecture that the mixing predicted by the FMS mapping gets altered by the quenching in a way that cannot be predicted by a simple leading order analysis. Also, higher order terms can allow for intermediate states that are described by the mass levels M_χ and M_ψ. This can then cause the overlap with both the states, as observed. The relative ratio between the states is also dependent on the Yukawa coupling, as confirmed by our data. Lastly, a lattice investigation contains nonperturbative information which might not be captured within the perturbative analysis in the FMS mechanism. On the other hand, only an unquenched lattice analysis can reveal whether these effect exist, and show other modifications to the mixing.

We can now conclude that the results we presented support that the physical spectrum is obtained by the correlators of the χ fermion, and by a bound state made of the scalar field X and the gauge variant fermion ψ. The masses are correctly predicted

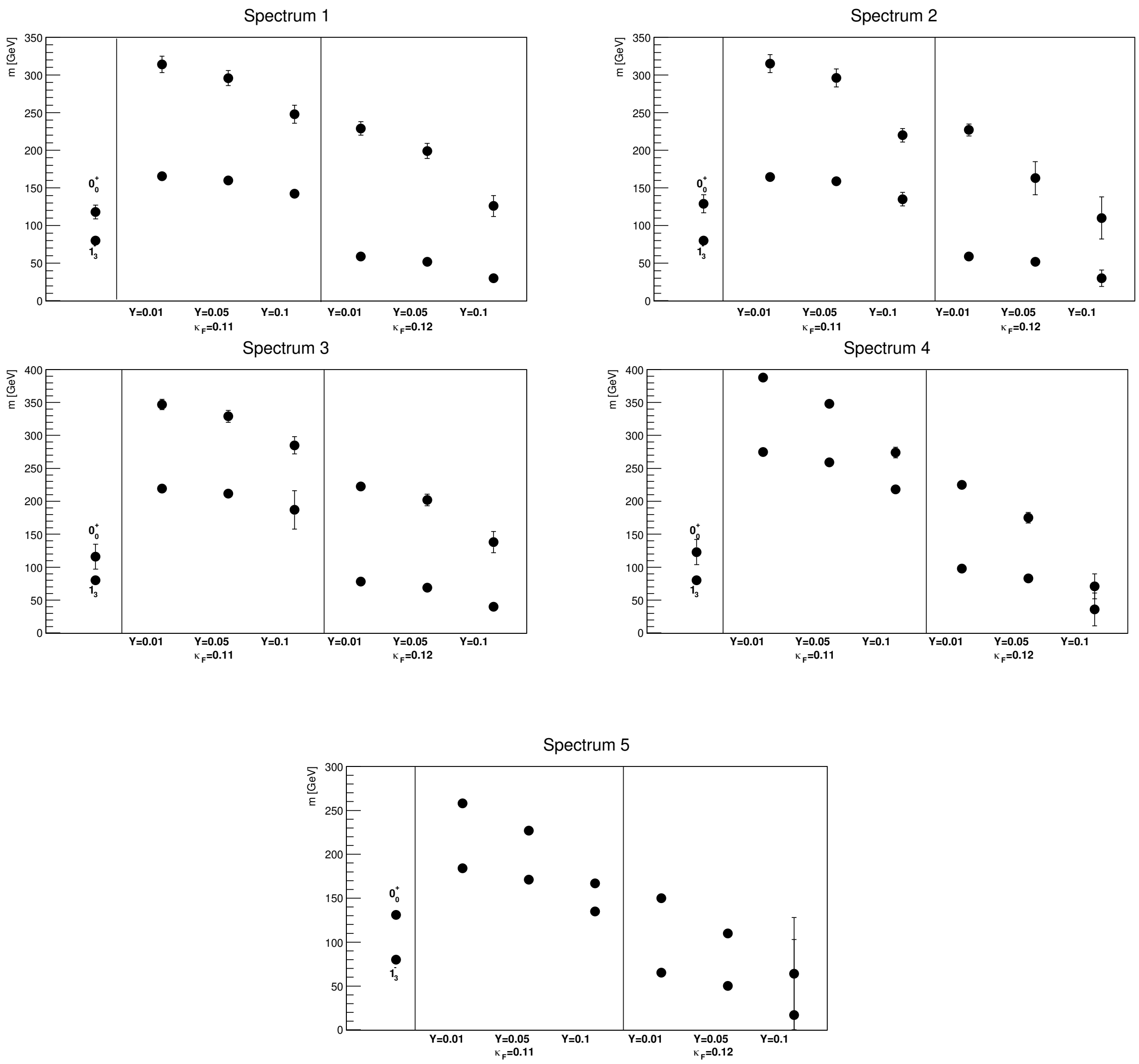

Figure 5.5.: Spectra for all setups. The bosonic sector is fixed, and plotted to the left, while the two states identified in the fermion channel, each being a doublet, are plotted for different parameter values to the right.

by the FMS mechanism, and correspond to the ones obtained in the analysis of the elementary fermion correlator, both gauge-variant and gauge-dependent. We can then provide the physical spectra for the five parameter sets analyzed in figure 5.5. Again, the spectrum is consistent with the FMS description both in the bosonic, and fermion sectors. We can also observe how a suitable choice of parameters can allow us to simulate the entire range of masses for the fermions, from very heavy to very light. In principle, there are no restrictions in tuning κ_f and Y in order to obtain the full range of fermion masses of the Standard Model, from the neutrino to the top quark. And also including heavier masses, to study beyond Standard Model theories.

6. Conclusions

Symmetries are the key element of a physical theory. In this work we assumed that the non abelian gauge symmetries cannot be spontaneously broken, and we classified states by using only operators which are invariant under such symmetries. We then focused on two important cases, that provide two key ingredients of the modern description of particle physics. The first case, analyzed in chapter 4, showed a way to obtain a massless vector state which is also a composite gauge invariant bound state, paving the way for an alternative construction of the photon in beyond standard model theories. In the second case, detailed in chapter 5, we provided a description of the fermions, which constitute all the matter known in the universe, as composite bound states with an Higgs valence component. In particular, a lattice implementation allowed us to analyze the spectral properties of the fermionic bound state.

In both cases, we first analyzed the bound state using the FMS mechanism, expanding over the classical vacuum expectation value of the Higgs, and obtaining a prediction for the on shell properties of the composite operators. We then confirmed both predictions by using nonperturbative lattice methods.

To recapitulate chapter 4, we have then obtained important numerical validations for a massless vector state in the Brout-Englert-Higgs phase of the SU(2) theory with a Higgs in the adjoint representation. This result is of fundamental importance in the construction of a great unified theory in a manifestly gauge invariant way. It also shows how it is possible to obtain a massless state in a theory with a broken global symmetry which is not a Goldstone boson. On the other hand, a determination of the scalar channel in the same theory would be an important continuation of the investigations concerning a gauge invariant construction of a GUT. It would also help other investigations on the vector channel. Further, the absence of massive states in our results is a sign of the necessity of a more thorough examination.

Results obtained in the fermionic theory of chapter 5 are evidence that the FMS mechanism works also for fermions in Higgsed gauge theories. Summarizing, we find that the physical fermion field is a combination of the ungauged fermion and of the fermion-Higgs bound state. The implications for the phenomenology of the near future colliders are substantial. Since the framework in which we obtained these results is basically the standard model, a discovery is guaranteed. Either the Higgs component is found, or there is a new mechanism that is acting, which would then be a potential signal of new physics.

These results continue a cycle of nonperturbative lattice tests of the FMS mechanism, which always proved to be successful in describing the underlying field theory of Higgs theories. Adding massless vector states and leptons is a fundamental contribution, given their importance in the phenomenology of particle physics.

Since the FMS mechanism is an integral part of the Higgs physics, it appears evident, after all the nonperturbative validations, how it should be taken into account for the phenomenological calculations in the future. Despite the first successful preliminary tests [57, 58], this is not an easy task. It would require firstly a dynamical fermion simulations, as an ideal continuation of the . In principle doing so would provide us enough information for obtaining the form factors, which are an ideal next goal in this line of research. We thus would get some first insight about the anomalous coupling of the Z, and also about the radius of the fermion-Higgs bound state. These two physical questions are accessible at the future linear collider that have been proposed. A continued effort both in the merely field theoretical direction, with more refined lattice simulations, and in the phenomenological analysis of the future colliders data is then of extreme importance and necessity, given the extent of the results discussed here about the gauge invariance of physically observable operators.

Appendices

Appendix A.

Details on the inversion algorithm

We write here explicitly the BiCGstab-M algorithm as formulated in [75]. The algorithm is used to solve the algebraic problem

$$(A+\sigma)x - b = 0\,.$$

In our implementation, we decided to vary the hopping parameter κ while keeping $\sigma = 1$. Given the initial residual r_0, the following sequences are realized

$$\begin{aligned} r_n &= Z_n(A)R_n(A)r_0 \\ w_n &= Z_n(A)R_{n-1}(A)r_0 \\ s_n &= Q_n(A)R_n(A)r_0\,, \end{aligned}$$

where $Z_n(z)$ and $Q_n(z)$ are the BiCG polynomials [114] and

$$R_n(z) = \prod_{i=1}^{n}(1-\chi_i z)\,.$$

The parameters χ_i are obtained with the minimization of the residuals. The shifted sequences are realized as

$$\begin{aligned} r_n^\sigma &= \zeta_n^\sigma \rho_n^\sigma Z_n(A)R_n(A)r_0\,, \\ w_n^\sigma &= \zeta_n^\sigma \rho_n^\sigma Z_n(A)R_n(A)r_0\,. \end{aligned}$$

The update of the solution, without the shift, is performed in the following form

$$x_{n+1} = x_n - \beta_n s_n + \chi_n w_{n+1}$$

The algorithm, which allows for a nontrivial shift parameter σ, is then realized as

$$
\begin{aligned}
& We\ \ set\ \ the\ \ following\ \ initial\ \ variables: \\
& x_0^\sigma = 0, r_0 = s_0^\sigma = b, \beta_{-1} = \zeta_{-1}^\sigma = \zeta_0^\sigma = \rho_0^\sigma = 1, \alpha_0^\sigma = 0, \\
& w_0\ \ so\ \ that\ \ \delta_0 = w_0^\dagger r_0 \neq 0, \phi_0 = w_0^\dagger A s_0/\delta_0 \neq 0 \\
& \text{for}\ \ i = 0, 1, 2, \cdots, n_{iter} \\
& \quad \beta_i = -\frac{1}{\phi_i} \\
& \quad \beta_i^\sigma = \beta_i \frac{\zeta_{i+1}^\sigma}{\zeta_i^\sigma} \\
& \quad \alpha_i^\sigma = \alpha_i \frac{\zeta_i^\sigma \beta_{i-1}^\sigma}{\zeta_{i-1}^\sigma \beta_{i-1}} \\
& \quad \zeta_{i+1}^\sigma = \frac{\zeta_i^\sigma \zeta_{i-1}^\sigma \beta_{i-1}}{\beta_i \alpha_i (\zeta_{i-1}^\sigma - \zeta_i^\sigma) + \zeta_{i-1}^\sigma \beta_{i-1}(1 - \sigma\beta_i)} \\
& \quad w_{i+1} = r_i + \beta_i A s_i \\
& \quad \chi_i = \frac{(Aw_{i+1})^\dagger w_{i+1}}{(Aw_{i+1})^\dagger A w_{i+1}} \\
& \quad \chi_i^\sigma = \frac{\chi_i}{1 + \chi_i \sigma} \\
& \quad \rho_{i+1}^\sigma = \frac{\rho_i^\sigma}{1 + \chi_i \sigma} \\
& \quad r_{i+1} = w_{i+1} - \chi_i A w_{i+1} \\
& \quad x_{i+1}^\sigma = x_i - \beta_i^\sigma s_i + \chi_i^\sigma \rho_i^\sigma \zeta_{n+1}^\sigma w_{n+1} \\
& \quad \delta_{i+1} = w_0^\dagger r_{i+1} \\
& \quad \alpha_{i+1} = -\frac{\beta_i \delta_{i+1}}{\delta_i \chi_i} \\
& \quad s_{i+1} = r_{i+1} + \alpha_{i+1}(s_i - \chi_i A s_i) \\
& \quad s_{i+1}^\sigma = \zeta_{i+1}^\sigma \rho_{i+1}^\sigma r_{i+1} + \alpha_{i+1}^\sigma \left(s_i^\sigma - \frac{\chi_i^\sigma}{\beta_i^\sigma} (\zeta_{i+1}^\sigma \rho_i^\sigma w_{i+1} - \zeta_i^\sigma \rho_i^\sigma r_i) \right) \quad \sigma \neq 0 \\
& \quad \phi_{i+1} = \frac{w_0^\dagger A s_{i+1}}{\delta_{i+1}}
\end{aligned}
$$

Appendix B.

Infinite volume behavior for fermion observables

We give some details about the volume dependence effect in the investigation discussed in chapter 5. Depending on the lattice parameters, these can be relevant. Especially when the comparison of masses of different states is needed. We therefore analyze the volume behaviour for the masses obtained. We use a fitting ansatz of the type [115]

$$m_N = m_\infty + \frac{a}{N} e^{-bN} . \tag{B.1}$$

Here the lattice extension N is used to determine the infinite-volume mass m_∞. This is done using the volumes of 8^4 to 20^4, on which the change is largest. We use results from the 24^4 lattices as a confirmation of fit results on the smaller lattices. We show as an example the finest lattice we simulated, which then has the most severe volume effects, in figure B.1. The results on the masses can confirm that we see already on the 20^4 lattice an infinite-volume behavior. In the previous section we then used only the infinite-volume masses [2].

The dependence for the r values appears far stronger. Also, we can see in B.1 that the behaviour is different, based on whether one uses the finite volume masses or the infinite volume extrapolated ones in the extraction of r. Also, conversely to the mass case, the Lüscher ansatz does not work. From a first analysis, it is evident that the results decrease for increasing volumes quicker than $1/N$. In the case with the masses from the finite volume fits, a quadratic fit can be performed, and it suggests a finite value above zero. We are not worried by the possibility that the results converge to a zero value. This case would suggest that the oscillations are predominant for intermediate Yukawa values, or at least that these have a strong volume dependence.

[2]Note that the values in table 5.1 are not extrapolated to infinite volume.

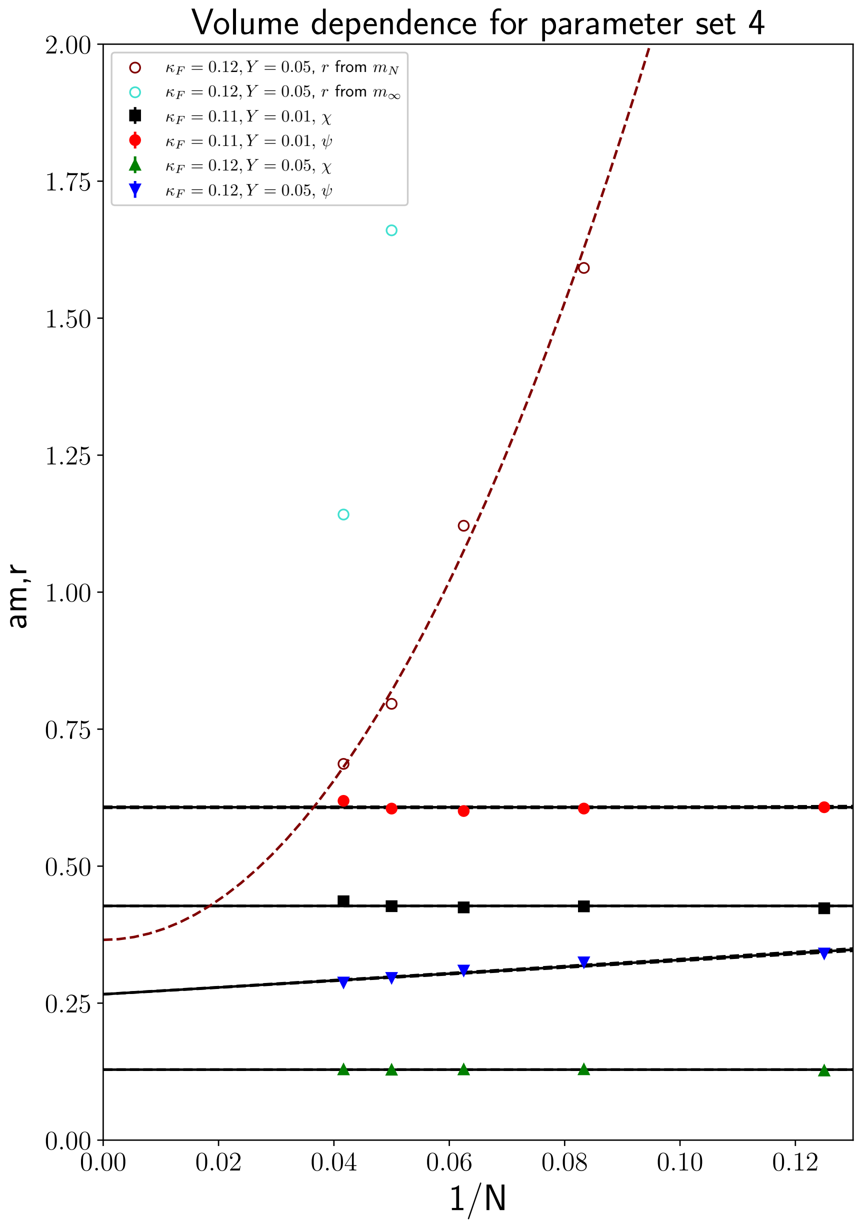

Figure B.1.: The volume dependence of some example non overlapping mass values, and the r quantity from (5.26), for the parameter set 4 are shown. The values of r are shown only in case there is an appreciable mixing between the states. A quadratic fit is also shown for the case with extrapolation with the masses at finite volume. For the masses a Lüscher type fit is shown.

Appendix C.

Lattice Sinh-Gordon model

This section describes my work at the University of Edinburgh on the Sinh-Gordon model, under the supervision of Prof. Luigi del Debbio.

C.1. Introduction

Our goal is to simulate a lattice regularized version of the sinh-Gordon model [116]. This model is the simplest example of an interacting field theory. It has only one particle in the spectrum and it is integrable. This means its S-matrix is known analytically. Furthermore it shows a remarkable duality property. Results obtained with the thermodynamical Bethe ansatz give interesting properties. For instance a mass formula is obtained [117]. These results also bring some dilemmas. In principle, the mass formula is not compatible with the duality of the theory. Also there is not a single UV behaviour of the theory, but there can be many values of the charge at infinity. A lattice analysis can be helpful to give numerical support to many of this nonperturbative results. In particular we focus on the analytical mass formula, by doing lattice perturbation theory and then lattice spectroscopy for comparison.

In section C.2 we give some information about of the theory in the continuum. In section C.3 we describe the lattice setup we implemented, and in section C.4 we show the results for lattice perturbation theory we obtained. In section C.5 we then use lattice spectroscopy and we compare our results to the continuum ones. Lastly, in section C.6 we discuss conformal bosonic theory on the lattice, and question the possibility of the Sinh-Gordon model becoming conformal over the self dual point.

C.2. Properties of Sinh-Gordon model in the continuum

The action that defines the model is

$$\mathcal{A} = \int d^2x \left\{ \frac{1}{2} \sum_{\nu} (\partial_\nu \phi)^2 + 2\mu \cosh(b\phi) \right\} . \tag{C.1}$$

The sinh-Gordon model has many remarkable properties. It is integrable, has a unique vacuum and the simplest symmetry Z_2: $\phi \to -\phi$. Due to the integrability of the model, the S-matrix is factorizable into 2 particle S-matrices, and it is known analytically

$$S(\theta) = \frac{\sinh(\theta) - i\sin(\pi\beta)}{\sinh(\theta) + i\sin(\pi\beta)}\,. \tag{C.2}$$

Here θ is the rapidity, and it is related to the energy and the momentum by

$$E = m\cosh(\theta)\ ;\ P = m\sinh(\theta)\,. \tag{C.3}$$

Here we introduced the function $\beta(b)$ defined by

$$\beta(b) = \frac{b^2}{8\pi}\frac{1}{1+b^2/8\pi}\,. \tag{C.4}$$

This result is obtained by analytic continuation from an analogous calculation in the sine-Gordon model, valid in the "Coleman bound", namely $b < \sqrt{8\pi}$. It is proven that the theory doesn't develop a mass gap over this bound.

This formula reveals an interesting property, which is not manifest in the Lagrangian, a duality symmetry given by

$$b/\sqrt{8\pi} \to \sqrt{8\pi}/b\ ;\ \beta \to 1-\beta\,. \tag{C.5}$$

The duality transformation does not change the position of the zeroes in the S-matrix.

C.2.1. Observables

Calculations of observable quantities have been made for this model. The action used in these calculations is

$$\mathcal{A} = \int d^2x \left\{ \frac{1}{16\pi}\sum_{\nu}(\partial_\nu\phi)^2 + 2\mu\cosh(b\phi) \right\} \tag{C.6}$$

This action is obtained through the redefinition $\phi \to 1/\sqrt{8\pi}\phi$, and by rescaling the coupling accordingly. In this way the Coleman bound is at $b = 1$, simplifying the calculations.

A notable example is obtained for the quantity $e^{a\phi}$ [118], namely

$$\begin{aligned}\langle e^{a\phi}\rangle = &\left[\frac{m\Gamma(\frac{1}{2+2b^2})\Gamma(1+\frac{b^2}{2+2b^2})}{4\sqrt{\pi}}\right]^{-2a^2} \times \\ &\exp\left\{\left\{\int_0^\infty \frac{dt}{t}\left[-\frac{\sinh^2(2abt)}{2\sinh(b^2t)\sinh(t)\cosh((1+b^2)t)} + 2a^2e^{-2t}\right]\right\}\right\},\end{aligned} \tag{C.7}$$

where [117]

$$m = \frac{4\sqrt{\pi}}{\Gamma(\frac{1}{2+2b^2})\Gamma(1+\frac{b^2}{2+2b^2})}\left[-\frac{\mu\pi\Gamma(1+b^2)}{\Gamma(-b^2)}\right]^{\frac{1}{2+2b^2}} . \tag{C.8}$$

The last equation gives the renormalized particle mass in terms of the bare parameter μ and the coupling b. It is remarkable that this formula does not have the duality symmetry, and that the mass goes to zero for $b = 1$ (which is equivalent to the Coleman bound, after the rescaling of $1/8\pi$ of the kinetic term). It has been obtained by analytic continuation from a mass formula for the breather in the Sin-Gordon model spectrum, valid for $b < 0.5$.

After the redefinitions $g = b\sqrt{8\pi}$ and $m_0 = 4b\sqrt{\pi\mu}$, the square of the renormalized mass can be expanded in g as

$$\begin{aligned} m^2 =& m_0^2 + \frac{m_0^2 g^2}{8\pi}\left(-\gamma_E + \psi(1/2) + 4\log 2 - \log m_0^2\right) + \\ &+ \frac{m_0^2 g^4}{384\pi^2}\Big[3\gamma_E(2+\gamma_E) - \pi^2 - 24(1+\gamma_E - 2\log 2)\log 2 + \\ &\qquad + 3\psi(1/2)\left(-2 - 2\gamma_E + 12\log 2 + \psi(1/2)\right) + \\ &\qquad + 6\log m_0^2\left(1+\gamma_E - 4\log 2 - \psi(1/2)\right) + 3\log^2 m_0^2\Big] + O(g^6) , \end{aligned} \tag{C.9}$$

where γ_E is the Euler–Mascheroni constant and the digamma function $\psi(x)$ is the logarithmic derivative of the gamma function.

We can also obtain a dimensionless quantity which is easy to estimate. It is given by

$$R = \frac{\langle e^{r\phi}\rangle \langle e^{s\phi}\rangle}{\langle e^{t\phi}\rangle \langle e^{u\phi}\rangle} . \tag{C.10}$$

The coefficients have to satisfy $r^2 + s^2 = t^2 + u^2$. When this condition is satisfied, all factors related to the scaling dimension cancel out, leading to the prediction

$$R = \exp\int_0^\infty \frac{dz}{z} - \left\{\frac{\sinh(2rbz)^2 + \sinh(2sbz)^2 - \sinh(2tbz)^2 - \sinh(2ubz)^2}{2\sinh(b^2 z)\sinh(z)\cosh((1+b^2)z)}\right\} . \tag{C.11}$$

The integral, owing to the aforementioned condition, is convergent for small values of z, while it can diverge at infinity for some values of the vertex parameter r. To avoid divergences, one must satisfy

$$r < \frac{b^2+1}{2b} . \tag{C.12}$$

This condition is obtained by observing the limit for z that goes to infinity in the integrand, and it is always satisfied for $r < 1$. For simulations we will take this bound into account, in order to avoid problems related to divergences.

C.3. Lattice setup

The lattice action (after rescaling the field as $\phi \to 1/\sqrt{8\pi}\phi$) is

$$\mathcal{A} = a^2 \sum_x \left[\frac{N_d}{8\pi}\phi(x)^2 + \frac{1}{8\pi}\sum_\nu \phi(x)\phi(x+a\nu) + 2\mu\cosh(b\phi(x)) \right] . \tag{C.13}$$

We can absorb a^2 in the dimensioned parameter μ by defining $\hat{\mu} = a^2\mu$. We simulate the model using the grid code, based on a HMC algorithm. We will use $a = 1$ as usual for the rest of the section. The forces for the HMC algorithm are given by

$$F(x) = \frac{N_d}{4\pi}\phi(x) + \frac{1}{4\pi}\sum_\nu \phi(x+\nu) + 2b\mu\sinh(b\phi(x)) . \tag{C.14}$$

For the simulations a lattice size of 256^2 has been used.

C.4. Comparing lattice perturbation theory with the continuum

Naive dimensional analysis shows that both the field and the parameter b are dimensionless, while μ has a dimension 2 in energy. Labeling the lattice parameter with an hat, we have $\hat{\mu} = a^2\mu$. Naively the continuum limit is obtained with $\hat{\mu} \to 0$. To compare lattice results with the continuum analytic results, we need to find the lines of constant physics.

We can get a good hint about them using lattice perturbation theory. Calculating the perturbative expansion of the two point function and setting the pole position equal to the mass gives a relation between $\hat{\mu}$ and b. This can be checked non-perturbatively doing lattice spectroscopy and checking the value of the physical mass obtained.

The theory has an infinite number of interaction terms

$$\mathcal{A} = \sum_x \frac{1}{2}\sum_\nu (\delta_\nu\phi(x))^2 + \frac{\hat{m}_0^2}{g^2}\cosh(g\phi) = \tag{C.15}$$

$$= \sum_x \left[N_d\phi(x)^2 + \sum_\nu \phi(x)\phi(x+\nu) + \frac{\hat{m}_0^2}{2}\phi(x)^2 + \frac{\hat{m}_0^2 g^2}{4!}\phi(x)^4 + \frac{\hat{m}_0^2 g^4}{6!}\phi(x)^6 + \dots \right] \tag{C.16}$$

which leads to an infinite number of Feynman rules for n-point vertex, with n even, namely

$$V_n = -\hat{m}_0^2 g^{n-2} . \tag{C.17}$$

We chose this action since it doesn't have a factor of the coupling in the bare mass. There is a relation to the b and μ parameters given by

$$g = \sqrt{8\pi} b \; ; \; m_0 = 4b\sqrt{\pi\mu} \,. \tag{C.18}$$

We can expand the two point function in perturbation theory over powers of the coupling g^2. In the continuum both the coupling and the field do not renormalize. There is only a multiplicative renormalization of the mass parameter, given by (C.8). Setting the two point function

$$D(p^2) = \frac{1}{\hat{p^2} + m^2} + O(\hat{p^2} + m^2) \tag{C.19}$$

for $p^2 \to -m^2$ one obtains

$$m^2 = m_0^2 + \frac{1}{2} m_0^2 g^2 T(m^2) + \frac{1}{8} m_0^2 g^4 T(m^2)^2 + O(g^6) \tag{C.20}$$

$$= m_0^2 (1 + \frac{1}{2} g^2 T(m^2) + \frac{1}{8} g^4 T(m^2)^2) + O(g^6) \tag{C.21}$$

We have obtained the tadpole integral

$$T(m^2) = \int_{-\pi/a}^{\pi/a} \frac{d^2k}{(2\pi)^2} \frac{1}{\hat{k^2} + m^2} \tag{C.22}$$

where $\hat{k^2} = \hat{k_x}^2 + \hat{k_y}^2$ and $\hat{k} = 2/a \sin(ka/2)$. The symmetry factors $1/2$ and $1/8$ are obtained by multiplying the factors $1/4!$ and $1/6!$ of the action by the number of possible connections between vertices and external legs when constructing the tadpole and double tadpole integral. It immediately appears that there must be a logarithmic divergence when one substitutes $l_\mu = ak_\mu$ and takes the limit $a \to 0$.

We can do a similar operation for the coupling, by setting the full four point function with zero external momentum equal to the renormalized coupling constant. We obtain

$$g_R^2 = g^2 + \frac{\hat{m}^2 g^4}{2} T(m^2) + \frac{3\hat{m}^4 g^4}{2} V(m^2) + O(g^6) \tag{C.23}$$

where $V(m^2)$ is a vertex correction integral. We invert this relation as well, obtaining

$$g^2 = g_R^2 \left[1 - \left(\frac{3\hat{m}^2}{2} T(m^2) - \frac{3\hat{m}^4}{2} V(m^2) \right) g_R^2 \right] + O(g_R^4) \tag{C.24}$$

We observe then that since $\hat{m}^2 = a^2 m^2$, it is evident that $g_R^2 = g^2 + \mathcal{O}(a^2)$, thus resulting in no renormalization correction in the continuum limit. We can substitute $\hat{m}_0^2$ with $\hat{m}^2$ in the integrals with an error of order g^6. We invert the series

$$m_0^2 = m^2 \left[1 - \frac{1}{2} g^2 T(m^2) + \left(\frac{1}{8} T(m^2)^2 + \frac{3\hat{m}^2}{4} (T^2 + \hat{m}^2 V T) \right) g^4 \right] + O(g^6) \,. \tag{C.25}$$

This formula gives us, given a physical value of the mass m, the bare parameter m_0 for a fixed value of the lattice spacing a. We still need to evaluate the tadpole and the vertex correction integrals.

C.4.1. Evaluation of the integrals

We substitute $l_\mu = ak_\mu$ in (C.22) obtaining

$$T(m^2) = \int_{-\pi}^{\pi} \frac{d^2 l}{(2\pi)^2} \frac{1}{\hat{l}^2 + a^2 m^2} = I_1(a^2 m^2)\,. \tag{C.26}$$

The integral has infrared divergences for $a \to 0$. We define, by introducing for simplicity the variable ξ

$$I_n(\xi^2) = \int_{-\pi}^{\pi} \frac{d^2 l}{(2\pi)^2} \frac{1}{(\hat{l}^2 + \xi^2)^n}\,, \tag{C.27}$$

where ξ is supposed to be small, since we want to set it equal to am. We can evaluate numerically the value of I_1 for $a \to 0$ by dividing the integral in two parts, one within a small radius ρ, and the other outside. We obtain

$$\begin{aligned} I_1(\xi^2) &= \int_{|l|<\rho} \frac{d^2 l}{(2\pi)^2} \frac{1}{l^2 + \xi^2} + \int_{|l|>\rho} \frac{d^2 l}{(2\pi)^2} \frac{1}{\hat{l}^2 + \xi^2} \\ &= \frac{1}{4\pi}\frac{\xi^2}{\rho^2} - \frac{1}{4\pi} \ln\left(\frac{\xi^2}{\rho^2}\right) + \int_{|l|>\rho} \frac{d^2 l}{(2\pi)^2} \frac{1}{\hat{l}^2} - \xi^2 \int_{|l|>\rho} \frac{d^2 l}{(2\pi)^2} \frac{1}{(\hat{l}^2)^2} + O(\xi^4) \\ &= Z_0 - \xi^2 C_0 - \frac{1}{4\pi} \ln\left(\xi^2\right) + O(\xi^4)\,. \end{aligned} \tag{C.28}$$

We have expanded both parts in powers of a^2, by defining $\xi^2 = a^2 m^2$. We also introduced the following quantities

$$Z_0 = \lim_{\rho \to 0} \int_{|l|>\rho} \frac{d^2 l}{(2\pi)^2} \frac{1}{\hat{l}^2} + \frac{1}{4\pi} \log\left(\rho^2\right) = 0.275794\,, \tag{C.29}$$

$$C_0 = \lim_{\rho \to 0} \int_{|l|>\rho} \frac{d^2 l}{(2\pi)^2} \frac{1}{(\hat{l}^2)^2} - \frac{1}{4\pi\rho^2}\,. \tag{C.30}$$

The first quantity has been obtained with numerical integration. In the case of the tadpole integral, the quantity C_0 is not influential for $a \to 0$, so we have the result

$$T(a^2 m^2) = Z_0 - \frac{1}{4\pi} \ln\left(a^2 m^2\right) + O(a^2)\,. \tag{C.31}$$

For the evaluation of the vertex corrections, we note that

$$V(m^2) = \int_{-\pi/a}^{\pi/a} \frac{d^2k}{(2\pi)^2} \frac{1}{(\hat{k}^2 + m^2)^2} = a^2 I_2(a^2m^2)\,. \tag{C.32}$$

We use the relation

$$I_2(\xi^2) = -\frac{d}{d\xi^2} I_1(\xi^2) = C_0 + \frac{1}{4\pi\xi^2} + O(\xi^2)\,. \tag{C.33}$$

We have the final result:

$$m_0^2 = m^2 \left[1 - \frac{1}{2} g^2 I_1(a^2m^2) + \left(\frac{1+6\hat{m}^2}{8} I_1(a^2m^2) + \frac{3\hat{m}^4 a^2}{4} I_1(a^2m^2) I_2(a^2m^2)\right) g^4\right] + O(g^6) \tag{C.34}$$

$$g^2 = g_R^2 \left[1 - \left(\frac{\hat{m}^2}{2} I_1(a^2m^2) - \frac{3\hat{m}^4 a^2}{2} I_2(a^2m^2)\right) g_R^2\right] + O(g_R^6)\,. \tag{C.35}$$

Comments We have shown that $T(m^2) = Z_0 - \frac{1}{4\pi}\log a^2m^2 + O(a^4m^4)$. From eq. (C.20), this implies that the coefficients of $\log a^2m^2$ at $O(g^2)$ and $(\log a^2m^2)^2$ at $O(g^4)$ match those in eq. (C.9).

C.4.2. Lattice renormalization group

We can obtain easily the anomalous dimension at first order for m_0^2 from C.20 by imposing

$$\begin{aligned} \frac{\partial}{\partial \ln a} m^2 =0 &= \frac{\partial}{\partial \ln a}\left[m_0^2\left(1 + \frac{1}{2} g^2 T(m^2) + \frac{1}{8} g^4 T(m^2)^2\right)\right] + O(g^6) \\ &= \left(\frac{\partial}{\partial \ln a} m_0^2\right)\left(1 + \frac{1}{2} g^2 T(m^2) + \frac{1}{8} g^4 T(m^2)^2\right) \\ &+ m_0^2 \frac{\partial}{\partial \ln a}\left(1 + \frac{1}{2} g^2 T(m^2) + \frac{1}{8} g^4 T(m^2)^2\right) + O(g^6)\,. \end{aligned} \tag{C.36}$$

One obtains

$$\gamma_{m_0^2} = \frac{1}{m_0^2} \frac{\partial}{\partial \ln a} m_0^2(a^2) = \frac{g^4}{4\pi} + \mathcal{O}(g^6) = 2b^2 + \mathcal{O}(b^6)\,. \tag{C.37}$$

This shows that the dimension of m_0^2 goes from the naive value of 2 to $2(1+b^2)$.

Also, we have shown that $g^2 = g_R^2 + O(a^2)$. This proves that the coupling has no divergences when taking the continuum limit, and also that it does not renormalize.

C.5. Mass scaling on the lattice

We are interested in verifying the assumptions provided by the mass formula (C.8). We want to do this by analyzing mass values obtainable within our lattice setup. We want to do this motivated also by the results of the last section. Since the coefficients in front of the logarithm matches, we want to use the result related to the resummation of the logarithm at every order, which gives the $\mu^{1/(2+2b^2)}$ behaviour. The coefficient in front of that will be a result of the lattice regularization, and will be affected heavily by lattice artifacts.

We used as spectroscopical operator the time sliced field

$$O(t) = \sum_x \phi(t,x)\,. \tag{C.38}$$

This can be used given the simplicity of the theory, and we also expect that no other spectroscopicS operators are needed. We chose one direction as the temporal one, and we summed over the other. Since the theory has no bound states, we expect that there shouldn't be contamination in the first time slices, and also that the majority of the signal should be in the first time slices. This is quite a different behavior with respect to other more complex lattice field theories, where the plateau is observed at later times. Given the correlation function

$$C(t) = \sum_{t'=0}^{N_t-1} O(t')(t'+t)\,, \tag{C.39}$$

we expect the following behaviour in initial times region

$$C(t) \approx e^{-m_{eff}t}\,. \tag{C.40}$$

We can extract the mass through using the quantity

$$m_{eff}(t+0.5) = \log\frac{C(t)}{C(t+1)}\,. \tag{C.41}$$

The mass is then visible in the plateau, which is observed already in the first time slices. This is expected to happen, since there is only one physical state possible in the system.

Inspired by (C.8), we want to observe a behaviour given by

$$m_{eff} = f(b)\,\mu^{\alpha}\,, \tag{C.42}$$

with $f(b)$ an unknown function of the parameter b, which can be sensible to lattice regularization artifacts, while we expect α to be close to the value obtained in the continuum, namely $1/(2+2b^2)$. We have shown in the previous section that the parameter b does not renormalize on the lattice, so we make the same assumption here. Hence, we will assume for this part of the analysis that for fixed b also a is fixed, so that we can check the relation between m and μ.

It's also interesting to note that, by imposing

$$\frac{\partial}{\partial \ln a} m = 0 = \frac{\partial}{\partial \ln a}\left[(a\mu)^{\frac{1}{2+2b^2}}\frac{1}{a}\right] \tag{C.43}$$

one obtains the anomalous dimension

$$\gamma_\mu(b) = 2b^2 \tag{C.44}$$

which matches the perturbative result at first order (C.37).

For fixed b values from 0.1 to 3 we proceeded to fit the masses obtained from spectroscopy, as functions of values of μ which range from 10^{-15} to 1. These values have been chosen in order to get effective masses between 0.001 and 1 approximately. Higher value of the masses would be too distant from the continuum limit, hence providing potentially substantial lattice artifacts. Nonetheless, lower values increase the autocorrelation times drastically, hence requiring significantly more computational time.

We show the results for our simulations with $b \leq 1$ in figure C.5. The green line represents the fit with the α parameter free to vary, while the red one fixes α to the theoretical value predicted in (C.8).

We expect the results to be close to the continuum limit for small values of the effective mass, since, given a fixed measured value of the physical mass m^*, it is related to the lattice mass simply by

$$am^* = \hat{m}_{lat} \tag{C.45}$$

with a being the lattice spacing. We used values of m_{lat} between 0.001 and 1. We believe that we are reasonably close to the continuum limit in this region. Lower values of the effective mass result in a theory with a really slowly growing potential, and the numerical algorhithms for these cases generate very correlated configurations. Higher values of the effective mass increase lattice artifacts considerably, and this can potentially invalidate our assumptions on the behaviour, so these will not be considered as well.

C.5.1. Violation of scaling

As noted in previous sections, the mass formula is valid up to $b = 1$. We show that nonperturbative lattice results cease toe support the anomalous dimension of the theory for $b > 1$. Simulations made on a lattice with $b > 1$ seem to violate the scaling

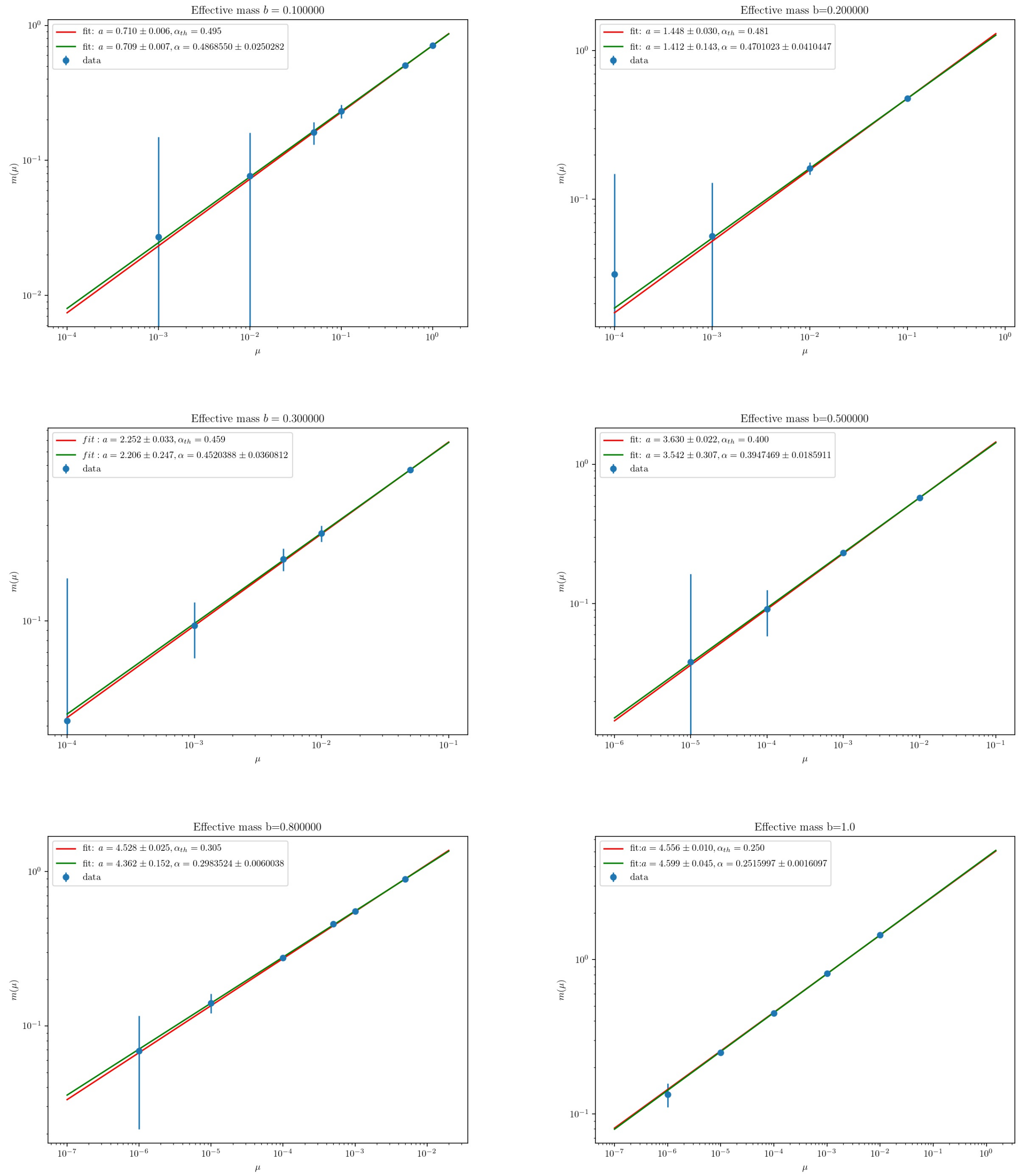

Figure C.1.: Spectroscopic results obtained for values of b smaller than 1 and values of μ in the range from 10^{-6} to 1. Two fits are also shown based on C.42, one in green that allows varying the exponent α, another red one that fixes it to the value $\alpha_{th} = 1/2 + 2b^2$.

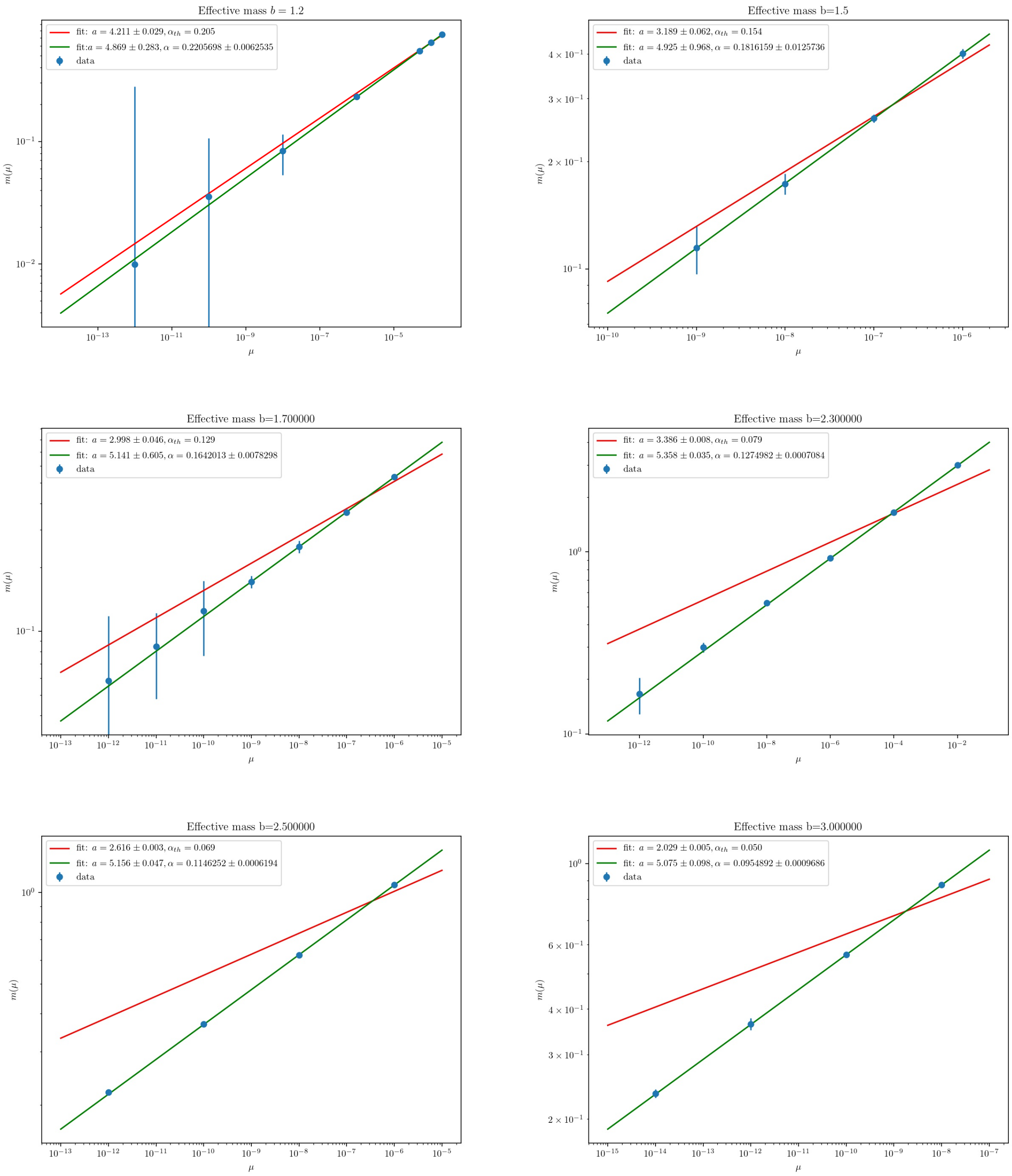

Figure C.2.: Spectroscopic results for values of b larger than the self dual point $b = 1$ are shown. Namely, the results are related to the values $b = 1.2, 1.5, 1.7, 2.3, 2.5, 3$. In the green fit the exponent α is free, while in the red one it is fixed to theoretical value given by the anomalous dimension $\alpha_{th} = 1/(2 + 2b^2)$.

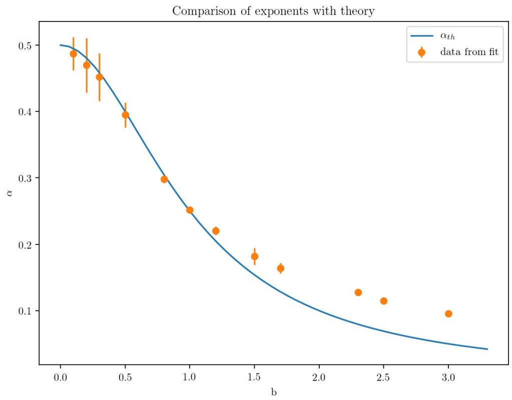

Figure C.3.: Values of the exponents obtained compared to the prediction $\alpha_{th}(b) = 1/(2 + 2b^2)$.

laws. Interestingly, there is still a μ^α behaviour, but $\alpha = 1/(2 + 2b^2)$ is not a correct prediction anymore.

In pictures C.2, we show the results for $b = 1.2, 1.5, 1.7, 2.3, 2.5, 3$. We can see clearly that the red line deviates from the green line, which is in good agreement with the data.

We can show the deviation from the expected behaviour, for $b > 1$ in figure C.3, where all the exponents from the fits are plotted alogside the function $\alpha_{th}(b) = 1/(2 + 2b^2)$.

We show now in figure C.4 a plot of the values obtained for the amplitudes in front of the exponential function. In principle this should be compared with the continuum equivalent described in (C.8). But as can be observed, the real part of that function goes to zero for $b = 1$, and it is not known whether it is valid for $b > 1$.

C.5.2. Finite volume effects

It is of utmost interest verifying that in our analysis finite volume effects are small and quantifiable. For a scalar theory which has a mass gap in the non-interacting limit, effects in the variation of the finite volume mass $\Delta m = m(l) - m(\infty)$ have been quantified to decrease exponentially as $-e^{-\frac{\sqrt{3}}{2}mL}$, where m is the mass gap of the theory and L the spatial length [119].

The hypothesis has been verified for different values of b, as shown in figure C.5. Based on the fit results obtained, it appears that with our working setup with a volume of 256^2, the finite volume effects are negligible.

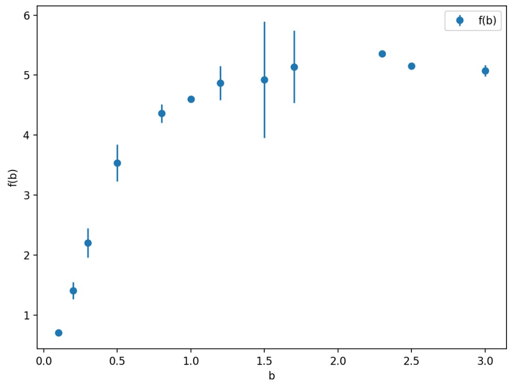

Figure C.4.: Obtained values of the unknown function $f(b)$.

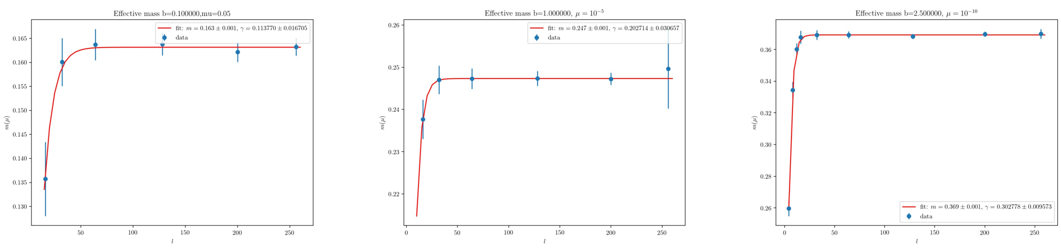

Figure C.5.: Mass value dependence with respect to smaller volumes is plotted, for values of the parameter $b = 0.1, 1, 2.5$. A Lüscher type of fit for the dependence is plotted along with the obtained values.

C.6. Bosonic free conformal field theory comparison

Lastly, we want to discuss how a conformal free field theory, in particular the free massless scalar field theory, with the action

$$\mathcal{S} = \int d^2x \, \frac{1}{2} \partial_\mu \phi \partial^\mu \phi \,, \tag{C.46}$$

can be described in terms of a lattice regularized version.

This theory is interesting for this work, since it is the limit for $\mu \to 0$ of the Sinh-Gordon action, and perturbation theory can be made around it, alternatively to our other choice of unperturbed action. Also, having a proper understanding of the properties of such theory in its lattice realization, can help us to interpret the results about the violation of scaling in section C.5.1. In the case that the theory actually becomes conformal in the region with $b > 1$, over the self dual point, this could explain why standard lattice spectroscopy can not follow the scaling law of the theory.

In the continuum, the theory is both ultraviolet and infrared divergent, so it needs two cutoffs. By naming the two cutoffs as a and R, we obtain the relations for the two point functions

$$G(z,\bar{z}) = \langle \phi(z,\bar{z})\phi(0,0)\rangle = -\frac{1}{2\pi}\log\frac{z}{a} - \frac{1}{2\pi}\log\frac{\bar{z}}{a}\,. \tag{C.47}$$

$$G(0,0) = -\frac{1}{4\pi}\log\frac{R}{a}\,. \tag{C.48}$$

From the propagators one can see that $\phi(x)$ is not a conformal field. But a conformal operator can still be constructed using derivatives, or the exponential operators $\tilde{V}_\alpha = e^{i\alpha\phi}$, called also vertex operators.

It can be shown that, since the action is quadratic, n-point functions of vertex operators can be computed directly from the functional integral, obtaining

$$\prod_{i=1}^{n} \langle \tilde{V}_{\alpha_i}(z_i)\rangle = \left(\frac{a}{R}\right)^{(\Sigma_i^n \alpha_i)^2} \prod_{i<j} \left(\frac{z_i - z_j}{a}\right)^{-\alpha_i\alpha_j} \,. \tag{C.49}$$

One can get rid of the ultraviolet cutoff dependence by defining the renormalized vector operator

$$\tilde{V}_\alpha(z) \to V_\alpha = \lim_{a\to 0} a^{-\alpha^2/2} e^{i\alpha\phi} \equiv : e^{i\alpha\phi} : \,. \tag{C.50}$$

It is interesting to think of an equivalent of this redefinition on the lattice. In principle, it is expected that the conformal invariance of the theory can be reobtained in an infrared regime. But it is explicitly violated in ultraviolet by the natural cutoff given by lattice spacing. The above redefinition takes into account ultraviolet quantities, in particular it is equivalent to subtracting all the tadpole divergences coming from the self interactions of the field $\phi(z)$.

We are interested in the two point function

$$\langle \tilde{V}_\alpha(x)\tilde{V}_{-\alpha}(0)\rangle = e^{-\alpha^2(\Delta(x)-\Delta(0))}\,. \tag{C.51}$$

We chose to use two opposite *charges* in order to remove the infrared divergence. In particular, we want to set the result for the two point function equal to the expected conformal result

$$\langle V_\alpha(x)V_{-\alpha}(0)\rangle = \frac{1}{x^{2\alpha^2}}\,. \tag{C.52}$$

In order to check if it is possible to recreate such a regime for correlation functions on the lattice, one can use the free field lattice propagator

$$\langle\phi(x)\phi(0)\rangle = \int_{-\pi}^{\pi}\frac{d^2p}{(2\pi)^2}\frac{e^{ipx}}{\hat{p}^2+m^2}\,. \tag{C.53}$$

We have added a mass, otherwise the propagator is also infrared divergent. We expect anyway a conformal like behavior in a region

$$\frac{x}{a} << \frac{1}{ma}\,. \tag{C.54}$$

Here we have indicated explicitly the lattice spacing a. One can use a computational algebra software to verify, via numerical integration, that this is the case, thus that correlation functions behave as $|x/a|^{-2\alpha^2}$.

In principle, this procedure can be used even in Sinh-Gordon case, with the addiction of a fictious mass term, in order to detect a conformal like behavior at the self dual point. In case it is detected, spectroscopy with standard lattice techniques ceases to be useful for that case.

A test of the described procedure at the self dual point $b = 1$ has been conducted. The observed results respect the Lüscher ansatz without the conformal behavior, even in the region indicated in equation (C.54). Thus the origin of the mass scaling law violation on the lattice has still to be investigated.

Bibliography

[1] M. E. Peskin and D. V. Schroeder, *An Introduction to quantum field theory* (Addison-Wesley, Reading, 1995).

[2] S. Weinberg, *The Quantum theory of fields. Vol. 1: Foundations* (Cambridge University Press, Cambridge, 1995).

[3] S. Weinberg, *The quantum theory of fields. Vol. 2: Modern applications* (Cambridge University Press, Cambridge, 1996).

[4] S. Tomonaga, Prog. Theor. Phys. **1**, 27 (1946).

[5] J. Schwinger, Phys. Rev. **75**, 898 (1949).

[6] W. E. Lamb and R. C. Retherford, Phys. Rev. **72**, 241 (1947).

[7] H. Fried and D. Yennie, Phys. Rev. **112**, 1391 (1958).

[8] C.-N. Yang and R. L. Mills, Phys.Rev. **96**, 191 (1954).

[9] S. Weinberg, Phys. Rev. Lett. **27**, 1688 (1971).

[10] P. W. Higgs, Phys. Lett. **12**, 132 (1964).

[11] P. W. Higgs, Phys. Rev. Lett. **13**, 508 (1964).

[12] P. W. Higgs, Phys. Rev. **145**, 1156 (1966).

[13] ATLAS Collaboration, G. Aad *et al.*, Phys.Lett. **B716**, 1 (2012), 1207.7214.

[14] CMS Collaboration, S. Chatrchyan *et al.*, Phys.Lett. **B716**, 30 (2012), 1207.7235.

[15] M. Shifman, *Advanced topics in quantum field theory: A lecture course* (Cambridge University Press, 2012).

[16] D. Gross and F. Wilczek, Phys. Rev. D **8**, 3633 (1973).

[17] H. Politzer, Phys. Rev. Lett. **30**, 1346 (1973).

[18] BaBar, J. Lees *et al.*, Phys. Rev. Lett. **109**, 101802 (2012), 1205.5442.

[19] H. Gies and L. Zambelli, Phys. Rev. **D92**, 025016 (2015), 1502.05907.

[20] H. Gies and L. Zambelli, Phys. Rev. **D96**, 025003 (2017), 1611.09147.

[21] H. Gies, R. Sondenheimer, A. Ugolotti, and L. Zambelli, (2019), 1901.08581.

[22] A. Maas and R. Sondenheimer, (2020), 2009.06671.

[23] H. Georgi and S. L. Glashow, Phys. Rev. Lett. **32**, 438 (1974).

[24] S. Dimopoulos and L. Susskind, **2**, 930 (1979).

[25] S. Elitzur, Phys. Rev. **D12**, 3978 (1975).

[26] K. Osterwalder and E. Seiler, Annals Phys. **110**, 440 (1978).

[27] E. Seiler, *Gauge Theories as a Problem of Constructive Quantum Field Theory and Statistical Mechanics* (Lect. Notes Phys., 1982).

[28] E. H. Fradkin and S. H. Shenker, Phys. Rev. **D19**, 3682 (1979).

[29] J. Fröhlich, G. Morchio, and F. Strocchi, Phys.Lett. **B97**, 249 (1980).

[30] J. Fröhlich, G. Morchio, and F. Strocchi, Nucl.Phys. **B190**, 553 (1981).

[31] E. Farhi, K. Rajagopal, and J. Singleton, Robert L., Phys. Rev. D **52**, 2394 (1995), hep-ph/9503268.

[32] A. Maas, Mod.Phys.Lett. **A28**, 1350103 (2013), 1205.6625.

[33] A. Maas and T. Mufti, JHEP **1404**, 006 (2014), 1312.4873.

[34] A. Maas and P. Törek, Annals Phys. **397**, 303 (2018), 1804.04453.

[35] A. Maas, R. Sondenheimer, and P. Törek, Annals of Physics **402**, 18 (2019), 1709.07477.

[36] P. Hasenfratz and R. von Allmen, JHEP **02**, 079 (2008), 0710.5346.

[37] A. Maas, Progress in Particle and Nuclear Physics **106**, 132 (2019), 1712.04721.

[38] R. Sondenheimer, Phys. Rev. D **101**, 056006 (2020), 1912.08680.

[39] M. Böhm, A. Denner, and H. Joos, *Gauge theories of the strong and electroweak interaction* (Teubner, Stuttgart, 2001).

[40] J. Fröhlich, Acta Phys. Austriaca Suppl. **15**, 133 (1976).

[41] J. Fröhlich, R. Israel, E. H. Lieb, and B. Simon, Commun. Math. Phys. **62**, 1 (1978).

[42] G. 't Hooft, NATO Adv.Study Inst.Ser.B Phys. **59**, 101 (1980).

[43] Particle Data Group, P. Zyla *et al.*, Prog. Theor. Exp. Phys. , 083C01 (2020).

[44] A. Djouadi, Phys. Rept. **457**, 1 (2008), hep-ph/0503172.

[45] S. Dawson, C. Englert, and T. Plehn, (2018), 1808.01324.

[46] A. Maas, Mod. Phys. Lett. **A27**, 1250222 (2012), 1205.0890.

[47] V. N. Gribov, Nucl. Phys. **B139**, 1 (1978).

[48] I. M. Singer, Commun. Math. Phys. **60**, 7 (1978).

[49] T. Banks and E. Rabinovici, Nucl.Phys. **B160**, 349 (1979).

[50] A. Ilderton, M. Lavelle, and D. McMullan, JHEP **03**, 044 (2007), hep-th/0701168.

[51] M. Lavelle, D. McMullan, and P. Sharma, Phys. Rev. **D85**, 045013 (2012), 1110.1574.

[52] M. Zubkov, Phys.Rev. **D82**, 093010 (2010), 1008.3076.

[53] M. Zubkov, Phys.Rev. **D85**, 073001 (2012), 1108.3300.

[54] M. Zubkov, Proceedings, 15th Lomonosov Conference on Elementary Particle Physics , 425 (2013), 1109.4077.

[55] B. Lucini, A. Patella, A. Ramos, and N. Tantalo, JHEP **02**, 076 (2016), 1509.01636.

[56] R. E. Shrock, Phys. Lett. **162B**, 165 (1985).

[57] L. Egger, A. Maas, and R. Sondenheimer, Mod. Phys. Lett. **A32**, 1750212 (2017), 1701.02881.

[58] S. Fernbach, L. Lechner, A. Maas, S. Plätzer, and R. Schöfbeck, Phys. Rev. D **101**, 114018 (2020), 2002.01688.

[59] G. Branco *et al.*, Phys.Rept. **516**, 1 (2012), 1106.0034.

[60] A. Maas and L. Pedro, Phys. Rev. **D93**, 056005 (2016), 1601.02006.

[61] J. Andersen *et al.*, Eur.Phys.J.Plus **126**, 81 (2011), 1104.1255.

[62] C. Gattringer and C. B. Lang, *Quantum chromodynamics on the lattice* (Lect. Notes Phys., 2010).

[63] A. Maas, SciPost Phys. **8**, 051 (2020), 1908.02140.

[64] H. B. Nielsen and M. Ninomiya, Phys. Lett. B **105**, 219 (1981).

[65] I. Montvay and G. Münster, *Quantum fields on a lattice* (Cambridge University Press, Cambridge, 1994).

[66] H. J. Rothe, *Lattice gauge theories: An Introduction* (World Sci. Lect. Notes Phys., 2005).

[67] N. Metropolis, A. Rosenbluth, M. Rosenbluth, A. Teller, and E. Teller, J. Chem. Phys. **21**, 1087 (1953).

[68] E. M. Ilgenfritz, M. Müller-Preussker, A. Sternbeck, A. Schiller, and I. L. Bogolubsky, Braz. J. Phys. **37**, 193 (2007), hep-lat/0609043.

[69] E.-M. Ilgenfritz, C. Menz, M. Müller-Preussker, A. Schiller, and A. Sternbeck, Phys.Rev. **D83**, 054506 (2011), 1010.5120.

[70] A. Maas, Phys. Rep. **524**, 203 (2013), 1106.3942.

[71] A. Cucchieri and T. Mendes, Nucl. Phys. **B471**, 263 (1996), hep-lat/9511020.

[72] C. Michael, Nucl. Phys. B **259**, 58 (1985).

[73] M. Luscher and U. Wolff, Nucl. Phys. B **339**, 222 (1990).

[74] B. Blossier, M. Della Morte, G. von Hippel, T. Mendes, and R. Sommer, JHEP **04**, 094 (2009), 0902.1265.

[75] B. Jegerlehner, (1996), hep-lat/9612014.

[76] A. Maas and T. Mufti, Phys. Rev. **D91**, 113011 (2015), 1412.6440.

[77] V. Afferrante, A. Maas, and P. Törek, Phys. Rev. D **101**, 114506 (2020), 2002.08221.

[78] A. Maas and P. Törek, Phys. Rev. **D95**, 014501 (2017), 1607.05860.

[79] L. Del Debbio, A. Patella, and C. Pica, Phys. Rev. **D81**, 094503 (2010), 0805.2058.

[80] M. Hansen, T. Janowski, C. Pica, and A. Toniato, EPJ Web Conf. **175**, 08010 (2018), 1710.10831.

[81] R. C. Brower, D. A. Kessler, T. Schalk, H. Levine, and M. Nauenberg, Phys. Rev. **D25**, 3319 (1982).

[82] S. Gupta and U. M. Heller, Phys.Lett. **B138**, 171 (1984).

[83] J. M. Drouffe, J. Jurkiewicz, and A. Krzywicki, Phys. Rev. **D29**, 2982 (1984).

[84] R. Baier, R. V. Gavai, and C. B. Lang, Phys. Lett. **B172**, 387 (1986).

[85] R. Baier, C. B. Lang, and H. J. Reusch, Nucl. Phys. **B305**, 396 (1988).

[86] A. Maas, S. Raubitzek, and P. Törek, Phys. Rev. **D99**, 074509 (2019), 1811.03395.

[87] A. Hasenfratz and P. Hasenfratz, Phys. Rev. **D34**, 3160 (1986).

[88] P. Boucaud *et al.*, Few Body Syst. **53**, 387 (2012), 1109.1936.

[89] L. von Smekal, K. Maltman, and A. Sternbeck, Phys. Lett. **B681**, 336 (2009), 0903.1696.

[90] A. Maas, Eur. Phys. J. **C71**, 1548 (2011), 1007.0729.

[91] V. G. Bornyakov, V. K. Mitrjushkin, M. Müller-Preussker, and F. Pahl, Phys. Lett. **B317**, 596 (1993), hep-lat/9307010.

[92] R. Lewis and R. Woloshyn, Phys. Rev. D **98**, 034502 (2018), 1806.11380.

[93] I.-H. Lee and J. Shigemitsu, Nucl. Phys. **B263**, 280 (1986).

[94] V. Afferrante, A. Maas, and P. Törek, (2019), 1906.11193.

[95] M. Wurtz, R. Lewis, and T. Steele, Phys.Rev. **D79**, 074501 (2009), 0902.1167.

[96] M. Lüscher, Nucl.Phys. **B364**, 237 (1991).

[97] C. Gattringer and M. Pak, Nucl. Phys. **B801**, 353 (2008), 0802.2496.

[98] Y. Igarashi and J. M. Pawlowski, Nucl. Phys. **B821**, 228 (2009), 0902.4783.

[99] N. Cundy, (2010), 1003.3991.

[100] D. M. Grabowska and D. B. Kaplan, Phys. Rev. Lett. **116**, 211602 (2016), 1511.03649.

[101] S. Catterall, (2020), 2010.02290.

[102] P. Swift, Phys. Lett. B **145**, 256 (1984).

[103] J. Smit, Acta Phys. Polon. B **17**, 531 (1986).

[104] I. Montvay, Phys. Lett. B **199**, 89 (1987).

[105] A. Borrelli, L. Maiani, R. Sisto, G. Rossi, and M. Testa, Phys. Lett. B **221**, 360 (1989).

[106] V. Afferrante, A. Maas, R. Sondenheimer, and P. Törek, (2020), 2011.02301.

[107] I.-H. Lee and R. E. Shrock, Phys. Rev. Lett. **59**, 14 (1987).

[108] I.-H. Lee and R. E. Shrock, Phys. Lett. B **201**, 497 (1988).

[109] A. Morel, J. Phys. (France) **48**, 1111 (1987).

[110] S. R. Sharpe, Phys. Rev. D **41**, 3233 (1990).

[111] C. W. Bernard and M. Golterman, Nucl. Phys. B Proc. Suppl. **26**, 360 (1992).

[112] C. W. Bernard and M. F. Golterman, Phys. Rev. D **46**, 853 (1992), hep-lat/9204007.

[113] M. Booth, G. Chiladze, and A. F. Falk, Phys. Rev. D **55**, 3092 (1997), hep-ph/9610532.

[114] H. A. Van der Vorst, SIAM Journal on scientific and Statistical Computing **13**, 631 (1992).

[115] M. Lüscher, Commun.Math.Phys. **104**, 177 (1986).

[116] A. Koubek and G. Mussardo, Phys. Lett. B **311**, 193 (1993), hep-th/9306044.

[117] A. B. Zamolodchikov, International Journal of Modern Physics A **10**, 1125 (1995).

[118] V. Fateev, S. Lukyanov, A. Zamolodchikov, and A. Zamolodchikov, Physics Letters B **406**, 83 (1997).

[119] M. Lüscher, Communications in Mathematical Physics **105**, 153 (1986).

Acknowledgements

The three years I spent working on this doctoral project have been full of people which have helped me, and also endured me.

Firstly, I want to thank my advisor Axel Maas for giving me the opportunity of working on these interesting and challenging topics. Thanks to his knowledge and his support, I have managed to overcome many hardships we encountered during the various parts of the work, and to learn many new concepts and a useful way to approach problem solving and how to distribute a workload. I am also grateful for giving me the occasion to attend different workshops and schools. Those have been really important for my formation, and i am truly grateful for them.

I am also really thankful for the experience I had in Edinburgh as visiting scientist. I had the occasion of working on a different topic under the supervision of Luigi del Debbio. It has been a fantastic way to improve as a scientist, by working on different projects and with new people. In this context, I am grateful to Gianluca, for its help and its patience when working on our project, and to Christian and Noel.

I want to say thanks especially to my parents, which supported me and have been close all the times during these years. I also say thanks to the remainder of my family, since i can always count on them, even if i am far away.

I want to talk about returning home, and how grateful i am to all my friends which always welcome me in every occasion i can return. I say thanks to Nicola, Pino, Raffaele, Umberto, Angelo, Angelo, Matteo, Daniele, Raffaele, Domenico and Gianluca.

I also want to talk about the city where i studied, and of all the people i met there. Returning to Rome always make me feel at home, and this is mostly due to the people i want to thanks, like Federico, which hosted and helped me many times in these years, but also to Alessandro and Alessandro, invaluable friends, even if only one of them can recognize a bad Doom movie. I also say thanks to Riccardo, Cristian, Giorgio, Alfonsomarco, Micol, Valentina, Lorenzo, Guido, Eugenio, Francesca, Silvia and Peppe.

Lastly i am especially grateful to all the colleagues i met here in Graz during my PhD. I felt part of this group immediately, and i had a really good time working here and collaborating. A particular thank goes to Pascal, which was of enormous help in my first project. His patience in explaining many fundamental concept for my research, and looking at many of my mistakes is something I truly value. Also many useful discussions have been done with my other colleagues, which i am really thankful. I say thanks to Mario, Angel, Christian, Maria, Michael, Milan, Pablo, Carlotta, Oliver, Jordi, Daniel, Marco, Bernd, Fabian, Elizabeth and Sean. I am again thankful to Michael and his advisor Prof. Andreas Wipf for giving me the opportunity of coming to Jena to present my work in a seminar. I also thanks René for discussions on our topic, and a critical reading of this manuscript's first chapters.

I am particularly grateful to all the people I mentioned here, because even if in the last times it has become harder to meet, and to be close together, I always felt their vicinity and affection. I consider this quite non trivial and important, and i appreciate it so much.